

3.2 First-Principles Calculation of Material Properties

Mechanisms of Semiconductor Interface Formation and its Electronic Properties based on Quantum Theory

Atsushi Oshiyama

Institute of Materials and Systems for Sustainability, Nagoya University

Furo-cho, Chikusa-ku, Nagoya 464-8601

In the fiscal year of 2018, on the basis of the density-functional theory we have clarified 1) an elementary process of the decomposition of ammonia and the incorporation of nitrogen into GaN network during the epitaxial growth of GaN [1,2], 2) the structure of carbon-related carrier traps at the SiC/SiO₂ MOSFET interface[3], and 3) the reason for the improvement of the SiC/SiO₂ interface using phosphorus [4,5]. In the following, I will explain the first issue.

Mechanisms of GaN MOVPE: NH₃ reactions on the growing surface

GaN is a principal material for optoelectronic devices and also emerging in power electronics. This is obviously due to its wide band gap and robustness. To endorse its superiority as power devices, however, growth of high-quality GaN films is an inevitable requirement and the clarification of atom-scale mechanisms of the growth of the GaN films is highly demanded. Metal Organic Vapor Phase Epitaxy (MOVPE) with trimethylgallium (TMG) and ammonia (NH₃) as gas sources is regarded as the most suitable technique of growing GaN films. Many experimental and theoretical efforts have revealed that TMG is decomposed in the gas phase and the growing surface is generally Ga rich. Knowledge of the decomposition and incorporation of NH₃ is,

however, extremely poor. We have performed first-principle total-energy electronic-structure calculations that clarify reaction pathways and corresponding energy barriers for the decomposition of NH₃ and the N incorporation on the growing GaN surface. On the contrary to a prevailed picture in the past, we find that the reaction is catalyzed by the presence of the surface [1,2].

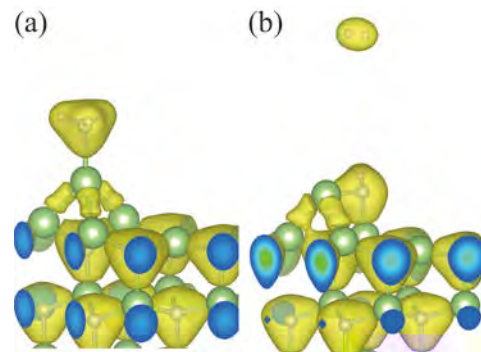


Fig. 1: The initial (a) and the final (b) atomic structures of the decomposition reaction of NH₃. Large and small balls depict Ga and N atoms, respectively. The electron density in each structure is shown as yellow iso-value surface. Adsorbed NH₃, surrounded by upper yellow surface in (a), is decomposed and the -Ga-N(H)-Ga- unit is formed in the subsurface region with an H₂ being desorbed (b).

We start with the identification of the growing surface. Preparing the (0001) bare surface, we have examined stable adsorption configurations for Ga atom as well as for other

molecular species. We have found that the most stable configuration for the additional Ga atom is so-called T4 configuration in which the Ga atom is adsorbed on the site above the second-layer N atom. This surface has been indeed shown to be thermodynamically stable below 1500 K under whole range of V/III ratio in MOVPE. We then examine the adsorption configuration of an NH₃ molecule on the Ga-atom surface. We have found that the NH₃ is adsorbed on the top of the Ga-atom site. The calculated electron density shows the formation of the bond between the Ga atom and the N atom in NH₃. It is also found that the Ga-Ga back bond is relatively weak as is evidenced by the less accumulation of the electron density [Fig. 1 (a)].

This Ga-Ga bond is a candidate for the N attacking site during the MOVPE. Hence we have explored reaction pathways for the NH₃ to be decomposed. We have found that the reaction, [NH₃ on GaN] → [NH in GaN] + [H₂ in gas phase], takes place. The initial and the final atomic structures in this reaction are shown in Figs. 1 (a) and (b), respectively. In the final structure, N in NH₃ intervenes in the weak Ga-Ga back bond, forming the network of - Ga atom - N(H) - Ga -. The N atom has been incorporated in GaN bond network after this reaction. The calculated energy profile along the reaction is shown in Fig.2. The energy barrier for the reaction is calculated to be 0.63 eV, being surprisingly small even though the Ga-Ga bond is destructed in this reaction. Further exploration of the reactions for H₂ desorption leads to a reaction channel toward the incorporated N surrounded by four Ga atoms with the energy barrier of 2 eV. This

barrier is overcome by the free-energy gain for the H₂ molecule in the gas phase: The hydrogen chemical potential at 1300 K in the gas phase is evaluated to be -2.1 eV, considering translation, vibration and rotation motions of H₂.

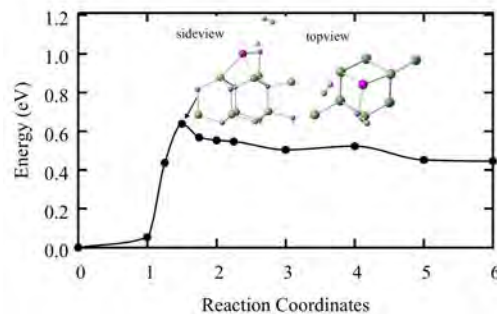


Fig. 2: Calculated energy profile for the reaction of the NH₃ decomposition and the NH incorporation (see text and Fig. 1) on the Ga-rich GaN(0001) growing surface. The transition-state geometry is also shown.

Related Publications

- [1] K. M. Bui, J.-I. Iwata, Y. Kangawa, K. Shiraishi, Y. Shigeta, and A. Oshiyama, *J. Phys. Chem. C* **122**, 24665 (2018).
- [2] K. M. Bui, J.-I. Iwata, Y. Kangawa, K. Shiraishi, Y. Shigeta, and A. Oshiyama, *J. Cryst. Growth* **507**, 421 (2019)
- [3] Y.-i. Matsushita and A. Oshiyama, *Jpn. J. Appl. Phys.* **57**, 125701 (2018).
- [4] T. Kobayashi, Y.-i. Matsushita, T. Okuda, T. Kimoto and A. Oshiyama, *Appl. Phys. Exp.* **11**, 121301 (2018).
- [5] T. Kobayashi, Y.-i. Matsushita, T. Kimoto and A. Oshiyama, *Jpn. J. Appl. Phys.* **58**, 011001 (2019).

Analyses on atomic, magnetic, and electronic structures in high-performance spintronics materials

Tatsuki ODA^{1,2}, Nurul IKHSAN², Tomosato KANAGAWA², Indra PARDEDE²,
Daiki YOSHIKAWA², Marleni WIRMAS², Hasan Al RASYID², Masao OBATA^{1,2}

¹*Institute of Science and Engineering, Kanazawa University, Kanazawa, Ishikawa 920-1192*

²*Graduate School of Natural Science and Technology, Kanazawa University, Kanazawa, Ishikawa, 920-1192*

We studied the several topics involved with this project; implementation of new approach on the magnetic anisotropy originating from spin dipole-dipole interaction and application to thin films. We also investigated the thickness dependence of magnetic anisotropy in Cr/Fe(x)/MgO.

Spin dipole-dipole interaction

We implemented the magnetic dipole interaction (MDI) in a first-principles planewave-basis electronic structure calculation based on spin density functional theory [1]. This implementation, employing the two-dimensional Ewald summation, enables us to obtain the total magnetic anisotropy energy of slab materials with contributions originating from both spin-orbit and spin dipole-dipole couplings on the same footing. The implementation was demonstrated using an iron square lattice. The result indicates that the magnetic anisotropy of the MDI is much less than that obtained from the atomic spin moment model due to the prolate quadrupole component of the spin magnetic moment

density. This new approach allows us to take a self-consistent treatment among the magnetic dipole field caused by the spin density and the exchange field originating from the exchange interaction. In this work, the implementation was performed in two dimensional system, however, the evaluation of spin dipole-dipole interaction can be extended to three dimensional system without any difficulty.

Application to thin films

The new implemented method was used to evaluate the shape magnetic anisotropy for the thin films of ferromagnetic and antiferromagnetic slabs as demonstration [2]. We found that in the ferromagnetic slab with Fe/MgO interfaces, the quadrupole component of atomic spin density suppresses the shape magnetic anisotropy energy in addition to the conventional suppression appearing as magnetic surface. In the antiferromagnetic MnPt slab, which has a perpendicular favor originating from the crystalline magnetic dipole interaction, a surface effect of the Mn

edge appears as an enhancement. This shape anisotropy was found to be comparable to those of the anisotropy originating from the spin-orbit interaction with different sign. Thus whole anisotropy of system may almost cancel out in MnPt system.

Interface systems of Cr/Fe(*x*)/MgO (*x*=1-9)

Electronic structure and magnetic anisotropy energy (MAE) of Cr buffered Fe/MgO interface were investigated in terms of thickness dependence by means of a fully relativistic density functional approach [3]. The electronic structure indicated that the interface state gets occupied unlike a typical rigid band picture as the number of Fe layers decreases, leading large perpendicular anisotropies in the oscillating behavior for its thickness dependence. The maximum of the MAE originating from spin-orbit interaction (SOI) reaches to 2 mJ/m². It is found that the saddle point nature and dispersionless at the Fermi level may be an origin of its large perpendicular magnetic anisotropy. To evaluate the MAE from SOI, the in-plane shape magnetic anisotropy from magnetic dipole interaction (MDI) was estimated. The calculated MAE from MDI required a suppression in the calculated total magnetization for realizing a fair agreement with an experimental MAE. With using a rescaled magnetization it was found that a possible perpendicular anisotropy may

appear in the thickness range of experimental data.

Fermi level smearing effect

Effects of the Fermi level smearing introducing temperature dependence of energy-band occupation numbers were investigated in terms of magnetic anisotropy by using a density functional theory [4]. In a perpendicular magnetization film Fe(0.7nm)/MgO, the magnetocrystalline anisotropy shows a decrease with respect to the smearing temperature; 0.4mJ/m² from 10.5K to 527K. This reduction is not negligible and is expected to be partially compensated by a reduction in the shape magnetic anisotropy, assuming reasonable values of the Curie temperature and saturated magnetic moment. The resulting temperature dependences in the total perpendicular magnetic anisotropy energy is in agreement with those of available experimental data semi-quantitatively.

References

- [1] T. Oda and M. Obata: J. Phys. Soc. Jpn. **87** (2018) 064803.
- [2] I. Pardede *et al.*: IEEE Trans. Magn. **55** (2018) 1300104.
- [3] N. Ikhsan *et al.*: The Sci. Rep. Kanazawa Univ. **62** (2018) 23.
- [4] N. Ikhsan *et al.*: The Sci. Rep. Kanazawa Univ. **62** (2018) 37.

Analyses on magnetic and electronic structures in high-performance spintronics materials

Tatsuki ODA^{1,2}, Indra PARDEDE², Daiki YOSHIKAWA², Tomosato KANAGAWA²,
Nurul IKHSAN², Hasan Al RASYID², Masao OBATA²

¹*Institute of Science and Engineering, Kanazawa University, Kanazawa, Ishikawa 920-1192*

²*Graduate School of Natural Science and Technology, Kanazawa University, Kanazawa, Ishikawa, 920-1192*

We studied the magnetic anisotropy and its electric field (EF) effect in the thin film related with spintronic devices. We obtained a sign change in electric field control perpendicular magnetic anisotropy energy at Fe/MgO interface. EF control on magnetic anisotropy energy (MAE) in the system which contains Fe/MgO interface with Cr underlayer was performed by means of first-principles electronic structure calculations. An opposite sign in EF coefficient γ was observed by introducing Fe/Cr intermixing. This intermixing leads to a substantial rearrangement in the electronic structure due to proximity effects of Fe and Cr. The origin of such an opposite sign in γ was discussed along the modulation of occupied and unoccupied d -band near the Fermi level. By introducing strain effect, the enhancements of MAE and γ were achieved with the maximum absolute values, 2.43 mJ/m² and 170 fJ/Vm respectively. The present result provides a new possible degree of freedom for the EF control in MAE as the underlayer configuration.

We systematically investigated EF effect in Fe/MgO interface systems with Cr underlayer by introducing the interchange of Cr and Fe layers. Our model using slab system, vacuum (0.79nm)/Cr(6ML)/Fe(1ML)/Cr(1ML)/Fe(3 ML)/MgO (5ML)/vacuum (0.79 nm) (system A) and vacuum(0.79nm)/Cr(5ML)/Fe (1ML) /Cr(1ML)/Fe(1ML)/Cr(1ML)/Fe (2ML)/MgO (5ML)/vacuum(0.79nm)(system B). The magnetic anisotropy energy (MAE) was calculated from the total energy difference between in-plane magnetization ([100]) and out-of-plane magnetization ([001]), $MAE = E[100] - E[001]$. To apply an EF, we used the effective screening medium (ESM) method. To obtain the EF inside the MgO layer, we took into account the dielectric constant (9.8 for MgO).

The MAE for system A and B in zero EF are 1.28 mJ/m² and 1.48 mJ/m², respectively. These values were largely enhanced, compared to the system which consists of Cr(6ML)/Fe (4ML)/MgO(5ML)(MAE = 0.59 mJ/m² without introduce Fe/Cr intermixing). In addition, this

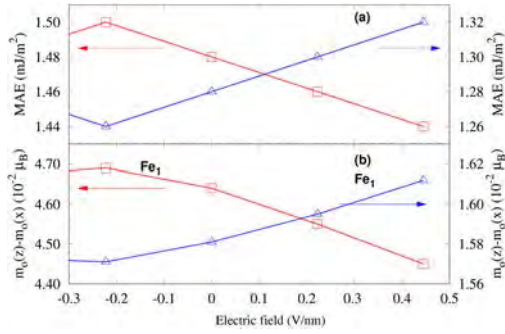


Fig. 1. (a) Electric field effect in MAE and (b) anisotropy of orbital magnetic moment for system A (triangle) and system B (square).

PMA value is comparable to the experimental result [2] after subtracting the shape anisotropy contribution, $K_{dt}=0.690\text{mJ/m}^2$. K_{dt} is estimated by using continuum model, $K_{dt} t_{Fe} = -\mu_0 M_s^2/2$, where μ_0 is the permeability of vacuum and M_s is saturation magnetization. In this estimation, we used $M_s=0.0785\text{ memu/cm}^2$ extracted from experimental data for $t_{Fe}=0.56\text{nm}$ (1ML \sim 0.14 nm)[2].

We calculated MAE as strain dependence for system B, as shown in Fig. 2(a). In this work, the variation of strain is taken in the range of -8.0% to 3.8% for the ratio with respect to Fe lattice constant (2.87\AA). As a result, MAE increases with increasing tensile strain (increase in lattice constant) and increasing compressive strain (reduce in lattice constant) with the maximum

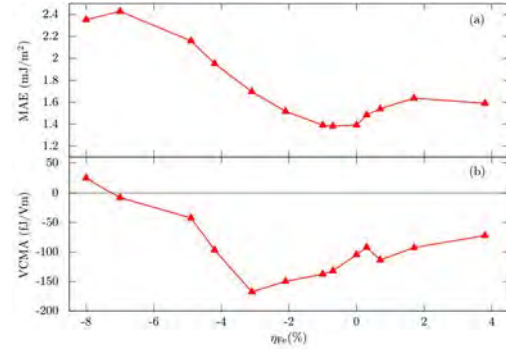


Fig. 2. Strain dependence of (a) MAE and (b) EF effect (VCMA) in Cr/Fe/MgO slab.

value of 2.43 mJ/m^2 . This MAE is strongly related to the spin-orbit-couplings of d -orbital component on the interface Fe, especially those of eigen-states near the Fermi level.

Furthermore, the electric field (EF) coefficient (γ) as strain dependence is shown in Fig. 2(b). The maximum absolute value of γ is 170 fJ/Vm at $\eta_{Fe}=-3.1\%$. This larger value can be related to a large amount of d -orbital states around the Fermi level.

References

- [1] I. Pardede *et al.*: IEEE Trans. Magn. **55** (2018) 1700104.
- [2] T. Nozaki *et al.*, Phys. Rev. Appl. **5**, (2016) 044006.

Functional property of electrodes

OSAMU SUGINO

Institute for Solid State Physics,

The University of Tokyo, Kashiwa-no-ha, Kashiwa, Chiba 277-8581

The water splitting and the fuel-cell reactions occurring on the electrode have recently become an important target of modern surface/interface science. Those reactions are known to occur efficiently catalyzed by platinum but novel class of catalysts such as TiO₂ has attracted attention because of technological importance; however, the reason why TiO₂ should play a role as electrocatalyst is not well known. As a step towards the understanding, we applied a thermodynamic approach to the oxygen reduction reaction (ORR), which has been successfully used to explain why existing electrocatalysts are far from ideal. The approach says that at least one of the elementary steps for ORR is an uphill reaction almost unexceptionally; this happens because adsorption energy of O₂H is linearly dependent on that of OH for most existing catalysts. This phenomenological rule implies that those adsorption energies cannot be modified independently of each other to satisfy the ideal condition by changing the catalyst materials. *In addition*, the adsorption energies follow a universal line that does not cross the point of ideal catalyst.

Our first-principles calculation, however, shows that the adsorption energies do not strictly follow a linear relationship on a rutile and

brookite TiO₂ surfaces when a surface Ti atom is doped with various transition metals [1]. That is, there is significant fluctuation in the E_{ads}(O₂H)-E_{ads}(OH) plot, where E_{ads} means the adsorption energy. It is also found that the adsorption energies approach much closer to the ideal point when doped with some transition metals.

The results of the calculation indicate that the universal relationship is exceptionally violated on TiO₂. They also indicate that, when there is a way to stabilize the dopants at a complex interface although they are not so stable on our model surface that is atomically flat, the dopants may strongly enhance the ORR. We conjecture that such reaction environment may be provided in some part of the real catalyst; we are planning to make it sure by performing an ab initio Monte Carlo simulation.

References

[1] Y. Yamamoto, S. Kasamatsu, and O. Sugino, *submitted*.

Theoretical Analyses on Various Properties Concerning Nanodevices

Satoshi WATANABE

*Department of Materials Engineering, the University of Tokyo
7-3-1 Hongo, Bunkyo-ku, Tokyo, 113-8656*

1 Introduction

Recently, possibilities of novel nanoscale information and energy devices have been explored with various materials and operation mechanisms. This requires deeper understanding on material properties at nanoscale. Considering this situation, we have been performing atomic/electronic level simulations (mainly based on density functional theory (DFT)), taking various nanostructures as target systems. In the followings, some of our results in the fiscal year 2018 are described.

2 Neural network potentials for ion diffusion under electric fields

Motivated by a recent proposal of novel memory device using Au (or Ni)/amorphous $\text{Li}_3\text{PO}_4/\text{Li}$ heterostructure [1], we have been examining Li ion diffusion behavior in amorphous Li_3PO_4 . To facilitate this study, we constructed high-dimensional neural network (HDNN) potentials for efficient prediction of ion diffusion behaviors [2]. Since the ion behaviors under applied electric fields is crucial in the switching in the proposed device, it is desirable to extend the HDNN potential method so that it can take account of applied electric fields. For this purpose, we have developed NN to predict Born effective charge.

The training data are Born effective charges evaluated with density functional perturbation theory for various atomic arrangements obtained via *ab initio* molecular dynamics (MD)

simulations starting from the $\gamma\text{-Li}_{12}\text{P}_4\text{O}_{16}$ structure (at 2000 K with a constant volume). The root mean square errors of the Born effective charge evaluated with the developed NN are 0.065 (e/atom) and 0.069 (e/atom) for the training and test data. We have also developed a MD code, where the forces acting on respective atoms are expressed as the sum of the forces calculated with the previously developed HDNN potential [2] and the force changes due to an applied electric field estimated using the present NN for the Born effective charge. To check the validity of this MD code is in progress.

3 Phonon-related properties of GaN

GaN is promising for power semiconductor device, blue light emitting diode (LED), etc. In such applications, phonon plays important roles, for example, in thermal management in power semiconductor device and emission efficiency in LED. Quantitative evaluation of such phonon-related properties is still a challenging task. Therefore, we have been studying such properties of GaN using DFT-based simulations. Here, we discuss 1) phonon band structures and thermal transport properties and 2) scattering rates due to electron-phonon interaction.

For the thermal transport, the evaluation of thermal conductivities using DFT has become possible recently. However, it is computationally very demanding, which hinders the application of this approach to systems with

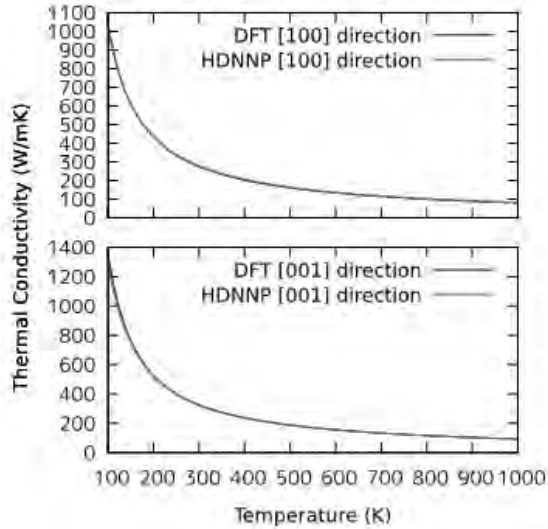


Figure 1: Temperature dependence of thermal conductivities of perfect wurtzite GaN crystal in (a) [100] and (b) [001] directions. Dark and light curves denote the results calculated using DFT and HDNN potential, respectively [3].

defects. So we have applied the HDNN potential techniques mentioned in the previous section to this problem. We have found that the HDNN potentials constructed our previous procedure [2] cannot provide sufficient accuracy of prediction of forces, while training the HDNN potential with forces can achieve good agreement with DFT results on phonon band structures and thermal conductivities of GaN as seen in the temperature dependence of thermal conductivities evaluated using the anharmonic lattice dynamics method (Fig. 1) [3].

For the electron-phonon interaction, we have examined the electron-phonon scattering rates from first principles using the density functional perturbation theory and maximally localized Wannier function. In doing so, we adopted EPW package [4, 5]. We have found that the scattering rates depend on the carrier wave number strongly. In addition, we have found that the applied strain changes the energy and wave number of carriers that suffer strong scattering from phonon.

4 Magnetism of adsorbed atoms and molecules on solid surfaces

The control of the perpendicular magnetic anisotropy (PMA) at the surface/interface of ferromagnetic metals is essentially important in novel magnetic devices based on the magnetic tunnel junctions. Since the interfacial PMA is sensitive to the electronic states at the surface/interface and these states are affected by adsorption of atoms and molecules, we started *ab initio* analysis of magnetism of adsorbed atoms and molecules on solid surfaces.

In the case of the PMA in an Fe(001) surface covered by Co-phthalocyanine (CoPc) molecule, as a preliminary results, we have found that the PMA is enhanced up to 18% by CoPc adsorption, which is in good agreement with experimental results. In the case of transition metal atoms on transition metal dichalcogenides, we have found that the stable adsorption sites changes with the applied strain, and magnetic moment of the adsorbed transition metal atom changes drastically in some combination of adsorbed atom species and transition metal dichalcogenides substrates.

References

- [1] I. Sugiyama, R. Shimizu, T. Suzuki, K. Yamamoto, H. Kawasoko, S. Shiraki, and T. Hitosugi: *APL Mater.* **5** (2017) 046105.
- [2] W. Li, Y. Ando, E. Minamitani, and S. Watanabe: *J. Chem. Phys.* **147** (2017) 214106.
- [3] M. Ogura: Master thesis, the University of Tokyo (2019).
- [4] F. Giustino, M. L. Cohen, and S. G. Louie: *Phys. Rev. B* **76** (2007), 165108.
- [5] S. Ponc e et al.: *Comput. Phys. Commun.* **209** (2016) 116.

First-Principles Study of Excited Electron, Positron and Atom Dynamics and Optical Responses of Nanostructures

Kazuyuki WATANABE, Yasumitsu SUZUKI,
Yoshihiro UEDA, Kazuki UCHIDA

*Department of Physics, Tokyo University of Science
1-3 Kagurazaka, Shinjuku-ku, Tokyo 162-8601*

In this project we investigated the following four topics on the basis of time-dependent density functional theory (TDDFT). 1) Secondary-electron emission from multi-layer graphene (MLG), 2) Multicomponent TDDFT for coupled electron-positron dynamics, 3) Finite temperature effects on laser-assisted field evaporation from a Si surface, and 4) Excitonic signature in dielectric functions of two-dimensional atomic layered materials.

1) *Secondary-electron emission (SEE) from MLG* [1]:

We calculated the amount of secondary electrons (*NSE*) emitted from MLG using real-time TDDFT simulations, and found its dependence on the layer number (L) of MLG and the incident energy of the electron wave packet (WP). *NSE* tends to converge to a certain value with increasing L , which is more conspicuous for a low-incident energy (~ 200 eV) electron WP than for a high-incident energy electron WP (~ 800 eV). The convergence stems from the attenuation of the incident electron WP upon scattering by each graphene layer. The attenuation was found to be proportional to the total number of excited electrons, which strongly depends on the incident energy. Our study enables the direct evaluation of *NSE* for layered and bulk materials and also provides useful insight into SEE from surfaces covered with layered materials. The simulations have been conducted by our home-

made TDDFT code, KENS. Parallelized calculations have been performed using System B.

2) *Multicomponent density functional theory for coupled electron positron dynamics* [2]:

We have developed time-dependent multicomponent density functional theory (TD-MCDFT) for coupled electron-positron systems. The TD-MCDFT is a first-principles method that treats both the electron and positron dynamics quantum mechanically. The TD-MCDFT was applied to LiH under a laser field. There was no simple relationship between the laser energy and the positron detachment probability, which indicates a complex coupling between electronic and positronic motion. We found that the attached positron significantly suppresses laser-induced electronic excitations, which suggests the possibility that the absorption spectrum and excited-state nuclear dynamics may also be changed. There are more promising applications of the theory, such as application to the positron migration in the bulk of the material to reveal how it is trapped in a defect or surface, and positron scattering by materials. These are basic processes in positron beam experiments, and the TD-MCDFT methodology developed this time will be valuable for the study of fundamental positron physics. The simulations have been conducted by our home-made code, TiMESS. Parallelized calculations have been performed using System B.

3) *Finite temperature effects on laser-assisted field evaporation from a Si surface* [3]:

We investigated finite temperature effects on laser-assisted field evaporation from a Si surface using real-time TDDFT. We focused on finite electron and lattice temperatures, both of which were characterized on different time scales. The results indicate that dangling bonds at clean surfaces support thermal excitation under finite electron temperature conditions. It was also determined that thermal excitation induces electron transfer from the surface to the interior of the Si bulk under an electrostatic field, resulting in ionization of the surface atoms. The finite electron temperature effect on evaporation dynamics was found to be negligible. Increases in the finite lattice temperature, however, apparently induce atomic motion both parallel and perpendicular to the surface, thus appreciably enhancing the evaporation rate under electrostatic and laser fields. The present TDDFT simulations provide theoretical support for finite temperature effects during laser-assisted field evaporation, and this method can be applied to various non-equilibrium thermal phenomena, such as laser ablation. The simulations have been conducted by our homemade TDDFT code, KENS. Parallelized calculations have been performed using System B.

4) *Excitonic signature in dielectric functions of two-dimensional atomic layered materials* :

We first calculated the dielectric function of bi-layer hexagonal boron nitride by many-body perturbation theory (MBPT) and found the excitonic signature that depends on its stacking type. We next calculate the dielectric functions of these systems by TDDFT with the meta GGA exchange-correlation potential and the bootstrap kernel and found the structures that are qualitatively similar to those by MBPT. Our study has shown the validity of TDDFT approach for the analysis of optical properties of complex two-dimensional atomic layered materials for which

the MBPT method needs an extremely long simulation time. All MBPT calculations and TDDFT calculations have been conducted using EXCITING (<http://exciting-code.org/>) and ELK (<http://elk.sourceforge.net/>) code, respectively. Parallelized calculations have been performed using System B.

References

- [1] Y. Ueda, Y. Suzuki, and K. Watanabe, *Appl. Phys. Express* **11**, 105101 (2018).
- [2] Y. Suzuki, S. Hagiwara and K. Watanabe, *Phys. Rev. Lett.* **121**, 133001 (2018).
- [3] K. Uchida, Y. Suzuki and K. Watanabe, submitted.

Reduction of Rare Metals in Formic Acid Decomposition Catalysts and Oxygen Storage Materials

Yuji KUNISADA

*Center for Advanced Research of Energy and Materials, Faculty of Engineering,
Hokkaido University, Sapporo, Hokkaido 060-8628*

We investigated the catalyst atom adsorption and diffusion properties on non-metal element doped graphene and MXene supports with the aid of the first principles calculation based on the density functional theory (DFT). We also investigated the corresponding catalytic activity. In addition, we investigated oxygen sorption properties of substituted brownmillerite oxides.

At first, we investigated adsorption and diffusion properties of Cu atoms on non-metal element doped graphene and MXene. We also investigated the catalytic activity using a theoretical volcano plot reported in previous study.[1] We performed the total energy and electronic structure calculations using The Vienna Ab initio simulation package (VASP). We installed parallelized VASP with Intel® MPI Library and Intel® Math Kernel Library. We found that the adsorption energies and diffusion activation barriers of Cu atoms increase by non-metal element doping into graphene lattice. From the adsorption energy of intermediates, we estimated the reaction activities. However, a single Cu atom catalyst shows low activity

because of its strong intermediate adsorption. This trend is also observed in the case of a MXene supported Cu atom.

We also investigated the oxygen sorption properties of $\text{Sr}_2\text{AlMnO}_5$ and $\text{Sr}_2\text{AlMnO}_5$. [2] We revealed that Sr substitution decreases the operating temperature, which indicates that the heteroatom substitution can control the operating temperature.

We also studied the plasmonic properties of an Ag nanoparticle dimer using Discrete Dipole approximation for Electron Energy Loss Spectroscopy (DDEELS). From comparison between simulated and experimental EELS spectra, we revealed that multipolar plasmon is observed in the EELS experiment. [3]

References

- [1] J. S. Yoo, F. A.-Pedersen, J. K. Nørskov, F. Studt: ACS Catal. 4 (2014) 1226.
- [2] Y. Kunisada, G. Saito, K. Hayami, T. Nomura, N. Sakaguchi: Surf. Inter. Anal. 51 (2019) 65.
- [3] N. Sakaguchi, S. Matsumoto, Y. Kunisada, M. Ueda: J. Phys. Chem. C 123 (2019) 6735.

Development of first-principles electronic-structure and transport calculation method based on real-space finite-difference approach

Tomoya ONO

*Center for Computational Sciences, University of Tsukuba
Tennodai, Tsukuba, Ibaraki 305-8577*

SiC has attracted considerable attention owing to its excellent physical properties, such as its high thermal conductivity, high breakdown strength, and large band gap. Among the numerous polymorphs of SiC, 4H-SiC has been recognized as the most promising candidate for power electronics devices. However, unlike Si MOSFETs, SiC MOSFETs have unacceptably low carrier mobility. One of the origins of the low carrier mobility is the generation of a large number of interface defects at SiC/SiO₂ interface. Although several experimental studies reported that carrier mobility increases when interface defect density is reduced by NO annealing after thermal oxidation, the carrier mobility is still much lower than that of SiC bulk and it has not been clarified role of N atoms at the interface yet. To improve the carrier mobility of SiC MOSFETs, it is important to understand and control the electronic structure of the SiC/SiO₂ interface after the annealing. In this study, we carried out density functional theory calculations to examine the atomic and electronic structures of the SiC(0001)/SiO₂ interface after annealing.

It is not straightforward to characterize the atomic structure of the SiC(0001)/SiO₂ interface because SiO₂ at the SiC/SiO₂ interface is mainly amorphous. Here, we assumed that crystalline structures exist locally at the SiC/SiO₂ interface and employed the most possible candidate for the interface atomic

structures reported in Ref. 1. Moreover, two types of atomic layers, h and k , with respect to the stacking orientation of 4H-SiC appear at the 4H-SiC(0001) surface. The effect of the two types of the interface structure was also investigated. The first-principles calculations were performed by RSPACE code.[2]

As for the atomic structures after the NO annealing, it is reported that the N atoms accumulate at the interface.[3] However, there still remain many discussions, whether N atoms exist in the SiO₂ or the SiC substrate. We assumed that the N atoms accumulate in the SiC substrate. For the comparison of the stability of the (oxy)nitrized SiC structure on SiC(0001) surface, we calculated the lattice constant of the (oxy)nitrized SiC by removing the Si atom and replacing the C atoms by the N atoms. It is well known that there are two types of atomic layers in 4H-SiC bulk, h and k . To imitate the atomic layers just below the interface and minimize the unfavorable effect of SiC part on the lattice constant, 2H- and 3C-SiCs were employed. Table 1 shows lattice constants of the (oxy)nitrized SiC, indicating that the lattice constant mismatch of the (oxy)nitrized SiC to SiC(0001) is small.

The computational models for the interfaces, in which N and O atoms are inserted, are shown in Fig. 1. The areal density of N atoms is 1.6×10^{15} (cm⁻²), which agrees well with experimental result obtained by secondary ion mass spectrometry and atom probe

Table 1: Lattice constants of (oxy)nitrized structure of SiC (in Å).

Polymorph	3C			2H		
	Structure	a	c	Structure	a	c
SiC	Si ₉ C ₉	3.07	7.54	Si ₆ C ₆	3.07	4.92
Nitrized	(SiC) ₅ Si ₃ N ₄	3.01	7.23	(SiC) ₂ Si ₃ N ₄	2.98	4.87
Oxynitrized	(SiC) ₄ Si ₄ N ₄ O ₂	3.07	7.39	(SiC)Si ₄ N ₄ O ₂	3.01	4.82

Table 2: Formation energy of (oxy)nitrized structure of SiC [in eV/SiC(0001)-3x1]. The zero of energy is the formation energies of h type interfaces.

	Interface		Bulk	
	h	k	h	k
Nitrized	0.00	+0.38	+0.64	+1.02
Oxynitrized	0.00	+0.40	+1.13	+1.65

field ion microscope.[3] Table 2 shows the formation energy of the interface, in which the minus of the formation energy means that the (oxy)nitrization occurs preferentially by the annealing. When we compare the (oxy)nitrized structures just below the interface and that in the bulk, the formation energy at the interface is smaller than that in the bulk, indicating that the N atoms introduced by the annealing accumulate just below the interface. Moreover, the previous theoretical calculations reported that the difference in the formation energies between the h and k type SiC/SiO₂ interfaces is comparable ($\sim 20\text{meV/SiC}(0001)\text{-}3\times 1$).[4] The formation energy of the k type nitrized interface is much smaller than that of the h type nitrized interface. Because the variation of the conduction band edge due to the coexistence of the h and k type SiC/SiO₂ interfaces causes the scattering,[5] we can conclude that the NO annealing improves the carrier mobility by preferentially generating the h type nitrized interface.

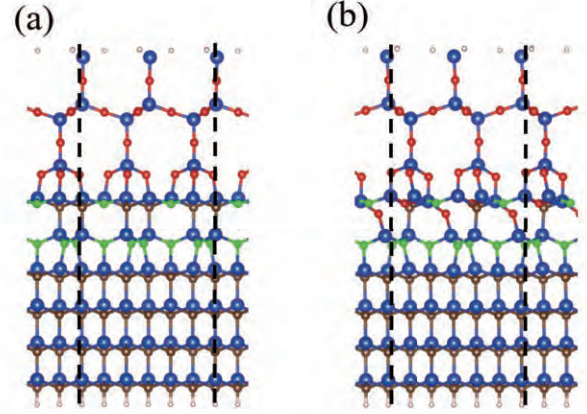


Figure 1: Computational models for (a) nitrized and (b) oxynitrized interfaces. Large (blue), small middle light (brown), and small dark (red) balls are Si, C, and O atoms, respectively. The vertical broken lines represent the boundary of the supercell.

References

- [1] T. Ono *et al.*, Phys. Rev. B **96** (2017) 115311.
- [2] K. Hirose, T. Ono, Y. Fujimoto, and S. Tsukamoto: First Principles Calculations in Real-Space Formalism (Imperial College, London, 2005).
- [3] K. Yamada *et al.*, The 78th JSAP Autumn Meeting (2017) 5a-A203-3.
- [4] C.J. Kirkham and T. Ono, J. Phys. Soc. Jpn. **85** (2016) 024701.
- [5] S. Iwase, C.J. Kirkham and T. Ono, Phys. Rev. B **95** (2017) 041302(R).

Study on the Temperature Induced Stability of Defects on Rutile $\text{TiO}_2(110)$ surfaces

Kenji YASUOKA

Department of Mechanical Engineering,

Keio University, Kohoku, Yokohama, Kanagawa 223-8522

TiO_2 , a wide-gap semiconductor, have attracted considerable attention due to its potential applications as solar cell, photocatalysts and biocompatible materials.[1] There are three major polymorphs of TiO_2 , rutile, anatase, and brookite. In particular, rutile TiO_2 (110) surface is known to be thermodynamically most stable surface and have been studied intensively as a model surface. Upon surface reaction on this surface, defects are known to take an important role,[2] however its microscopic property remains largely unknown.

In this study, we have approached this problem using first-principles molecular dynamics (MD) of interface between defective surface and water. By using this method, we were explicitly able to treat the dynamics of water and their chemical reaction with the TiO_2 (110) surface. This calculation was performed with multi-leveled parallelism on multiple computer nodes by taking advantages of the node-node data transmission technology such as the "enhanced hypercube" topology and $4\times$ FDR InfiniBand $2\times$ used in the System B.

As a result, bond formation between water

molecule and surface Ti defect were observed. This result suggests that stability of Ti defect on the surface is stabilized by forming a bond. Since behavior of water is expected to depend largely on temperature, it can be anticipated that this mechanism is largely temperature dependent. This result is also in agreement with the experimental reporting by Wendt et al. [2], where they suggested importance of Ti defect at near-surface regions. The stabilization mechanism in this study may contribute to modifying theoretical estimate of surface defect concentration. It must be noted however, due to heavy computational cost, complete sampling of phase space is not taken yet. Thus, further calculation and statistical analysis is required to draw a final conclusion.

References

- [1] U. Diebold: Surf. Sci. Rep. **48** (2003) 53.
- [2] S. Wendt, P. T. Sprunger, E. Lira, G. K. H. Madsen, Z. Li, J. Ø. Hansen, J. Matthiesen, A. Blekinge-Rasmussen, E. Lægsgaard, B. Hammer and F. Besenbacher: Science **320** (2008) 1755.

Interaction between osmolytes in water revealed by ab initio molecular dynamics simulation

Tatsuhiko OHTO

Graduate School of Engineering Science,

Osaka University, 1-3 Machikaneyama, Toyonaka, Osaka 560-8531

Trimethylamine N-oxide (TMAO) and urea (shown in Fig. 1), which are small organic molecules solvated in water, coexist in cells of marine animals to control the osmotic pressure. TMAO stabilizes protein structure, whereas urea destabilizes it. But, the mechanism of cancellation of the effects due to TMAO and urea is not clear. In this work, we have identified how TMAO and urea interact in water by ab initio molecular dynamics (AIMD) simulation. We show that the interaction between both osmolytes is favored by hydrophobic association from the potential of mean force (PMF) shown in Fig. 2.

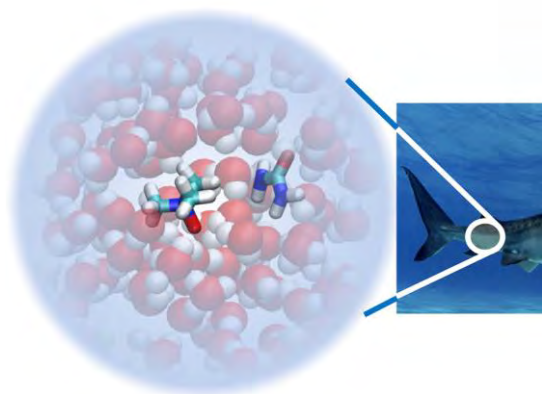


Fig. 1: Structures of the SAM-water interface and the snapshot.

Because one of the reviewers suggested that a

simulation with a hybrid functional is necessary, we did it with revPBE0-D3 using the resource of the class D. Thanks to the additional calculations, the paper was published[1], although the data is not shown in the main text due to the short trajectory.

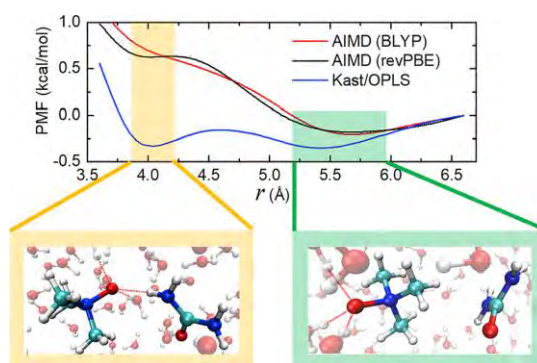


Fig. 2: PMF calculated with BLYP-D3, revPBE-D3, and a classical force field.

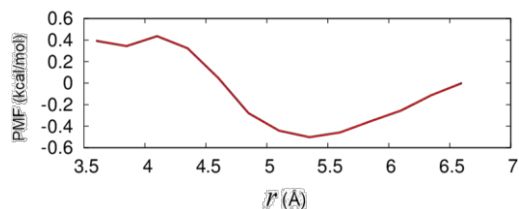


Fig. 3: PMF calculated with revPBE0-D3.

References

- [1] W. J. Xie et al. *Chem* **4**, 2615 (2018).

First-principles molecular dynamics simulation of the interface between water and a supramolecular self-assembled monolayer

Tatsuhiko OHTO

Graduate School of Engineering Science,

Osaka University, 1-3 Machikaneyama, Toyonaka, Osaka 560-8531

Ab initio molecular dynamics (AIMD) simulation is a powerful tool to describe heterogeneous systems such as the water/solid interface. Although AIMD is computationally expensive, it describes electronic states beyond classical force fields,[1] which is important for interfaces.

We have simulated sum-frequency generation (SFG) spectra at the self-assembled monolayer (SAM)-water interface, shown in Fig. 1, using AIMD simulations. The SFG response of the N-H, C-H stretch is the key to understand the orientation and conformation of the SAM. In particular, the hydrogen bond network between melamine and barbituric acid can be detected from the sign of the N-H stretch resonances, if the stretch frequencies are well separated. We employed CP2K code [2], based on the Gaussian plane wave (GPW) method. About 20 ps of trajectory could be accumulated. We will continue running the AIMD and analyze the results after completing the AIMD simulations.

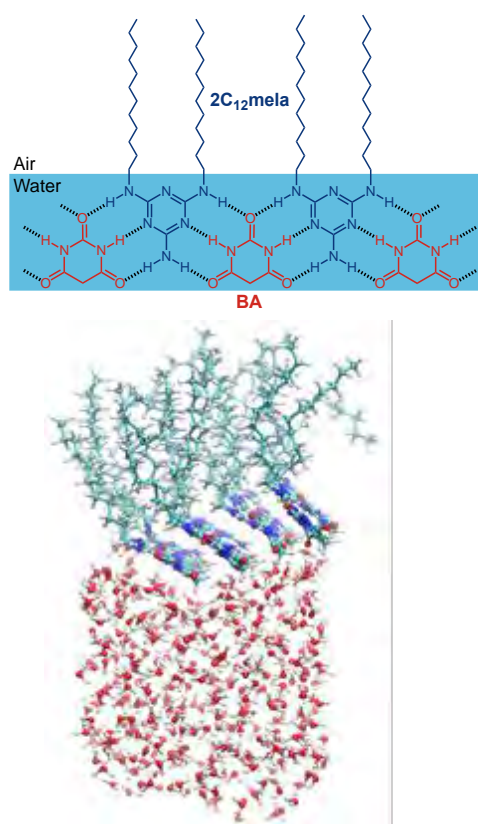


Fig. 1: Structures of the SAM-water interface and the snapshot.

References

- [1] T. Ohto et al. *Phys. Chem. Chem. Phys.* **19**, 6909 (2017).
- [2] The CP2K developers group, <http://cp2k.berlios.de/>

Ab initio molecular dynamics simulation of doped-graphene/water interfaces

Tatsuhiko OHTO

Graduate School of Engineering Science,

Osaka University, 1-3 Machikaneyama, Toyonaka, Osaka 560-8531

Ab initio molecular dynamics (AIMD) simulation is a powerful tool to describe heterogeneous systems such as the water/solid interface. Although AIMD is computationally expensive, it describes electronic states beyond classical force fields,[1] which is important for interfaces.

We have simulated sum-frequency generation (SFG) spectra of isotopically diluted water at the water-graphene and water-hexagonal boron-nitride (hBN) sheet interfaces, using ab initio molecular dynamics simulations. The simulations themselves were performed using ISSP several years ago and recently the paper was published.[2] A sharp ‘dangling’ O-D peak around $\sim 2640\text{ cm}^{-1}$ appearing in both simulated SFG spectra evidences that both graphene and hBN are hydrophobic. The dangling O-D peak is 10 cm^{-1} red-shifted at the water-hBN interface relative to the peak at the water-graphene interfaces. This frequency difference manifests a stronger O-D...N intermolecular interaction between water and hBN than a O-D...C interaction between water and graphene.

To modify the hydrophobic interaction, we calculated doped-graphene water interfaces

using the CP2K code [3]. We prepared 2 % B-doped, 2 % N-doped and 10 % N-doped graphene sheets. We tried to accumulate the 80 ps trajectory for each system and completed 80 % of AIMD runs. We will continue running the AIMD and analyze the results after completing the AIMD simulations.

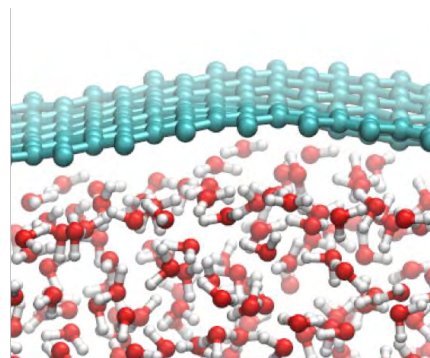


Fig. 1: Structures of the graphene-water interface.

References

- [1] T. Ohto et al. *Phys. Chem. Chem. Phys.* **19**, 6909 (2017).
- [2] T. Ohto et al. *Phys. Chem. Chem. Phys.* **20**, 12979 (2018)
- [3] The CP2K developers group, <http://cp2k.berlios.de/>

Solid State Quantum Chemical Analysis of Fluorinated Polymer Electret

Seonwoo KIM, and Yuji SUZUKI

Department of Mechanical Engineering

The University of Tokyo, Hongo, Bunkyo-ku, Tokyo 113-8656

Electret is a dielectric with quasi-permanent charges. The electrons/ions trapped in the electret material can independently form electrostatic field more than tens of years. In recent years, a vibration-driven electret energy harvester that efficiently converts ambient vibration into electricity gathers much attention as a power source for low-power electronics. In order to improve the harvester's performance, it is essential to develop a new electret material with high surface potential and long-term charge stability.

An amorphous polymer electret CYTOP (AGC Inc.) has desirable characteristics for energy harvesting (low dielectric constant, hydrophobicity, high thermal stability, etc.). Performance of CYTOP as electret is dependent on its end-group, even the number of fluorinated repeat unit is much larger than that of the end-group. Figure 1. shows

three kind of CYTOP series with different end-group. In recent study, we adopted long-range-corrected density functional theory (LC-DFT) analysis to calculate electron affinity (EA) of CYTOP series [1]. Calculated EA made qualitative agreement with material's performance as electret (surface potential, thermal stability of trapped charge). Yet, calculated EA was found to have considerable overestimation tendency, because the analysis is only performed for a free molecule in vacuum state, which is different from real solid polymeric system.

In this study, the authors aim to analyze real electron affinity of CYTOP electret. Solid state quantum chemical analysis is performed, acknowledging morphological diversity and influence of molecules surrounding the trap site to LC-DFT calculation.

Firstly, amorphous CYTOP system is prepared with molecular dynamic (MD) simulation. MD force field parameters are fitted with reference quantum mechanical (QM) calculation results, in order to make mimic QM behavior. Each system is made of 89 CTX-S hexamers and 1 CTX-X (X=S, A, M) hexamer to reflect ratio of end-group and repeat unit in real CYTOP. The system is firstly

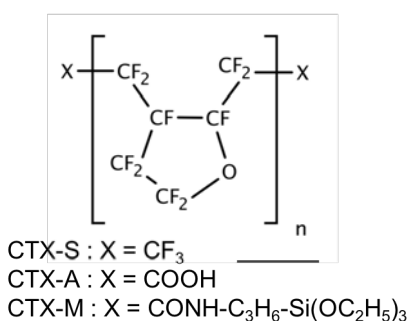


Fig. 1. Chemical structure of CYTOP series.

mixed randomly at 1,000 K to form 1,000 identical random geometry, and then slowly cooled down to 300 K to create morphology of electron-trapped CYTOP system. The energy of molecule is calculated considering three terms; the first is QM term which we can obtain from CAM-B3LYP/6-31+G(d,p) level energy calculation. The second term is electrostatic energy shift. Wavefunctions obtained from QM calculation are converted to multipoles of rank 1-4 using multipole analysis package GDMA [2]. Influence of surrounding molecule to the charge trapping site is acknowledged by calculating multipole-multipole interaction between molecules. The third term is the multipole induction. Multipoles calculated in the second term influence each other thus correction term should be introduced. With these terms in hand, one can calculate solid state energy of a molecule at certain electronic state. Electron affinity is calculated while comparing molecular energy at neutral (0) and negatively-charged (-1) state. Normalized histogram is obtained from 1,000 identical cases, and portrayed as density of state (DoS). Figure 2. shows result of solid state electron affinity analysis. Obtained DoS makes gaussian-like distribution. The medians of distribution are, 3.41 eV (CTX-S), 3.94 eV (CTX-A), and 4.56 eV (CTX-M). The electron affinity of CTX-S makes agreement with EA measured by LEIPS (3.6 eV) within error range [1], implying that the present method reflects real amorphous polymer electret system well.

The calculation is performed with SGI ICE

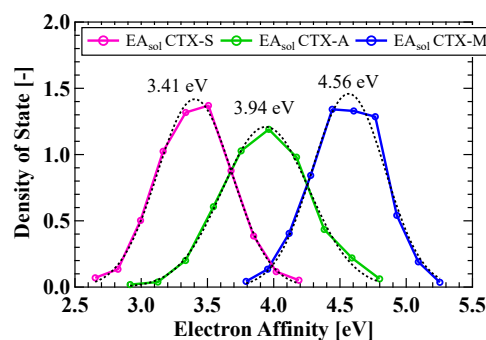


Fig. 2. Solid state electron affinity of CYTOP series.

XA ISSP system B, using quantum mechanical simulation package NWChem [3], molecular dynamic simulation package GROMACS [4], and solid state analysis package VOTCA-CTP [5]. Every calculation is held with 1 node (24 CPUs). In case of CYTOP hexamers, the calculation cost was approximately 150 CPU hours for QM calculation, 100 CPU hours for MD simulation, 5 CPU hours for multipole analysis and solid state analysis. In total, 765,000 CPU hours are used for analysis of CTX-S, CTX-A, and CTX-M.

This work was partially supported by JST CREST Grant Number JPMJCR15Q3.

References

- [1] S. Kim et al., *Sci. Technol. Adv. Mater.*, **19**, (2018), 486-494.
- [2] A. J. Stone, *J. Chem. Theory Comput.*, **1** (2005) 1128-1132.
- [3] M. Valiev et al., *Comput. Phys. Commun.* **181**, (2010) 147.
- [4] S. Pronk et al., *Bioinformatics*, **29**, (2013) 845-854.
- [5] V. Rulhe et al., *J. Chem. Theory Comput.*, **7**, (2011), 3335-3345.

First-principles calculation for muon and positron experiments of wide gap semiconductors

Mineo SAITO

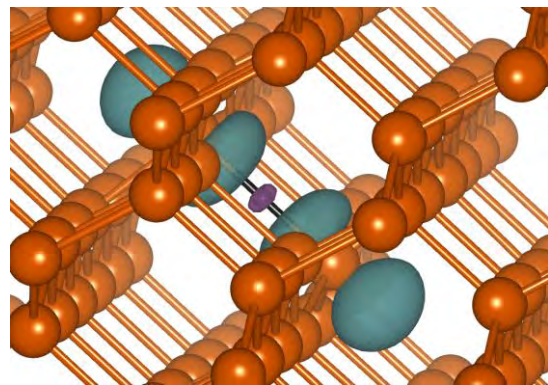
Institute of Science and Technology, Kanazawa University

Kakuma, Kanazawa, 920-1192 Japan

The muon spin resonance is an effective tool to determine the dynamics of hydrogen in semiconductors since muonium bears similarities to hydrogen. Recently, application of this technique to wide gap semiconductors attract scientific interests. To confirm the reliability of density functional theory calculations, we study bond-centered muonium in silicon since this system has been intensively studied but there are still unresolved problems. In this study, we carry out a reliable calculation and quantitatively reproduce the experimental Fermi contact interaction constants (FCIC); the deviation is only 4 %. We find that a large size of supercell is necessary to obtain reliable results. We clarify that the spin density is negative at the muon site whereas it is positive at the nearest Si sites (Fig. 1). The negative spin density at the muon site is found to induce the negative FCIC.

Spin polarized positron annihilation technique detected some spin polarized vacancies in

semiconductors. We systematically study the magnetic properties of vacancies in BN, AlN, GaN, BeO, ZnO, ZnS, and CdS by using the spin-polarized density functional theory. The magnetic moments in all nitride semiconductors are 3 μB whereas the other systems have the magnetic moments of 2 μB . In the case of GaN, we find that the real-space distribution of the majority spin density is narrower than that of the minority spin density, predicting that the positron-electron pair momentum density of the majority spin is broader than that of the minority spin.



.Fig. 1

Development and application of first-principles simulation methods: from structure prediction to superconductivity

Shinji TSUNEYUKI

Department of Physics, School of Science,

The University of Tokyo, 7-3-1 Hongo, Bunkyo-Ku, Tokyo 113-0033

Institute for Solid State Physics,

The University of Tokyo, Kashiwa-no-ha, Kashiwa, Chiba 277-8581

We are developing and applying post-processes of first-principles simulations based on density functional theory (DFT) to tackle with structure prediction, superconductivity and dynamical phenomena in condensed matter. I summarize important achievements in FY2018 in the below.

(i) Data assimilation for crystal structure prediction

Theoretical prediction of unknown crystal structure has been a hard and longstanding problem in science since the number of possible structures increases rapidly with the number of atoms and elements in the unit cell. The problem is especially severe when we use first-principles simulations that require large computational cost even for one-shot calculation.

In this project, we are developing a method of structure prediction supported by experimental data. The method is designed to utilize powder diffraction data whose range of diffraction angle is limited by experimental setup or whose quality is insufficient for Rietveld analysis just like ultra-high-pressure

experiments. In this method, instead of finding the global minimum of the multi-dimensional potential energy surface $E(\mathbf{R})$ as a function of the atomic positions \mathbf{R} , we define the effective potential $F(\mathbf{R})$ by the sum of $E(\mathbf{R})$ and a penalty function which increases when the simulated diffraction pattern deviates from the experimental one:

$$F(\mathbf{R}) = E(\mathbf{R}) + \alpha ND[I_{\text{obs}}, I_{\text{calc}}(\mathbf{R})].$$

Here, D is a function of experimental data I_{obs} and the calculated data $I_{\text{calc}}(\mathbf{R})$. N is the number of atoms in the simulation cell and α is a control parameter. There are various possibilities for the mathematical expression of D , but in this project, we use crystallinity [1] or correlation coefficient.

In FY2018, we made a program that utilizes DFT for the calculation of $E(\mathbf{R})$ and realized simulated annealing with $F(\mathbf{R})$. We used the program to find structures of H_3S at ultra-high pressure and Y_2CH_3 successfully [2].

(ii) Spin fluctuation effect in superconducting DFT

Recently an extension method has been proposed that incorporates the effect of spin

fluctuation into the superconducting transition temperature calculation method based on the superconducting DFT (SCDFT) (Essenberger et al., 2014). We applied the method to non-magnetic iron at high-pressure and clarified that the energy dependence of the spin-fluctuation-mediated interaction can raise the transition temperature through the retardation effect.

(iii) Multiscale simulation of non-thermal ablation of metals

Laser processing is used in a wide range of applications. It is widely known that we have to use a laser with a pulse width of femtoseconds to perform metal microfabrication, but the physical mechanism is not well understood. Many differences between experimental and theoretical calculations have also been reported. Therefore, the optimum laser irradiation conditions at the time of laser processing often rely on empirical rules, and it is difficult to determine from simulation or theory. Our goal is to elucidate the physical mechanism of metal microfabrication.

Based on the results of finite-temperature DFT calculations, we have proposed an electronic entropy induced mechanism for the laser ablation that the entropy of electrons excited under non-equilibrium conditions plays

a dominant role [3]. In FY2018, to discuss the validity of our mechanism, we made a multi-scale simulation method based on the two-temperature model, where we simulate the electronic temperature with finite difference method and the atomic motion with molecular dynamics. For this method, we made an interatomic potential model that depends on the electron temperature and formulated the equations of atomic motion so that the simulation satisfies the energy conservation law. With this method, we simulated laser ablation of Copper with changing laser fluence and successfully found atomic emission at low fluence, spallation and so-called phase explosion at high fluence [4].

References

- [1] N. Tsujimoto, D. Adachi, R. Akashi, S. Todo and S. Tsuneyuki, *Phys. Rev. Materials* 2, 053801 (2018).
- [2] N. Tsujimoto, Ph.D. Thesis, The University of Toyo (2019).
- [3] Y. Tanaka and S. Tsuneyuki, *App. Phys. Exp.* 11, 046701 (2018) (Spotlights 2018).
- [4] Y. Tanaka, Ph.D. Thesis, The University of Toyo (2019).

Analyses on self-organization processes using dissimilarity sampling

Yasuteru SHIGETA

Center for Computational Sciences,

University of Tsukuba, Tsukuba, Ibaraki, 305-8577

Self-organization is a phenomenon in which well-designed molecules spontaneously gather to produce unique structures and is a common process in nature and has great potential for providing a confined nanospace for molecular recognition, transfer, reaction, and catalysis. In particular, it is one of the essential elementary processes in the formation of structures of biological molecules, such as double helix DNAs and tertiary/quaternary structures of proteins, a membrane by the self-assembly of lipid bilayers, the formation of amyloid fibers, and so on. The molecular self-assembly in biological systems plays a crucial role in the function of cells. In order to design and synthesize a new molecular nanoarchitecture, understanding the formation mechanisms is quite essential.

Hiraoka *et al.* developed a hexameric aggregate, nanocube, assembled from gear-shaped amphiphiles (GSAs) **1** in a solvophobic environment. However, the formation process of **1**₆ has not been completely explored yet. Generally, it is very difficult to elucidate self-assembly processes by conventional molecular dynamics (MD) simulations. Instead, we used a dissimilarity sampling method [2] for investigating the dissociation process of **1**₆ into 6 monomers. Figure 1 shows the representative structures from pentamer to dimer [3]. Judging

from the dissociation processes we suggested the formation process and important structures. Once a stable trimer, **1**₃, is formed, it creates a hydrophobic core to absorb hydrophobic guest molecules in the space in contact with three HMEs. These guest molecules further stabilize **1**₃ and might accelerate the formation of the nano-cube, because more non-covalent interactions strengthen the stability not only of **1**₆, but also of other oligomeric structures, especially **1**₂ or **1**₅. Conversely, a hydrophobic molecule of suitable size, say two tribromomesitilenes, serves as a nucleation core to form a quite stable nanocube.

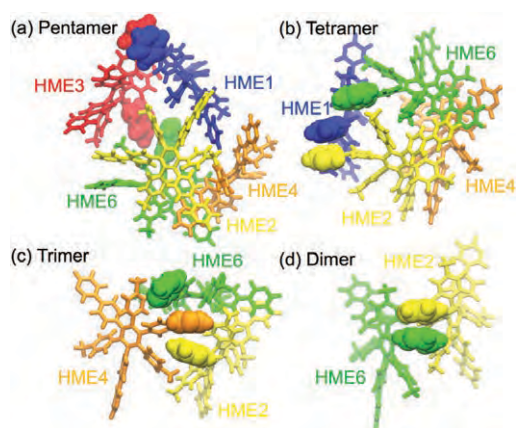


Figure 1 Structures of n -mers ($n = 2$ to 5)

References

- [1] S. Hiraoka, K. Harano, M. Shiro and M. Shionoya, *J. Am. Chem. Soc.* **130** (2008), 14368–14369.
- [2] R. Harada, T. Mashiko, M. Tachikawa, S. Hiraoka, Y. Shigeta: *Phys. Chem. Chem. Phys.* **20** (2018) 9115.

Optical properties of six isomers of a carbon nanocage

Yoshifumi NOGUCHI

Department of Applied Chemistry and Biochemical Engineering, Graduate School of Engineering, Shizuoka University, Johoku 3-5-1, Hamamatsu, Shizuoka 432-8561, Japan

In 2014, a carbon nanocage ($C_{96}H_{80}$), which corresponds to the joint part of a branched carbon nanotube, was successfully synthesized and its optical properties were measured in solution [1]. However, because benzene rings connected through a single C-C bond can rotate each other, the external experimental and environmental conditions can easily reverse the order of stability of the energetically close six isomers; thus, isomers have not yet been identified through the measured the UV-vis absorption spectra in the solution.

In this study, we applied the first-principles GW+Bethe-Salpeter method based on the many-body perturbation theory and attempted to identify the isomers through a comparison between the simulated and experimentally measured UV-vis absorption spectra. In our simulation, we used an original first-principles program, in which employs an all-electron mixed basis approach. With this program, the GW+Bethe-Salpeter calculation for a 176 atoms system can be completed within 3 days, when 288 INTEL XEON processors (or 3456 CPU cores) and total 18 TB memory on a

system B supercomputer are used.

The experimental UV-vis absorption spectra were measured in the solution at a finite temperature [1] and the theoretical spectra were simulated for the most stable (labeled as D2) and most unstable (labeled as T) isomers in vacuum at zero temperature [2]. The peak top position is 3.92 eV for the experimental spectrum, 4.02 eV for D2, and 3.93 eV for T. Although both isomers are in a good agreement with the experimental results, the most unstable isomer, T, is clearly better than D2. In addition, the other spectral parameters such as the height of the second peak and the peak width show better results for T. The results of this study suggest that the T isomer is more strongly stabilized by the external experimental conditions such as by the solvation effect.

References

- [1] K. Mitsui, Y. Segawa, and K. Itami: *J. Am. Chem. Soc.*, **136** 16452 (2014).
- [2] Y. Noguchi, D. Hirose, and O. Sugino: *Eur. Phys. J. B.* **91** 125 (2018).

Direct coupling of replica exchange Monte Carlo method with first-principles calculations for thermodynamic sampling of configurational disorder in solids

Shusuke KASAMATSU

Academic Assembly, Yamagata University

1-4-12 Kojirakawa, Yamagata-shi, Yamagata 990-8560

Metal and oxide alloy systems have varying degrees of disorder which determine the physical properties of those systems. To simulate such disorder, a natural approach may be to combine first-principles calculations based on density functional theory (DFT) with Metropolis Monte Carlo sampling. However, due to the high computational cost of DFT calculations, many previous works have relied on lightweight models fitted to density functional calculations. Due to the difficulty in obtaining reliable *and* lightweight models, this approach has seen limited use in many-component systems. Thus, in this project, we decided to reexamine the feasibility of bypassing the use of fitted models through efficient use of cluster supercomputers.

To we decided to rely on the replica exchange Monte Carlo (RXMC) method [1]. The Figure shows our computational scheme. There are N_{rep} Metropolis samplers running in parallel. Each of the samplers spawns parallel DFT processes (we used VASP [2]) to perform local structural relaxation and energy calculation at every Metropolis step. We

benchmarked the scheme on the calculation of the degree of cation disorder in MgAl_2O_4 and found that it is efficient enough to perform sampling without resorting to fitting models [3]. In other words, we showed that it is now possible to sample configurational disorder in solid state systems directly from first principles through a combination of parallel sampling algorithms and state-of-the-art supercomputers,

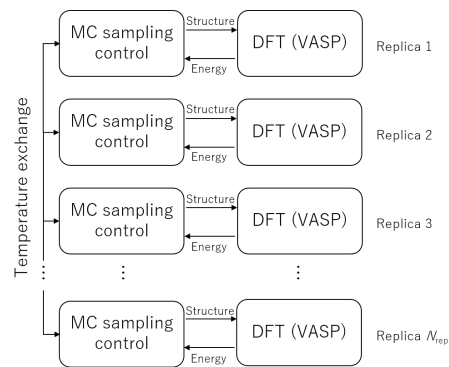


Fig. .: Our RXMC-DFT sampling scheme.

References

- [1] K. Hukushima and K. Nemoto: *J. Phys. Soc. Jpn.* **65** (1996) 1604.
- [2] G. Kresse and J. Furthmüller: *Phys. Rev. B* **54** (1996) 11169.
- [3] S. Kasamatsu and O. Sugino: *J. Phys.: Condens. Matter* **31** (2019) 085901.

First-principles quantitative approach to the interplay of charge and spin fluctuations in superconductors

Ryosuke AKASHI

Department of Physics, University of Tokyo

Hongo, Bunkyo-ku, Tokyo 113-0033

In this project, we investigated the interplay of the dynamical charge and spin fluctuation effects in the superconductors. Many superconductors are classified as "conventional", where the electronic pairing is dominated by the mechanism mediated by the phonon exchange between the electrons. In such systems, the effects of the electron-electron Coulomb interaction is secondary, but still have quantitative impact on the superconducting T_c . The screened static Coulomb interaction strongly suppresses the pairing. On the other hand, the dynamical fluctuations of charge and spin degrees of freedom, which also originates from the Coulomb interaction, can affect the pairing via more complex mechanisms. In the uniform electron gas, the former is expected to enhance the pairing (plasmon mechanism [1, 2]), whereas the latter, which is presumably uniform ferromagnetic fluctuation induced by the exchange effect, suppress the phonon-induced singlet pairing [3]. But for non-uniform realistic cases the situation is thought to be more complicated.

Recently, there has been progress in the first-principles calculation method for superconductors. The density functional theory for superconductors (SCDFT [4, 5]) has been extended to include the charge [2] and spin fluctuation [6] effects. This enables us to elucidate the abovementioned complicated interplay of the fluctuation effects in real superconductors from first principles.

We addressed the superconducting phase in iron emerging under pressure. Although the elemental iron is ferromagnetic metal, at pressure of several ten GPa, its crystal structure changes into the hcp one, the magnetic

order vanishes and superconductivity occurs with $T_c \simeq 3 K$ [8]. This superconducting phase is obviously on the verge of the magnetic transition point and coexistent with strong spin fluctuation and its role on the superconducting phenomenon should be non-trivial.

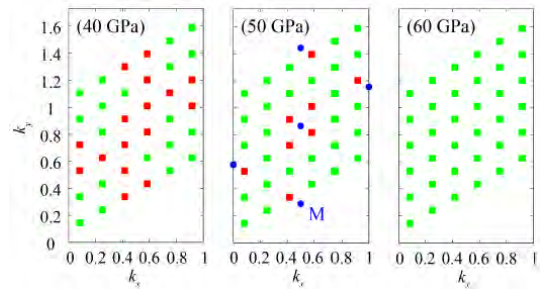


FIG. 1. \mathbf{q} -point grid in the primitive hcp Brillouin zone on the $q_z = 0$ plane. Red points indicate where the sign change of the eigenvalues of D (see Eq. (2)) occurs, whereas at the green points D is positive definite. The sign change represent the strong spin fluctuation with wavenumber $\mathbf{q} = M$

According to the SCDFT, the superconducting order parameter at temperature T is determined by the following gap equation

$$\Delta_{n\mathbf{k}} = -\mathcal{Z}_{n\mathbf{k}}\Delta_{n\mathbf{k}} - \frac{1}{2} \sum_{n'\mathbf{k}'} \mathcal{K}_{n\mathbf{k}n'\mathbf{k}'} \frac{\tanh \frac{\beta E_{n'\mathbf{k}'}}{2}}{E_{n'\mathbf{k}'}} \Delta_{n'\mathbf{k}'}. \quad (1)$$

Δ is the order parameter and $n\mathbf{k}$ labels the Kohn-Sham band index and crystal wavenumber, respectively. $E_{n\mathbf{k}} = \sqrt{\xi_{n\mathbf{k}}^2 + \Delta_{n\mathbf{k}}^2}$ and β is the inverse temperature. The gap equation kernels \mathcal{Z} , \mathcal{K} have been formulated so that the mass-renormalization and pairing effects mediated by the phonons and electron-electron Coulomb interactions, and can be

evaluated with the output of the normal-state Kohn-Sham equation and phonon properties obtained with the density functional perturbation theory [5–7]. We examined the spin fluctuation effects on the superconducting phase by evaluating the T_c with the gap equation using the formulas of \mathcal{Z} and \mathcal{K} with and without the spin fluctuation.

First, in a certain pressure range, we found numerical divergence of the kernels. To clarify its origin, we analyzed the dynamical spin susceptibility χ calculated with the following formula in the plane-wave basis $\{\exp[i\mathbf{G} \cdot \mathbf{r}]\}$

$$\sum_{\mathbf{G}_2} \left[\delta_{\mathbf{G}\mathbf{G}_2} - \sum_{\mathbf{G}_1} \chi_{\mathbf{G}\mathbf{G}_1}^{\text{KS}}(\mathbf{q}, i\omega_n) J_{\mathbf{G}_1\mathbf{G}_2}^{\text{xc}} \right] \chi_{\mathbf{G}_2\mathbf{G}'}(\mathbf{q}, i\omega_n) = \chi_{\mathbf{G}\mathbf{G}'}^{\text{KS}}(\mathbf{q}, i\omega_n),$$

where χ^{KS} denotes the independent particle polarizability calculated with the Kohn-Sham states. This formula is abbreviated by the matrix representation

$$D\chi = \chi^{\text{KS}}. \quad (2)$$

The divergence of χ occurs when any eigenvalues of D changes from positive to negative through zero. We found that this sign change occurs with $\omega_n = 0$ around a certain \mathbf{q} point in the Brillouin Zone as shown in Fig. 1. This divergence is thought to be an artifact originating from the approximate formula Eq. (2), but at least indicates large spin fluctuation with the corresponding wavenumber. We hence limited the calculation with the spin fluctuation to the high pressure regime where D is positive definite.

The calculated superconducting T_c with and without the spin fluctuation is shown in Fig. 2. First we note that in the pressure regime where the superconducting phase is experimentally observed ($\lesssim 30$ GPa), the calculation yields the ferromagnetic phase as the ground state (in the pressure region indicated by “FM” with an arrow), at odds with the experiment. We then assume that the generalized gradient approximation (GGA [9]) for

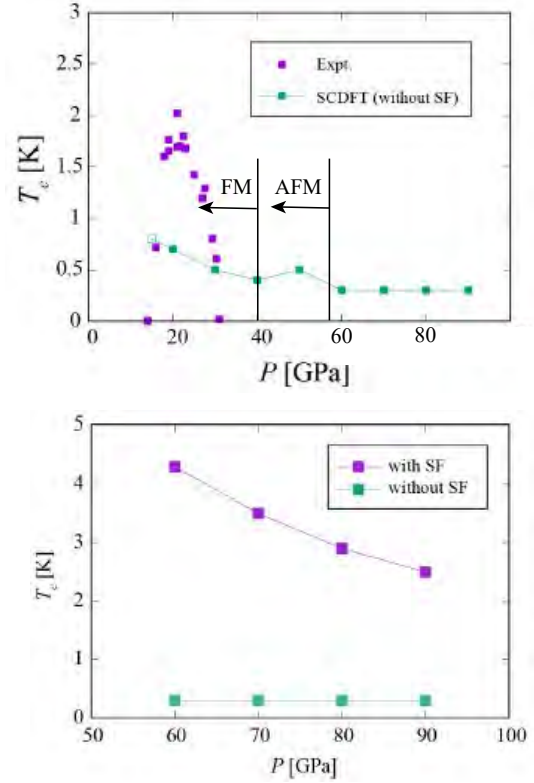


FIG. 2. Calculated and experimentally observed T_c s of Fe under pressure. (upper) Experimental values and the calculated results without the spin fluctuation (SF) effect. The arrows indicate the pressure regions where ferromagnetic phase is stabilized and antiferromagnetic fluctuation diverges numerically. (lower) The calculated results with and without the SF effect.

the exchange correlation functional tends to overestimate the stability of the magnetic order. The calculated T_c without the spin fluctuation effect shows little pressure dependence as shown in the left panel. On the other hand, with the spin fluctuation effect, T_c shows a decreasing trend with increasing the pressure. This could corresponds to the right half of the dome-like dependence observed experimentally. Interestingly, the spin fluctuation enhances the T_c , which cannot be explained with the simplistic uniform electron gas picture mentioned above. This result suggests a novel superconducting mechanism could be possible where the spin fluctuation is the main driving force of the superconducting pairing in the

compressed iron.

The above results have been published as a dissertation [10]. The first-principles electronic structure calculations were done with the plane-wave basis code package QUANTUM ESPRESSO (5.1)(Ref. [11]). The phonon and electron-phonon properties were calculated with the PHonon program in this pack-

age, which is based on the density functional perturbation theory [12]. The Brillouin-Zone integration for the metallic systems were done with the optimized tetrahedron method [13]. The GGA-PBE [9] exchange-correlation potential was used. Parallel calculation was performed with respect to \mathbf{k} points (*-npool* option) as implemented in *ph.x* code. The calculations were mainly done in System B.

-
- [1] Y. Takada, J. Phys. Soc. Jpn. **45**, 786 (1978).
 [2] R. Akashi and R. Arita, Phys. Rev. Lett. **111**, 057006 (2013).
 [3] N. F. Berk and J. R. Schrieffer, Phys. Rev. Lett. **17**, 433 (1966).
 [4] M. Lüders, M. A. L. Marques, N. N. Lathiotakis, A. Floris, G. Profeta, L. Fast, A. Continenza, S. Massidda, and E. K. U. Gross, Phys. Rev. B **72**, 024545 (2005).
 [5] M. A. L. Marques, M. Lüders, N. N. Lathiotakis, G. Profeta, A. Floris, L. Fast, A. Continenza, E. K. U. Gross, and S. Massidda, Phys. Rev. B **72**, 024546 (2005).
 [6] F. Essenberger, A. Sanna, A. Linscheid, F. Tandetzký, G. Profeta, P. Cudazzo, and E. K. U. Gross, Phys. Rev. B, **90** 214504 (2014).
 [7] R. Akashi, M. Kawamura, S. Tsuneyuki, Y. Nomura, and R. Arita, Phys. Rev. B **91**, 224513 (2015).
 [8] K. Shimizu, T. Kimura, S. Furomoto, K. Takeda, K. Kontani, Y. Onuki, and K. Amaya, Nature **412**, 316EP (2001).
 [9] J. P. Perdew, K. Burke, and M. Ernzerhof, Phys. Rev. Lett. **77**, 3865 (1996).
 [10] Y. Hizume, Master thesis “Theoretical study on the effect of spin-fluctuation in superconductivity in iron under high pressure” (Department of Physics, The University of Tokyo, 2019).
 [11] P. Giannozzi *et al*, J. Phys.: Condens. Matter **21**, 395502 (2009); <http://www.quantum-espresso.org/>.
 [12] S. Baroni, S. de Gironcoli, A. Dal Corso, and P. Giannozzi, Rev. Mod. Phys. **73**, 515 (2001).
 [13] M. Kawamura, Y. Gohda, and S. Tsuneyuki, Phys. Rev. B **89**, 094515 (2014).

First-principles study of ionization and diffusion of metal atoms at metal/solid interfaces in electric fields: toward semiconductor and organic substrates

Takashi NAKAYAMA

Department of Physics, Chiba University

1-33 Yayoi, Inage, Chiba 263-8522

Metal/solid interfaces are essential structures for various electronic/optical devices. During the fabrication and operation of devices, however, a variety of defects are often generated, particularly from their interfaces in electric fields, which produces various carrier traps and promotes the degradation of devices. However, there are little theoretical works on defect formations around metal/solid interfaces. In this works, we studied the formations of various point defects, such as interstitial metal atoms, atom vacancies, and impurity dopants, around metal/solid interfaces in electric fields using first-principles calculations.

To simulate the interfaces, we adopt (2×2) – (4×4) metal/solid repeated-slab models made of 4 ML metal atoms and 16 ML inorganic/organic solids. The formation energy of a point defect was calculated as a function of the distance from the interface by the standard first-principles method in the density functional theory. We employ a primitive method to produce an electric field perpendicular to the interface by simply removing electrons from the present slab system. All atom positions are optimized for all interfaces.

Figs. 1(a)–1(c) show the formation energies of C-vacancy, P-dopant, and Al-dopant defects in SiC layers around Au/2H-SiC interfaces, respectively, as a function of the distance from the interface, for various values of electric fields. The formation energies of point defects gradually increase with increasing the distance from the interface in the case without an electric field, which is a general trend observed for point defects around metal/solid interfaces. The most remarkable feature is that, with increasing the electric field, the formation

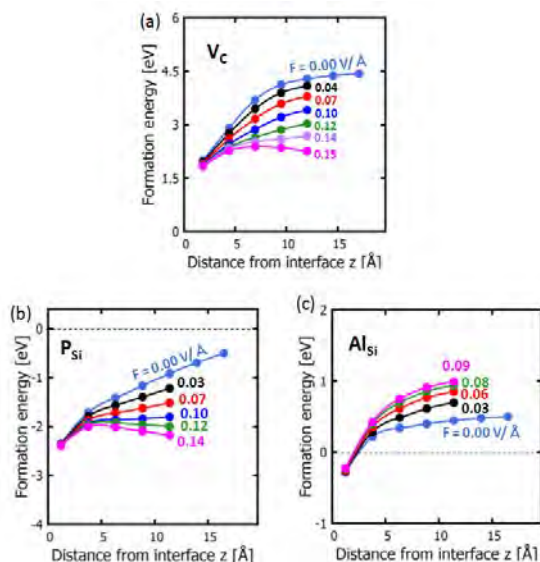


Fig.1. Calculated formation energies of (a) C-vacancy, (b) P dopant, and (c) Al dopant as a function of the distance z of a defect from the Au/2H-SiC interface. The cases with various electric fields ($F = 0$ – 0.15 V/Å) are shown in different colors.

energies in inner 2H-SiC layers decrease for the former two defects, while it increases for the latter defect. We also studied various point defects and found that formation of anion vacancies and donor-type dopants is easy, while the formation of acceptor-type dopants becomes difficult around the metal/solid interfaces when the positive voltage is applied to the metal electrode.

To understand the variation of formation energy, we show the ionization charges of C-vacancy in Fig. 2(a), as a function of the distance from the interface. We can clearly see that the ionization charge increases with increasing the electric field. This variation is explained by considering the capacitor model shown in Fig. 2(b). When the C vacancy is produced in 2H-SiC layers, the electron-

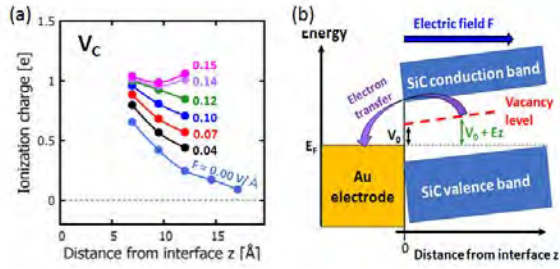


Fig.2. (a) Calculated ionization charge of C-vacancy as a function of the distance from the Au/2H-SiC interface for various values of electric fields ($F = 0-0.15$ V/Å). (b) Schematic picture to explain the electron transfer between electronic state of defect and metal electrode around metal/solid interface in electric field, for the cases of C-vacancy.

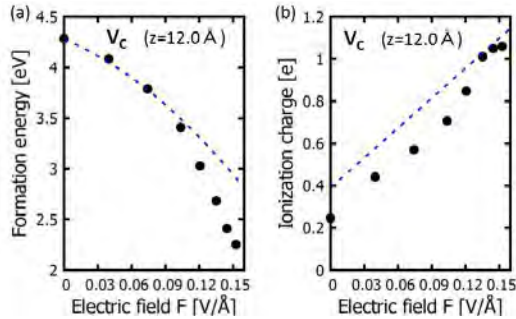


Fig.3. (a) Calculated formation energy and (b) ionization charge of C-vacancy at $z = 12$ Å around the Au/2H-SiC interface, as a function of the electric field. Dots are obtained by the first-principles calculation, while blue dashed lines are by the capacitor model.

occupied vacancy state appears in the band gap of 2H-SiC. Since the Fermi energy of Au electrode E_F is located below this state, the electron transfer q occurs from the vacancy state to the Au layers as shown by the arrow in Fig. 2(b). By considering the energy gain and loss by this electron transfer, we obtain the formation energy and ionization charge of C-vacancy as $E_{\text{form}}(F, z) = E_0 - \epsilon SF^2 z/2 - \epsilon SFV_0 - \epsilon SV_0^2/2z$ and $q = \epsilon SF + \epsilon SV_0/z$, where E_0 is the formation energy in bulk SiC, F the electric field, z the distance from the interface, S the effective area of ionization charge, V_0 the energy position of vacancy state, and ϵ the dielectric constant of SiC.

Figures 3(a) and 3(b) show the variations of the formation energy and ionization charge of C vacancy at the fixed $z = 12$ Å position. We can

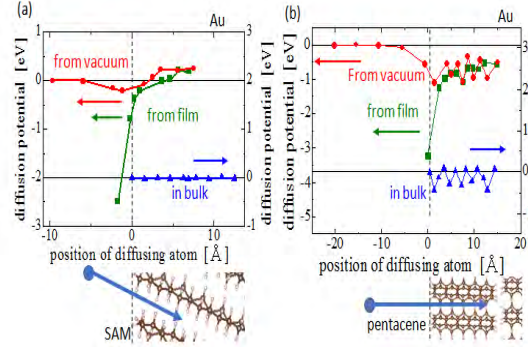


Fig.4. Calculated diffusion potentials for Au metal atom in (a) SAM and (b) pentacene solids, as a function of metal-atom position. Lower pictures display the corresponding position.

see that such variations are well explained by the present capacitor model. In this way, the electron transfer between defect and metal electrode is the key to understand the variation of defect formation energies around the metal interface in electric field.

Then, we consider the cases of metal/organic solid interfaces. Figures 4(a) and 4(b) show the diffusion potentials of Au atom around Au/SAM and Au/pentacene interfaces. In the case of SAM, metal atom easily penetrates and diffuses in solids reflecting the weak interaction between metal atom and molecules. In case of pentacene, on the other hand, since the interaction between metal atom and molecules is attractive and strong, metal atom actively enters into solids and is tightly bonded to molecules. The difference in metal-atom behavior comes from the difference in electronic structure between SAM and pentacene, which are respectively σ - and π -orbital molecular systems.

All these calculations were performed using the xTAPP, VASP, and pspwf codes. In order to realize the calculations for the present interface systems in electric fields, because the system is made of a large number of atoms (300-1000 atoms), the advanced computing facility having multi-task and higher-speed CPU (more than 64 cores \times 2.5GHz), larger-size memory (around 128GB), and larger-size storage (more than 1 TB) is indispensable. These conditions are realized only by the ISSP supercomputing systems.

Redox-driven spin transition in layered battery materials

Atsuo YAMADA

*Department of Chemical System Engineering,
The University of Tokyo, Bunkyo-ku, Hongo, Tokyo 113-8656*

Electronic spin plays a crucial role in determining the physical and chemical properties of transition-metal compounds. In battery ceramics electrode materials containing transition-metals M , it is likely that M exhibits a hitherto unreported redox-driven spin transition (RDST), which might considerably influence the operating potential of the electrodes.

In the present study, we have discovered an existence of RDST occurring for the $\text{Co}^{3+}/\text{Co}^{2+}$ redox couple in layered transition-metal oxides using density functional theory calculations, leading to a colossal potential hysteresis (> 1 V) between the cathodic (low spin (LS) Co^{3+} to LS Co^{2+}) and anodic (high spin (HS) Co^{2+} to HS Co^{3+}) reactions.

All the calculations are performed using Vienna Ab-initio simulation package (VASP). The projector-augmented-wave (PAW) method and a plane-wave basis set with a kinetic energy cutoff of 550 eV were used. We applied GGA+U where values of $U_{\text{eff}} = 3.9, 4.0, 3.4, 6.0$ eV were used for the d electrons of Mn, Fe, Co, and Ni atoms, respectively.

Our work points to the considerable influence of the spin-state variance on their

battery performance. In a practical sense, redox-driven spin transitions cause a large voltage hysteresis and a large loss in energy efficiency. Thus, $\text{Co}^{3+}/\text{Co}^{2+}$ should be used with care as the redox couples in battery electrodes.

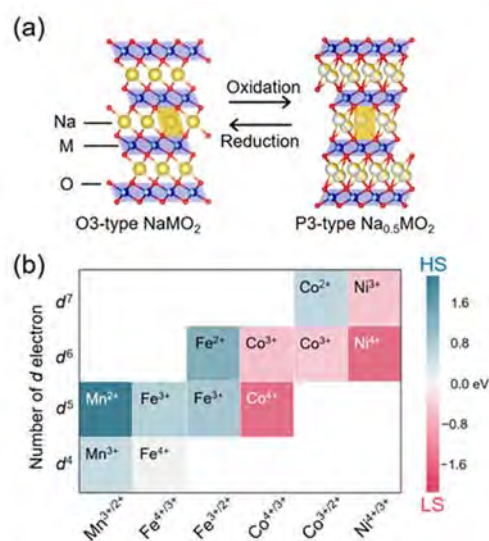


Fig. 1: (a) Schematic illustration of Na_xMO_2 upon Na^+ (de)intercalation. (b) Stable spin states of M^{m+} in $\text{Na}_x\text{Ti}_{0.5}M'_{0.5}\text{O}_2$ and $\text{Na}_x\text{Al}_{0.5}M'_{0.5}\text{O}_2$. [1]

References

- [1] Eriko Watanabe, Masashi Okubo, Atsuo Yamada et al, *Chem. Mater.*, **31** (2019) 2358.
- [2] Eriko Watanabe, Yuki Yamada, Masashi Okubo, Atsuo Yamada et al, *Chem. Rec.*, **19** (2019)

First-Principles DFT Calculations for Topological-Insulator Multilayers

Kunihiko YAMAUCHI

ISIR-SANKEN, Osaka University, Ibaraki, Osaka 567-0047

Based on *Ab-initio* approach, we have theoretically designed heterostructure of various tetradymite-type topological insulators. A three-dimensional topological insulator exhibits the non-trivial quantum states which can be characterized by the insulating bulk states and the spin-polarized metallic surface states. The latter is known to have a Dirac cone dispersion and show the helical spin structure, as having an appealing potential for future spintronics device applications. Although the highly insulating bulk state and the tunable Dirac cone in the bulk band gap are desired for the applications, many of topological insulators have been found to be metallic due to the existence of impurities and/or structural disorder.

In order to tune the Dirac points energy, we control the artificial multilayer composed of Bi_2Se_3 -related topological quintuple layers. Band-structure calculations are performed by using a projector augmented wave method implemented in Vienna Ab initio Simulation Package (VASP) code with generalized gradient approximation. After the crystal structure was fully optimized, the spin-orbit coupling was included self-consistently. MPI parallelization was performed over bands and plane wave coefficients using 16 ~ 96 cores in system B.

After we tested several combinations of hetero-structural slabs, some successful results are obtained as shown in Fig. 1. Here the Dirac point is located exactly at the middle of the band gap at the $\bar{\Gamma}$ point, while the bulk

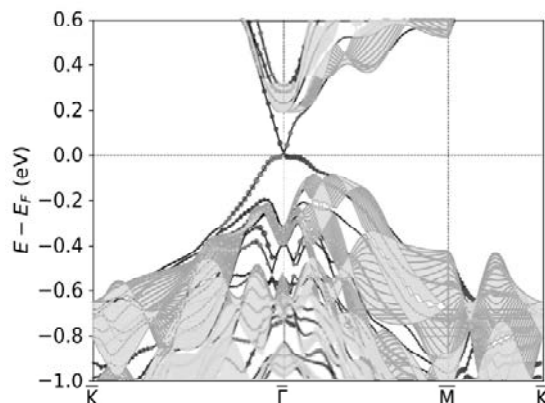


Figure 1: Calculated bandstructure of a multilayer slab which consist of ternary tetradymite topological insulators. The spin-polarized surface states are indicated by open and filled circles. The bulk band projection is also shown.

band structure keeps rather large band gap. In order to understand the shift of the surface-state energy, the work function of slab structure was evaluated. It reveals that the surface energy is determined by the difference in work function between surface and bulk materials. Our finding provides a way to obtain the ideal Dirac cone state in artificial multilayers of topological insulator that is appealing for the future spintronics applications.

References

- [1] T. Kosaka, K. Yamauchi, and T. Oguchi: in preparation.

Large scale ab initio calculations on the fundamental processes of solar energy convergence devices and on designing principles for new materials

Koichi YAMASHITA

Department of Chemical System Engineering, School of Engineering,

The University of Tokyo, 7-3-1, Hongo, Bunkyo-ku, Tokyo 113-8656

1. Defect structures and anion orderings on perovskite photocatalysts for water-splitting

Water-splitting photocatalysts are expected as hydrogen production devices using sunlight, but, its energy-conversion efficiency is still low for practical use. Recent studies have reported that the defects and anion orderings improve the physical properties of semiconductors. Therefore, we investigated the defects or anion orderings.

Defective perovskite oxides $\text{Sr}_{1-x}\text{NbO}_3$ have recently been reported as water-splitting photocatalysts. Its band structure is metallic, but it can split water into oxygen or hydrogen by specific sacrificial reagents, and the carrier mobility is expected to be high. In this work, we performed density functional theory (DFT) calculation to identify the bands and k -points that can absorb light nearby experimental optical gap, which suggested that the Fermi level is shifted due to the formation of Sr defects and O vacancies, the optical gap is changed, and the absorption of light can be controlled by the defect amount. Besides, the defect dependence of the optical gap suggests that Sr defects and O vacancies may coincide. [1]

The band gaps of certain perovskite oxynitri-

des are suitable for water-splitting under visible light irradiation. However, due to the myriad of anion orderings, traditional DFT calculations can only investigate some of them. In this work, we combined DFT calculations with machine learning to rapidly predict the large size anion ordering of BaNbO_2N , which can oxidize water under light irradiation up to 740 nm. The machine learning model was trained to predict the energy and band gap obtained by DFT calculation from the anion ordering. Our method has reduced more than 99.99% of the calculation cost of predicting total energy using only DFT calculation. Besides, by using the Metropolis method, we were able to predict the stable anion configuration of a large supercell, which is difficult to calculate using DFT calculations. This work demonstrates a means of predicting the properties of functional materials based on more realistic elemental ordering with a reasonable computational load. [2]

2. Device-Scale Simulations of Organic Photovoltaics for Performance Improvement

Organic photovoltaics, OPVs, are promising energy harvesting devices, but their power conversion efficiencies are lower than traditional silicon ones. Morphology—the degree of phase

separation and miscibility of the organic semiconductors—is a key factor for performance improvement since it strongly affects exciton dissociation and charge collection. Bulk heterojunction, BHJ, morphologies are widely adapted because of both of nanoscale phase separation (~ 10 nm) and bicontinuous transport pathways. There are many experimental techniques to observe morphologies; especially, conductive atomic force microscopy (C-AFM), a contact-mode variant of AFM, offers high-resolution (from a few to dozens of nanometers) examination of components under the probe tip. It is, however, challenging to experimentally obtain three-dimensional high-resolution information about morphologies.

In this work, C-AFM of BHJ morphologies was simulated by dynamic Monte Carlo algorithm [3] to obtain three-dimensional information from two-dimensional images. The system was ITO/P3HT:PCBM/Al as a model since it has been well studied. The device scale (50^3 nm³, 1-nm grid) morphologies were generated by Metropolis Monte Carlo of reptation [3]. Charge injection, hopping, recombination, and extraction were stochastically simulated. We analytically solved Laplace equation of a bispherical coordinate system to obtain the electric potential arising from the applied voltage and the difference of Fermi levels of the electrodes. Simulations were performed for all the probe points, *i.e.* lattices on the surface, and the currents were evaluated.

The cross-sections of morphologies and hole injection current are shown in Fig. 1 Hole

injection current ranges from a few picoamperes to a few hundreds of picoamperes when a probed lattice was donor, which agrees with experiments. On the other hand, electron injection current was low (0.02 pA at maximum) due to high injection barrier and low potential gain, resulting in no charge recombination. Morphologies with smaller interfacial areas tended to show higher current because of their favorable transport pathways.

In this work, only a few morphologies were examined as model cases. This simulation is viable for high throughput computations, which will enable to predict three-dimensional morphologies from experimental C-AFM images with such technique as machine learning.

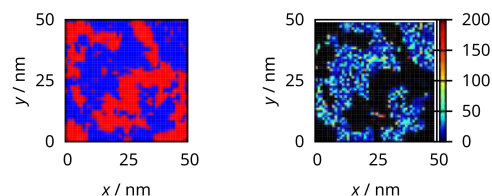


Fig. 1: (left) A cross-section and (right) a simulated C-AFM image (hole injection current divided by pA) of a BHJ morphology. Blue and red lattices represent donor and acceptor, respectively.

References

- [1] M. Kaneko, K. Mishima, and K. Yamashita: *J. Photochem. Photobiol. A: Chem.* **375** (2019) 175–180.
- [2] M. Kaneko, M. Fujii, T. Hisatomi, K. Yamashita, and K. Domen: *J. Energy Chem.* **36** (2019) 7–14.
- [3] E. Kawashima, M. Fujii, and K. Yamashita: *Phys. Chem. Chem. Phys.* **18** (2016) 26456–2646.

Singular atomic structure and its electronic property in oxide material

Kazutoshi INOUE¹, Mitsuhiro SAITO², and Yuichi IKUHARA^{1,2,*}

¹ *Advanced Institute for Materials Research, Tohoku University, Sendai, Miyagi, 980-8577*

² *Institute of Engineering Innovation, The University of Tokyo, Yayoi, Tokyo, 113-8656*

We found a formation of singular atomic structures in MgO thin films around grain boundaries and grain-boundary triple junctions through a combination of scanning transmission electron microscopy (STEM) and first-principles calculations [1]. The atomic arrangements possess a two-dimensional random arrangement of one-dimensionally ordered atomic columns which is different from the known solid states — crystal, quasicrystal and amorphous. The structure is referred to as the “one-dimensionally (1D) ordered crystal” which can be a metastable phase in a confined region. They consist of the structural units that are similar to the ones found in coherent grain boundaries.

The MgO thin film was deposited on metallic thin films by RF-magnetron sputtering in high vacuum at room temperature. STEM observations were carried out with a 200kV STEM with a sub-Å resolution. Atomic models were constructed from STEM images. Then, density-functional theory calculations were carried out using Vienna Ab-initio Simulation Package (VASP) within projector augmented wave scheme with an energy cut-off of 500 eV. We applied the generalized gradient approximation of Perdew, Burke, and Ernzerhof to address exchange-correlation functional. Sampling of the irreducible Brillion Zone (BZ) was performed with a regular Monkhorst-Pack grid of Gamma centered $9\times 9\times 9$ and $13\times 13\times 13$ k-points for the 1D ordered crystal and the MgO bulk, respectively. Full relations of all atoms were iterated under the conjugate gradient algorithm until the magnitude of Hellmann-Feynman force on each atom

converged to less than 0.03 eV/Å. Total energy was calculated using the linear tetrahedron method with Blöchl correction.

To obtain accurate electronic properties for the 1D ordered crystal and its bulk counterpart, the hybrid HSE06 functional was adopted to determine the electronic density of states (DOS). A set of Gamma-centered $5\times 5\times 7$ k-points and a Gaussian smearing scheme with a converged width of 0.05 eV for integrating BZ were applied. The energy tolerance was converged less than 10^{-5} eV. The HSE06 gives a much more accurate prediction of the band gap of 6.5 eV for the bulk MgO. The total DOS indicates a significantly reduced band gap of 3.0 eV for the 1D ordered crystal which is obviously smaller than that of the bulk MgO.

To confirm the theoretical predictions, we also measured the band gaps using low-loss electron energy loss spectroscopy (EELS) with a monochromated STEM. The band gaps of the 1D ordered crystal and the bulk MgO are measured to be 3.2 eV and 7.4 eV, respectively, in a good agreement with the theoretical prediction. These results suggest that the MgO 1D ordered crystal should be a wide-band-gap semiconductor.

The discovery of the 1D ordered crystals is of fundamental scientific interest and will encourage more efforts for exploring the potential applications.

References

- [1] D. Yin, C. Chen, M. Saito, K. Inoue, Y. Ikuhara: *Nat. Mat.*, 18 (2019) 19-23.

Large-scale device-material research by massively parallel electronic structure calculation and data science

Takeo Hoshi

*Department of Applied Mathematics and Physics, Tottori University,
4-101 Koyama-Minami, Tottori 680-8550, Japan.*

The present project was carried out for the joint research between electronic structure calculations and data science. Related mathematical studies and software development were also carried out. The main collaborators are Yusaku Yamamoto (U. Elec. Comm.), Koji Hukushima (U. Tokyo), Takatoshi Fujita (IMS), Hiroyuki Matsui (Yamagata U.), Toshio Hyodo and Ayahiko Ichimiya (KEK).

The large-scale electronic-state and transport calculations were carried out for flexible organic devices. As a main achievement, principal component analysis (PCA) was carried out so as to analyze large-scale electronic state calculation data for exploration of organic polymer device materials [1-3]. The method is given by the dimensional reduction of electronic wavefunctions, since the original data size is huge. The reduction is realized, when the participation ratio of wavefunctions, a measure of quantum localization, is chosen as the descriptor. The computation was carried out for electronic states for 40,000 samples of disordered organic polymers with 1,200 atoms by our large-scale electronic state calculation code ELSESES (<http://www.elses.jp/>) on the K computer. As

results, the polymer samples are classified into four groups correctly and the physical meaning of the principal components is clarified. The present method is general and forms a rigorous foundation of the data-driven material science. Numerical methods for large-scale electronic state calculations were developed for efficient contour integral [4], intermediate eigenpair computation [5], middleware for parallel eigenvalue computation with the performance prediction function by Bayesian inference [6]. In addition, preliminary researches were carried out for large-scale exciton calculation of organic interface [7] and large-scale electronic state calculation of disordered pentacene thin film [8], the development of data analysis on positron diffraction experiment [9].

As mathematical studies, we developed a new preconditioner for the CG method which combines the block red-black ordering with relaxed modified incomplete Cholesky factorization. Numerical experiments on a multicore processor shows that the preconditioner is both effective and scalable [10]. We also developed a new algorithm for the nonlinear eigenvalue problem based on signed singular values [11].

References

- [1] T. Hoshi, H. Imachi, K. Oohira, Y. Abe, and K. Hukushima, 'Principal component analysis with electronic wavefunctions for exploration of organic polymer device materials', International Meeting on High-Dimensional Data-Driven Science, Kyoto, 10-13. Sep. 2017
- [2] T. Hoshi, H. Imachi, Y. Abe, K. Oohira, K. Hukushima, 'Principal component analysis with large-scale electronic state calculation for ultra-flexible device materials', Waseda U., 18th SIAM Conference on Parallel Processing for Scientific Computing (SIAM-PP18), 7-10, Mar. 2018.
- [3] (Award) T. Hoshi, 'Organic-device material research based on 100-nano-meter electronic structure calculation and data science', Excellent achievement award of HPCI projects, 2. Nov., 2017.
- [4] H. Kohashi, K. Sugita, M. Sugihara and T. Hoshi, 'Efficient methods for computing integrals in electronic structure calculations', JSIAM Letters 9, pp. 81-84 (2017)
- [5] D. Lee, T. Hoshi, T. Sogabe, Y. Miyatake, S.-L. Zhang, 'Solution of the k-th eigenvalue problem in large-scale electronic structure calculations', submitted; Preprint (<http://arxiv.org/abs/1710.05134>).
- [6] T. Hoshi, T. Fukumoto, T. Fukaya, Y. Yamamoto, 'Analysis and prediction of the performance in generalized eigenvalue solvers on Oakforest-PACS', International Workshop on Eigenvalue Problems: Algorithms; Software and Applications, in Petascale Computing (EPASA2018), 5-6, Mar. 2018.
- [7] MD K. ALAM, T. Fujita, T. Hoshi, 'Excited-state calculation for large size C60/Pentacene interface based on the fragment molecular orbital method', Meeting of The Japan Society of Applied Physics, Hakata, 5-8, Sep 2017.
- [8] T. Hoshi, Y. Abe, A. Kuwata, K. Kakuda, T. Fujita, H. Matsui, 'Large-scale electronic state calculation in disordered pentacene thin film', Meeting of The Japan Society of Applied Physics, Waseda U., 17-20, Mar. 2018 (Japanese)
- [9] T. Hoshi, K. Tanaka, I. Mochizuki, T. Hyodo, A. Ichimiya, Y. Nakanishi, K. Hukushima, 'Development of data analysis software for positron diffraction', 2nd Workshop on Positron Diffraction, organized by T. Hyodo and T. Hoshi, KEK Tsukuba, 30. Mar. 2018. (Japanese)
- [10] A. Shioya and Y. Yamamoto, 'The danger of combining block red-black ordering with modified incomplete factorizations and its remedy by perturbation or relaxation', Jpn. J. Ind. Appl. Math., 35, pp 195-216 (2018).
- [11] K. Ooi, Y. Mizuno, T. Sogabe, Y. Yamamoto and S.-L. Zhang, 'Solution of a nonlinear eigenvalue problem using signed singular values', East Asian J. Appl. Math. 7, pp. 799 - 809 (2018).

DFT sampling studies on interfacial properties of batteries and catalysts

Yoshitaka TATEYAMA

Center for Green Research on Energy and Environmental Materials (GREEN), National Institute for Materials Science (NIMS), 1-1 Namiki, Tsukuba, Ibaraki 305-0044; Elements Strategy Initiative for Catalysts & Batteries (ESICB), Kyoto University, Goryo-Ohara, Nishikyo-ku 615-8245.

We are working on (1) developments of theoretical, computational and data-driven techniques [1-3] as well as (2) understanding of surface and interface reactions, essential in the energy and environmental technologies such as battery and catalyst [1,4]. Recently, we have developed some multiscale techniques involving the DFT-level calculations.

In this report, we introduce a study via DFT-based surface microkinetics simulations of NO + CO reaction on Rh surface, which is widely used as a model reaction on the NO_x reduction by the three-way catalyst [1]. Though there are many DFT microkinetics studies, inclusion of surface reactions and development of automated protocol were still very rare.

We assumed that the catalysis cycle consists of the following elementary reaction steps; NO dissociation, N₂O formation, N₂ formation, and CO₂ formation. The adsorption energies, reaction energies, and activation energies were all evaluated with the DFT calculations. For the exchange-correlation interaction, the RPBE functional was used. All the DFT calculations

were done by VASP 5.4. The microkinetic analysis was carried out with the DFT-calculated energetics.

In Figure 1, the reaction rates of NO consumption, N₂O formation, N₂ formation and CO₂ formation were plotted with respect to temperature (T). The results show that the N₂O formation is faster than the N₂ formation at low T, while the opposite behavior is observed at high T. This agrees with the experiments in which N₂O and N₂ were reported as the main product at low and high T regions, respectively. The surface coverage, shown in Figure 1 (right), shows good correspondence with change of the reaction rate: At T = 300 - 400 K, the NO dissociation takes place and thus the surface NO is consumed while N and O coverage increases. At T = 500 - 600 K, the surface O is consumed because of the CO₂ formation and at higher T range the surface N decreases as the N₂ formation occurs. The surface coverage changes strongly suggest that accumulation of the N species on the surface is crucial for N + N → N₂ reaction to take place.

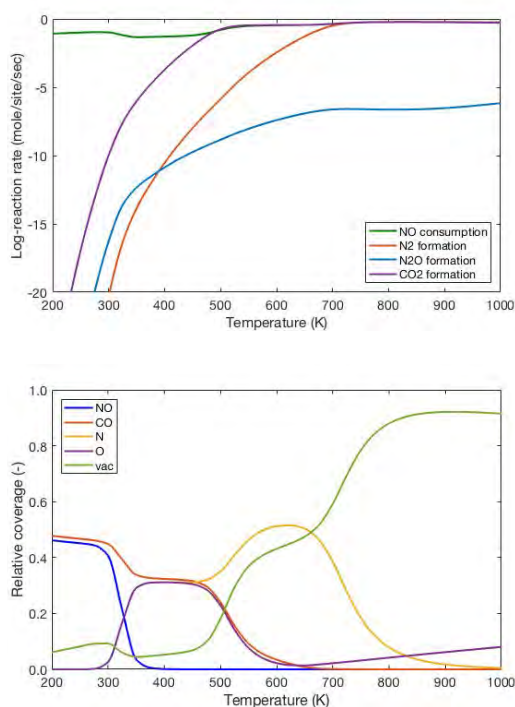


Figure 1: (upper panel) The reaction rates of four elementary reaction steps in the NO + CO reaction and their changes with respect to the

temperature. (lower panel) the change in the surface coverages of reaction intermediates as the function of the temperature.

References

- [1] A. Ishikawa, Y. Tateyama: *J. Phys. Chem. C* **122** (2018) 17378-17388.
- [2] R. Jalem, M. Nakayama, Y. Noda, T. Le, I. Takeuchi, Y. Tateyama, H. Yamazaki: *Sci. Tech. Adv. Mater.* **19** (2018) 231-242.
- [3] K. Sodeyama, Y. Igarashi, T. Nakayama, Y. Tateyama, M. Okada: *Phys. Chem. Chem. Phys.* **20** (2018) 22585-22591.
- [4] L. Szabova, M. F. Camellone, F. N. Ribeiro, V. Matolin, Y. Tateyama, S. Fabris: *J. Phys. Chem. C* **122** (2018) 27507-27515.

First-principles study of quantum transport in nanostructures

NOBUHIKO KOBAYASHI

*Institute of Applied Physics, University of Tsukuba
1-1-1 Tennodai Tsukuba Ibaraki 305-8573*

1 Introduction

The aim of this project is to reveal and predict charge, heat and spin transport in materials from first-principles. Theoretical studies on transport properties are indispensable for the recent developments of high-performance electronic devices. Quantum nature is essential in nanoscale systems, and atomistic analysis based on detailed electronic states calculations are indispensable to discuss the transport property. In order to investigate transport properties, we have developed the nonequilibrium Green's function (NEGF) method, and the $O(N)$ time dependent wave-packet diffusion (TD-WPD) method on the basis of the density functional theory (DFT). Using these methods, we have investigated charge, heat and spin transport properties of materials. [1, 2]

2 $O(N)$ TD-WPD method and application to organic semiconductors

Organic semiconductors have attracted much attention for their applications to flexible, printable, lightweight, and low-cost electronic devices. They are crystals that are assemblies of π -conjugated molecules weakly bonded by van der Waals interactions, and single crystallization has been achieved, enhancing the mobility. It is expected that the mechanism of carrier transport in organic semiconductors can be elucidated and that materials exhibiting high mobility can be developed by novel molecular synthesis.

We developed the $O(N)$ TD-WPD method for the quantum transport calculation of huge

systems of up to 100 million atoms a decade ago. We calculated the conductance and the mobility of the system with micron-order lengths at room temperature at the atomistic levels. Using this method we can study the transport properties from diffusive to ballistic regimes including the effect of realistic electron-phonon scattering, and determine the mean free path and relaxation time from an atomistic viewpoint. We performed DFT calculations of electronic structures and interactions between molecules of single-crystal organic semiconductors including the effect of the van der Waals interaction, and applied the TD-WPD method to the analysis of transport properties of the organic semiconductors.

We analyzed the transport properties of various organic semiconductors, and confirmed that the calculated mobilities and their temperature dependences are quantitatively in good agreement with those obtained in experiments. The essence of the requirements to quantitatively evaluate mobility is employing the proper computation method of diffusion coefficient defined using the velocity correlation function. Moreover, quantitative accurate evaluations of both two-dimensional transfer-integral networks based on DFT and effects of dynamic disorder induced by all phonon modes on the electronic states are also required. Since our methodology enables quantitative prediction of the transport properties of various soft materials using first-principles calculations, our method becomes a powerful tool when developing new materials. [3]

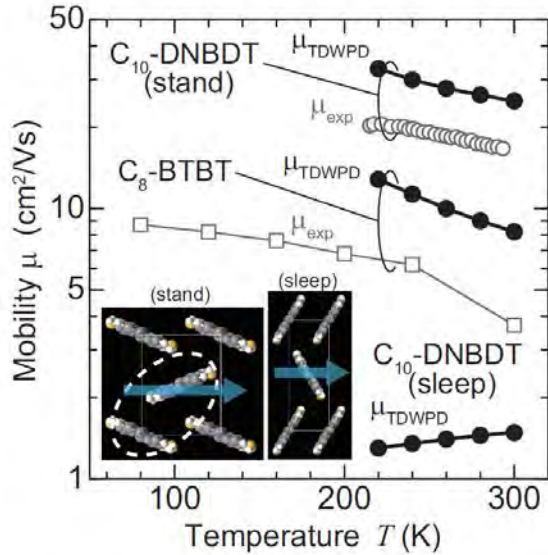


Figure 1: Mobility of C10-DNBDT (sleep), C10-DNBDT(stand) and C8-BTBT are shown by solid circles. The two different crystal structures of the C10-DNBDT polymorphs are shown in the insets. The mobilities are calculated along the column direction shown by the arrow. The experimental data points for C10-DNBDT (stand) and C8-BTBT are shown by circles and squares.

3 NEGF method and application to thermoelectricity

We have developed an efficient numerical calculation code for the ab-initio electron transport based on the DFT and NEGF formalism. We have applied the method to analyses of thermoelectricity of magnetic semiconductors.

Thermoelectric materials have attracted considerable attention from viewpoints not only of materials science but also of applications for energy harvesting by waste heat, and intensive works have been devoted to enhance conversion efficiency from thermal energy into electricity. The efficiency is expressed as a function of the figure of merit $ZT = \sigma S^2 T / \kappa$, where σ , S , κ and T are the electrical conductivity, the Seebeck coefficient, the thermal conductivity and the temperature, respectively, and the thermoelectric power factor is written as σS^2 . Enhancement of thermoelectric efficiency is not an easy task since the Seebeck coefficient, the electrical conductivity, and the thermal conductivity are not independent of

each other. There is the trade-off between σ and S , and materials with high electric conductivity tend to have high thermal conductivity.

We analyze the thermoelectric properties of a magnetic semiconductor by NEGF-DFT. The electronic transport properties, Seebeck coefficient, and the figures of merit are estimated for doped systems and thin films. We theoretically demonstrate the enhancement in the figure of merit by doping, which is in agreement with experimental work, and show further enhancement by the optimized doping.[4, 5]

References

- [1] N. Kobayashi, H. Ishii, K. Hirose, Jpn. J. Appl. Phys. 57, 08NA01 (2018).
- [2] N. Kobayashi, H. Ishii, K. Hirose, in *3D Local Structure and Functionality Design of Materials* eds H. Daimon, Y. C. Sasaki (World Scientific, 2018) p133.
- [3] H. Ishii, J. Inoue, N. Kobayashi, K. Hirose, Phys. Rev. B 98, 235422 (2018).
- [4] H.Takaki, K.Kobayashi, M.Shimono, N.Kobayashi, K.Hirose, N.Tsujii, T.Mori, Materials Today Physics 3 85e92 (2017).
- [5] H.Takaki, K.Kobayashi, M.Shimono, N.Kobayashi, K.Hirose, N.Tsujii, T.Mori, Jpn. J. Appl. Phys. (2019) in press.

van der Waals density functional theory study of molecular adsorption on metal surfaces

Ikutaro HAMADA

*Department of Precision Science and Technology, Graduate School of Engineering,
Osaka University, 2-1 Yamada-Oka, Suita, Osaka 565-0871*

Molecular adsorption on the electrode surface is one of the important building blocks in diverse devices relevant to energy harvesting and storage, such as fuel cell, solar cell, and secondary battery, to name only a few. The accurate description of the molecular adsorption is challenging in the conventional density functional theory based on the local density and generalized gradient approximations (GGA), because they cannot capture the dynamic and nonlocal nature of the van der Waals interaction, crucial in the molecule-surface interaction. In this work, we use rev-vdW-DF2[1], an offspring of the van der Waals density functional (vdW-DF)[2], which has been shown to describe the molecular adsorption on solid surfaces accurately.

All the calculations were performed using STATE[3], our in-house plane-wave pseudopotential code. We used an efficient algorithm[4] of the self-consistent vdW-DF.

In this work, we studied small water clusters on a Cu(110) surface, to investigate the origin of the formation of one-dimensional water chain made from pentagon. We constructed water clusters one by one, starting from

monomer to octamer. Overall, the structures obtained with vdW-DF are similar to those obtained in previous studies using GGA with slightly larger adsorption energies. We found that the water pentamer is stable, and hexamer is slightly less stable than the pentagon based cluster (i.e., pentamer plus additional water molecule). For octamer, we found that the pentagon based structure is also stable. We concluded that the pentagon based structure is formed as a result of a delicate balance between hydrogen bonding between water molecules and the interaction between water molecule and substrate.

References

- [1] I. Hamada: Phys. Rev. B **89** (2014) 121103(R)
- [2] M. Dion et al.: Phys. Rev Lett. **92** (2014) 246401.
- [3] Y. Morikawa, H. Ishii, and K. Seki: Phys. Rev. B. **64** (2004) 041403.
- [5] J. Wu and F. Gygi: J. Chem. Phys **136** (2012) 224107.
- [6] A. Shiotari and Y. Sugimoto: Nat. Commun. **8** (2017) 14313.

Rashba effects in surface-Bi nanostructures

Yoshihiro GOHDA

*Department of Materials Science and Engineering, Tokyo Institute of Technology
J1-3, Nagatsuta-cho 4259, Midori-ku, Yokohama 226-8502, Japan*

Systems exhibiting the Rashba effect is of fundamental importance due to their characteristic spin textures. The Rashba effect is possible not only in two-dimensional surface structures, but also in one-dimensional surface nanostructures. As a possible candidate for technological applications, spin-filtering exploiting the Rashba effect is promising, which is caused by band structures with opposite spin directions at the Fermi energy for the positive and negative electron momenta with each other. Even though such a band structure is proposed using an application of the magnetic field [1], it has not been realized yet without an external magnetic field. As a constituent element of the one-dimensional nanostructure, Bi is expected to be promising because of large spin-orbit coupling coming from its large atomic number.

In this study, we investigated a new one-dimensional Rashba system, Bi-adsorbed In atomic chains, using first-principles calculations [2]. First-principles calculations were performed on the basis of density functional theory with the generalized gradient approximation by the OpenMX code [3]. One of the most stable structures in the system shows unconventional spin textures, which is the reversal of the spin polarization direction in Rashba bands. This band structure is caused by a gap-opening due to the avoided-crossing of two Rashba bands. We have confirmed using a group-theoretical analysis that four relevant Rashba bands are classified into two irreducible representations as in Fig. 1 (a). The avoided-crossing is caused by the hybridization

of two Rashba bands belonging to the same irreducible representation. The schematic representation of this hybridization is shown in Fig. 1 (b). Together with the shift of the Fermi level within the gap, our results suggest a new spin-filtering mechanism through atomic chains. In addition, our mechanism has a great advantage; previous spin-filtering mechanisms require the external magnetic field [1], whereas ours does not need the magnetic field. This feature is suitable for spintronic applications.

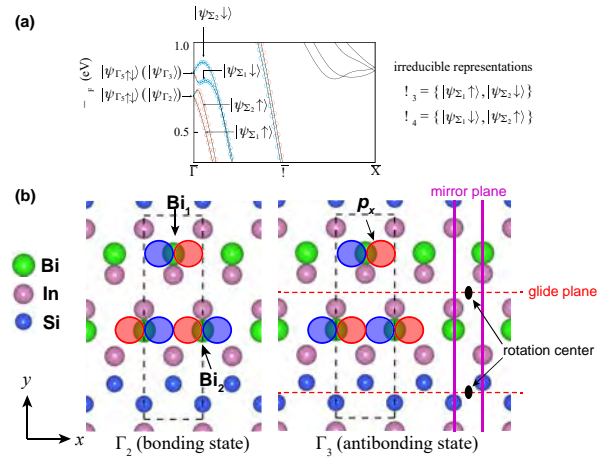


Figure 1: (a) Spin-polarization components parallel to the y axis as open circles with the band dispersion. The classification of the four Rashba bands into the irreducible representations are also shown. (b) Schematic illustrations of the hybridization together with the symmetry elements. The drawn orbitals represent p_x orbitals of Bi.

- [1] C. H. L. Quay *et al.*, Nature Phys. **6**, 336 (2010).
- [2] T. Tanaka and Y. Gohda, Phys. Rev. B **98**, 241409(R) (2018)
- [3] T. Ozaki, Phys. Rev. B. **67**, 155108 (2003).

Study on Removal Mechanism in Catalyst-Referred Etching of Single Crystalline SiC with Pure Water

Pho Van BUI, Daisetsu TOH, Kouji INAGAKI, Yoshitada MORIKAWA

Graduate School of Engineering,

Osaka University, 2-1 Yamada-oka, Suita, Osaka 565-0871

Polishing is an extremely important technique used in the finishing processes for optical and semiconductor surfaces and determines the performance of the final products. To produce a smooth surface without introducing any crystallographically damaged surface, the only pure chemical etching method is desired. Recently, catalyst-referred etching (CARE) method using Pt catalyst and water (as an etchant) has been proposed [1-3]. CARE can planarize SiC and various crystalline semiconductor materials to atomically smooth surfaces. However, the removal rate (RR) was sufficiently slow for crystalline materials (to be lower than several tens of nm/h) [4]. Our recent studies indicate that the etching via CARE is hydrolysis reaction, in which the catalyst assists water dissociation and stabilization of hypervalent states, an increasing rate of the

reaction, as seen in Fig. 1 [5].

The research is carried out to clarify the catalytic mechanism by finding new catalysts having suitable binding energy with OH using first-principles calculations.

Reaction heats for the below reaction were previously calculated over the most close-packed surface of a number of metals at a quarter monolayer coverage [6].



where H_2O and H_2 are in the gas phase and * denotes a site on the surface. The positive value means that the final state is less stable, i.e. the binding energy with OH is weak and vice versa. The results are summarized in Fig. 2.

Until now, Pt was selected as a catalyst because of its corrosion resistance and stability. However, the RR can be improved by using a new catalyst with higher catalytic activity. I have

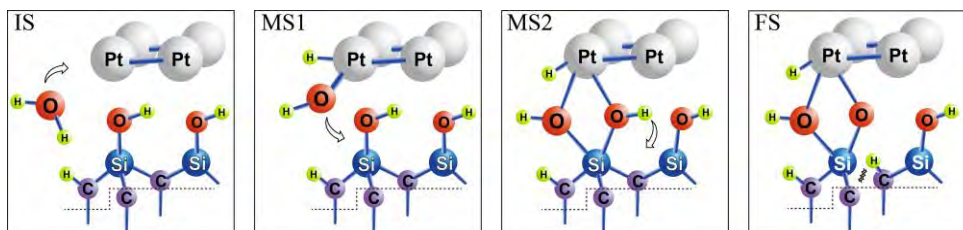


Fig. 1: Mechanistic reaction pathway of SiC in water using a Pt catalyst.

tested the performance of CARE using some catalysts and found that the RRs using a Ni and Ru are ca. 3 and 6 times higher than that using a Pt, respectively [6]. Our experimental results agreed well with the calculated results showing that Ni and Ru have higher binding energy with OH compared to Pt, promoting the water dissociation (Fig. 2).

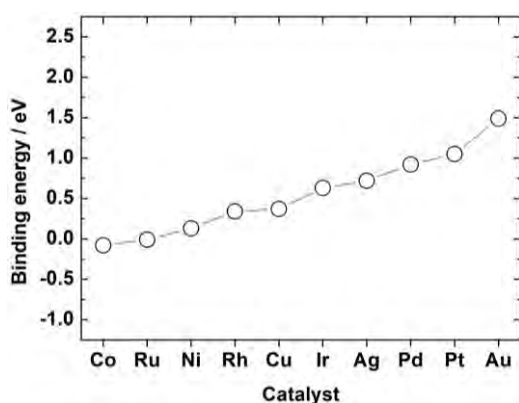


Fig. 2: M—OH binding energies on some metal surfaces.

Due to the high stability under ambient conditions and high RR, we investigate the interaction of water on the Ru surface by using massive parallel computer simulations. The adsorption energy and activation barrier of water on Ru are calculated and shown in Fig. 3.

The calculated results showed that the water dissociation capability of Ru is quite good. Additionally, we employ the Ru surface as a catalyst for SiC removal. The method and model are described elsewhere [5]. The calculated results revealed the catalytic mechanism of Ru is similar to that of a Pt catalyst.

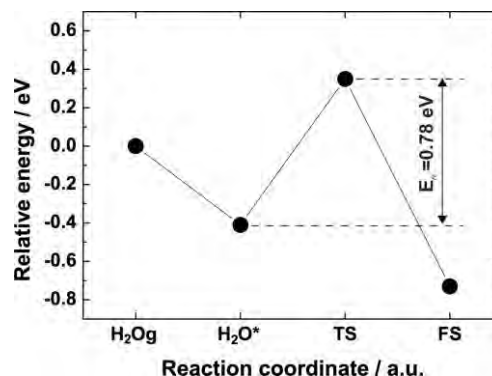


Fig. 3: Adsorption energy and activation barrier of Ru, where H₂O_g, H₂O*, TS, and FS is the isolated, molecularly adsorbed, transition and final/dissociated states.

References

- [1] H. Hara, Y. Sano, H. Murata, K. Arima, A. Kubota, K. Yagi, J. Murata, and K. Yamauchi: *J. Electron. Mater.* **35** (2006) L11.
- [2] T. Okamoto, Y. Sano, K. Tachibana, K. Arima, A. N. Hattori, K. Yagi, J. Murata, S. Sadakuni, and K. Yamauchi: *J. Nanosci. Nanotech.* **11** (2011) 2928.
- [3] H. Hara, Y. Sano, K. Arima, K. Yagi, J. Murata, A. Kubota, H. Mimura, K. Yamauchi: *J. Sci. Technol. Adv. Mater.* **8** (2007) 162.
- [4] A. Isohashi, P. V. Bui, D. Toh, S. Matsuyama, Y. Sano, K. Inagaki, Y. Morikawa, and K. Yamauchi: *Appl. Phys. Lett.* **110** (2017) 201601.
- [5] P. V. Bui, D. Toh, A. Isohashi, S. Matsuyama, K. Inagaki, Y. Sano, K. Yamauchi, and Y. Morikawa: *Jpn. J. Appl. Phys.* **57** (2018) 055703.
- [6] J. K. Nørskov, J. Rossmeisl, A. Logadottir, and L. Lindqvist: *J. Phys. Chem. B* **108** (2004) 17886.
- [7] P. V. Bui, D. Toh, S. Matsuyama, Y. Sano, K. Yamauchi: *euspen conference proceeding* (2019).

Bronsted Acidity on Oxide Surface Induced by Neutralization of Lewis Acid Sites by Molecules

Ryuhei Sato and Shu Yamaguchi

Department of Materials Engineering,

The University of Tokyo, Bunkyo-ku, Hongo, Tokyo 113-0032

Proton activity on oxide surface is paid considerable attention for the application to catalysts like sulfated zirconia for strong solid acid and Cu/ZnO for methanol synthesis. Since these catalysts utilize the reactions with local proton and electron migration, the acid-base and Red-Ox property on the surface strongly influence on their efficiency. However, in conventional methods like titration and electrophoretic measurement, acid-base property on the surface is only evaluated macroscopically without considering the difference of acidity between the sites on the surface. In addition, the mechanism about the emergence of Brønsted acidity on Lewis acid-base sites like metal and oxide ion sites on oxide surface by molecular adsorption is still unclear. Therefore, we cannot evaluate the change in acidity on the surface by the adsorption of reactants and products during reactions, which makes it difficult to design the new strong solid acid and solid base with surface modification and predict the catalytic efficiency of metal/oxide catalysts. Under such circumstance, here, we studied the adsorption of acid-base molecules and subsequent

emergence of Brønsted acidity and discuss the relationship between this Brønsted acidity and strength of adsorption to develop a new approach to evaluate pKa from adsorption energy.

Adsorption reaction of H₂O, HCOOH, CH₃OH, H₂S, CH₃SH, and HCSSH on cubic ZrO₂ (110) surface is analyzed by *ab initio* molecular dynamic (AIMD) simulation. Also, for HCOOH, CH₃OH, and H₂S adsorbed surface, subsequent hydration reaction is also analyzed. All the simulations were performed by home-made code written by F. Shimojo et al. [1]. The GGA/PBE functional and PAW method were employed with L4cpu and L36cpu queues.

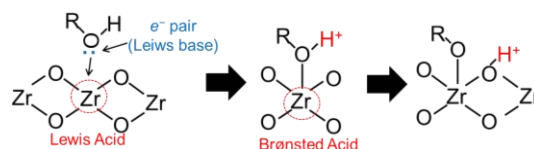


Figure 1. Schematic image of adsorption and subsequent deprotonation of acid-base molecules on ZrO₂ surface.

From the observation of adsorption reaction of these acid-base molecules, it is found that there is a common mechanism about adsorption and subsequent emergence of Brønsted acidity. That is, these molecules as a Lewis base

neutralize the metal ion sites (strong Lewis acid) by the adsorption, subsequently dissociate protons, and work as Brønsted acid (Fig. 1). Therefore, it is considered that pK_a for chemisorbed molecules could be determined from adsorption energy, since the strength of O(S)-H bond is inversely proportional to that of Zr-O(S) bond to reduce the number of atomic bonding around O(S) atom.

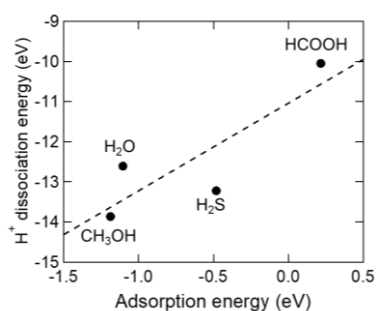


Figure 2. H⁺ dissociation energy vs adsorption energy of single molecule on ZrO₂ (110) surface calculated from the total energy difference of DFT simulation.

Figure 2 shows the relationship between H⁺ dissociation energy and adsorption energy of single acid-base molecule on bare cubic ZrO₂ (110) surface. As shown in this figure, there is a linear relationship between H⁺ dissociation energy and adsorption energy, implying that pK_a could be determined from adsorption energy. Actually this kind of pK_a evaluation is already shown in molecular system [2], where the linear relationship between pK_a for adducts of Lewis acid and Brønsted base molecules (i.e. NH₃ and H₂O) and strength of Lewis acidity of combined Lewis acid molecules is already shown from simple DFT calculation. However, the problem of pK_a estimation of adsorbate on

oxide surface is the strong solvation effect and the interaction between adsorbates. Therefore, to extract the parameter to discuss the relationship between deprotonation and adsorption property of molecules, the change in electronic states of atoms during hydration reactions of these adsorbates is analyzed. Density of states (DOS) analysis shows the electronic states of Zr ion sites do not change before and after the adsorption and H⁺ dissociation. In addition, by comparing the DOS of H atom in these molecules and that of O(S)-H bond, it is found that H atom does not have electrons and electrons are localized in O(S)-H bond. Therefore, it is considered that by analyzing the change in electronic states of O(S) atom in adsorbates and bonds around it, the deprotonation and adsorption property with solvation effect and interaction between adsorbates could be discussed. However, it is also found that the projection function to decompose the total energy into the energy of each atom has non-negligible error to discuss the chemical reaction. Therefore, to find the way to overcome this error induced by projection function will be the next challenge to develop the method to evaluate pK_a from adsorption energy.

References

- [1] F. Shimojo, R.K. Kalia, A. Nakano, P. Vashishta, *Comp. Phys. Comm.* **140** (2001) 303.
- [2] A. P. Lathem, Z. M. Heiden, *Dalton Trans.* **46** (2017) 5976.

First-Principles Molecular-Dynamics Study of Structural and Electronic Properties of Covalent Liquids and Glasses under Pressure

Fuyuki SHIMOJO, Akihide KOURA, Hiroyuki KUMAZOE, Kho UJIHARA

Institute for Solid State Physics,

Department of Physics, Kumamoto University, Kumamoto 860-8555

The investigation of the dynamic properties of molten materials under pressure is important from perspectives of geophysics as well as fundamental liquid-state science. A remarkable feature in the pressure dependence of the diffusivity of covalent liquids, such as liquid boron oxide and liquid zinc chloride, is that while the two diffusion coefficients of elements are almost the same at relatively low pressures, the difference between them increases with pressure after they exhibit a maximum [1], i.e., the dynamic asymmetry appears.

Our calculations of liquid magnesium forsterite Mg_2SiO_4 also shows a noticeable pressure dependence of the dynamic properties. Figure 1 shows the self-diffusion coefficients of elements as a function of pressure. Being different from other covalent liquids, the dynamic asymmetry is seen at pressures below 5 GPa; the three self-diffusion coefficients are largely different from each other. With increasing pressure, the self-diffusion coefficient of magnesium approaches that of oxygen, and they have almost the same values

with similar pressure dependence above approximately 15 GPa. The self-diffusion coefficient of silicon is lower than those of other elements in the whole range of pressure investigated in this study. It is important to consider the microscopic origin of this anomalous pressure dependence of the diffusivity in connection with the change from low- to high-coordinated structures.

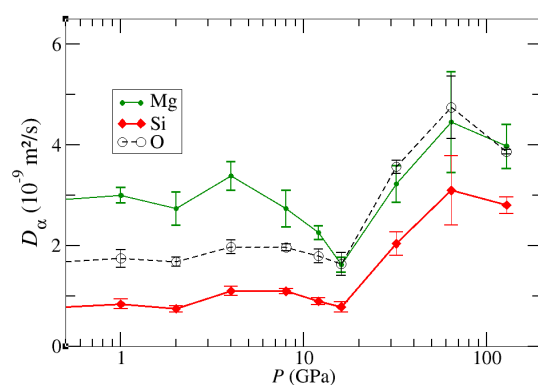


Fig. 1: Pressure dependence of self-diffusion coefficients of elements in liquid Mg_2SiO_4 .

References

- [1] A. Koura, S. Ohmura and F. Shimojo, J. Chem. Phys. **138**, 134504 (2013); A. Koura and F. Shimojo, Phys. Status Solidi B **255**, 1800103 (2018)

First principles calculations and development of graph analysis method for magnetic alloys and amorphous grain boundary phases in permanent magnets

Asako TERASAWA

*Department of Materials Science and Engineering, Tokyo Institute of Technology
J1-3, Nagatsuta-cho 4259, Midori-ku, Yokohama 226-8502, Japan*

Improvement of Nd-Fe-B magnets without heavy rare earth elements is one of the topics of increasing importance in the applied physics and materials science. The key for high-coercivity Nd-Fe-B magnets lies in the Nd-rich grain boundary (GB) phases [1]. However, the details of structural and magnetic properties of those GB phases are not clarified yet. Some experiments revealed the relationship between the crystallinity of GB phases and the relative angles between the interfaces and the *c*-plane of neighboring grains [2], which indicates the complexity of the physics in grain boundary phases in Nd-Fe-B magnets.

Considering these backgrounds, we targeted the amorphous grain boundary phase for a computational study of magnetism in Nd-based permanent magnets. The problem of amorphous grain boundary phases involves two important topics; the origin of the difference in crystallinity of grain boundary phases depending on the composition ratio and the magnetism of grain boundary phases depending on the composition ratio and the local structures.

To tackle these problems, we performed coupled analyses of structure and magnetism of Nd-Fe amorphous alloys having different composition ratios. To simulate the grain boundary phase, we created a model of amorphous Nd-Fe alloy containing 54 atoms computationally on the basis of density functional theory

(DFT). For the DFT calculations, we adopted OpenMX [3] code. For the systems created, we performed structural analyses using the Delaunay [4] and Gabriel graphs [5]. It was shown by the comparison of radial distribution functions (RDFs) that the Gabriel graphs depict the nearest neighbor networks in amorphous Nd-Fe alloys well. We also examined the 2D histogram of coordination numbers statistically from the MD simulation results, as well as the angular distribution functions between two adjacent edges in the Gabriel graphs. It was shown that the extent of short-range order becomes weak at the Nd composition ratio of 41 %, which is close to the Nd composition of amorphous grain boundary phase observed in the experiment [2]. We published these results in Journal of Chemical Physics [6].

Even though the structural properties of amorphous grain boundary phases started to unveil by such efforts, investigation of their magnetic properties is still a difficult problem, because it is difficult to determine the spin alignment of such a complicated structure. To solve this problem, we implemented the Liechtenstein formula to calculate exchange coupling constants from the output of OpenMX. We derived the explicit form of Liechtenstein formula on the non-orthogonal local orbital basis with Green's function formalism. We adopted the finite pole approximation [7] of Fermi function

for fast computation of energy integral.

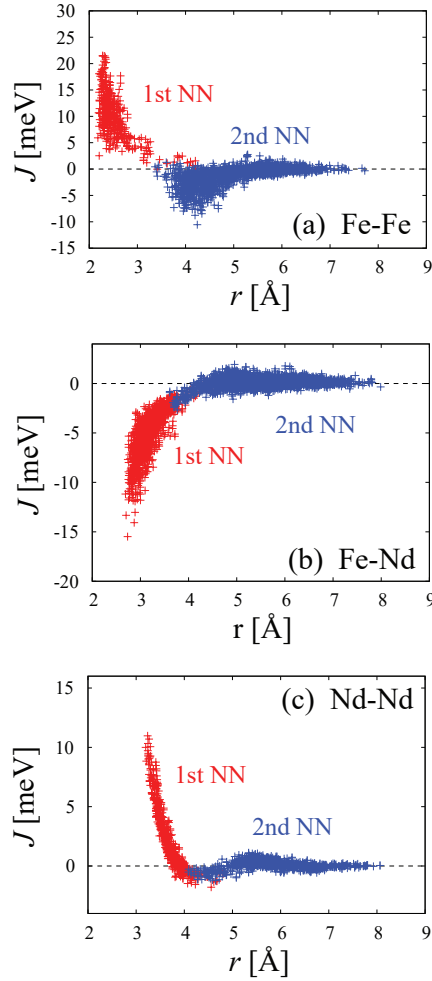


Figure 1: Exchange coupling constants in Nd-Fe amorphous alloys of Nd composition ratio at 41%, for element pair component of (a) Fe-Fe, (b) Fe-Nd, and (c) Nd-Nd. (Color online)

Using this formula, we calculated the exchange coupling constants between two atoms in the Nd-Fe amorphous using Liechtenstein method [4]. We obtained strong distance dependences and fluctuations of exchange coupling constants J_{ij} (see Fig. 1). The distance dependence curves of J deform gradually depending Nd composition ratio. These features indicate that the exchange couplings do not only depend on atomic species and distance between two atoms, but also for surrounding environment.

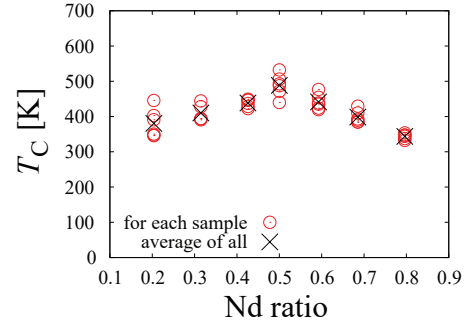


Figure 2: The Curie temperature as a function of Nd composition ratio for independent 6 samples.

It is also possible to calculate the Curie temperature from all the non-negligible J_{ij} in the whole system under the mean field approximation. Figure 2 shows the Curie temperature as a function of Nd composition ratio. As seen in Figure 2, the Curie temperature reaches maximum at around the Nd composition ratio of 50%.

Calculations and interpretations of magnetism of amorphous materials had been a big challenge for materials science for many decades, and our approach can open up a new perspective to the amorphous magnetism.

References

- [1] K. Hono *et al.*, *Scripta Mater.* **67**, 530 – 535 (2012).
- [2] T. T. Sasaki *et al.*, *Acta Mater.* **115**, 269 (2016).
- [3] T. Ozaki, *Phys. Rev. B* **67**, 155108 (2003).
- [4] B. Delaunay, *Bulletin de l'Académie des Sciences de l'URSS.* **6**, 793 – 800 (1934).
- [5] K. R. Gabriel *et al.*, *Society of Systematic Biologists*, **18**, 259 – 270 (1969).
- [6] A. Terasawa and Y. Gohda, *J. Chem. Phys.* **149**, 154502 (2018)
- [7] T. Ozaki, *Phys. Rev. B* **75**, 035123 (2007).

First-principles study on the nanoscale physics of $\text{Nd}_2\text{Fe}_{14}\text{B}$

Yasutomi TATETSU

Meio University, Biimata, Nago, Okinawa 905-8585

In 1970's, $\text{Re}_2\text{Fe}_{17}$, where Re represents rare earth elements, could be considered as permanent magnets. However, the Curie temperature ($T_c = 330\text{K}$) was not high enough for permanent magnets. B was introduced into $\text{Re}_2\text{Fe}_{17}$ by Sagawa [1], who is the inventor of Nd-Fe-B sintered magnets, in order to increase the magnetic properties, for example, magnetic moment, magnetization, Curie temperature, etc. of $\text{Re}_2\text{Fe}_{17}$. This led to creating $\text{Nd}_2\text{Fe}_{14}\text{B}$ known as the main phase of Nd-Fe-B sintered magnets. However, the role of B in $\text{Nd}_2\text{Fe}_{14}\text{B}$ was not clearly studied from nanoscale physics.

We systematically studied the effects of B in $\text{Nd}_2\text{Fe}_{14}\text{B}$ on the magnetic properties and electronic states through first-principles calculations [2]. We used OpenMX [3] mainly on System B for the present study. In order to understand how B changes the magnetic moment and magnetization of $\text{Nd}_2\text{Fe}_{14}\text{B}$, we calculated these two physical quantities of $\text{Nd}_2\text{Fe}_{14}\text{B}$, $\text{Nd}_2\text{Fe}_{14}\text{B}_0$ and $\text{Nd}_2\text{Fe}_{14}$. $\text{Nd}_2\text{Fe}_{14}\text{B}_0$ has the same lattice parameters and the atomic positions of $\text{Nd}_2\text{Fe}_{14}\text{B}$, but B is not present in it. $\text{Nd}_2\text{Fe}_{14}$ is a hypothetical material and its lattice parameters and atomic positions are optimized, therefore, these are not the same as $\text{Nd}_2\text{Fe}_{14}\text{B}$. We find that B does not increase the magnetic

moment and magnetization of $\text{Nd}_2\text{Fe}_{14}\text{B}$. We check the stability of $\text{Nd}_2\text{Fe}_{14}\text{X}$ (X = B, C, N, O, F) by comparing the formation energies of $\text{Nd}_2\text{Fe}_{17}\text{X}$. We find that the formation energies of $\text{Nd}_2\text{Fe}_{14}\text{B}$ or $\text{Nd}_2\text{Fe}_{14}\text{C}$ become negative relative to that of $\text{Nd}_2\text{Fe}_{17}\text{B}$ or $\text{Nd}_2\text{Fe}_{17}\text{C}$ (see Fig.1). Our calculation result is in good agreement with the experimental fact that $\text{Nd}_2\text{Fe}_{14}\text{B}$ and $\text{Nd}_2\text{Fe}_{14}\text{C}$ stably exist. The main role of B in $\text{Nd}_2\text{Fe}_{14}\text{B}$ is not to increase the magnetic properties but stabilizes the structure of $\text{Nd}_2\text{Fe}_{14}\text{B}$ itself.

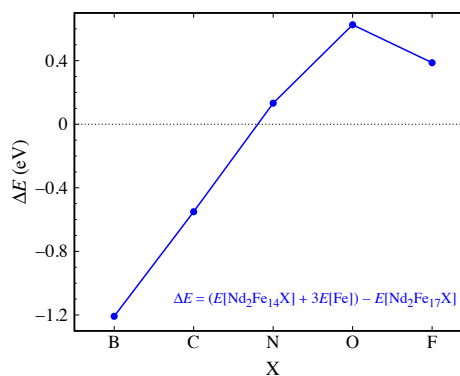


Figure 1. The formation energy of $\text{Nd}_2\text{Fe}_{14}\text{X}$.

References

- [1] M. Sagawa *et al.*, J. Appl. Phys. **55**, 2083 (1984).
- [2] Y. Tatetsu *et al.*, Phys. Rev. Mater. **2**, 0744100 (2018).
- [3] <http://www.openmx-square.org>

Development of *ab initio* many-body perturbation calculation software RESPACK and its applications to Ta₂NiS₅ and Ta₂NiSe₅

Kazuma NAKAMURA

*Quantum Physics Section, Kyushu Institute of Technology
1-1 Sensui-cho, Tobata, Kitakyushu, Fukuoka, 804-8550*

As progress of this year, I have released a new version of the software RESPACK [1] for many-body perturbation calculation and effective low-energy model derivation. RESPACK is possible to calculate the maximally localized Wannier function, response function with random phase approximation and related optical properties, and frequency-dependent electronic interaction parameters, etc, and the new version includes the GW calculation. RESPACK supports *ab initio* band calculation codes using norm conserving pseudopotentials plus plane wave basis set, and officially supports xTAPP [2] and QUANTUM ESPRESSO [3] packages. An automatic generation script from these band-calculation output to input files for RESPACK is prepared. An input file for specifying calculation conditions is designed pursuing simplicity and is given in a namelist format. RESPACK has a wide application including simple metals, semiconductors, *3d/4d* transition-metal compounds, organic and aromatic compounds, etc. It supports OpenMP/MPI and intel/GNU compiler environments. The new version also includes utility such as interfaces to model-analysis solvers mVMC [4] and $\mathcal{H}\Phi$ [5]; users can automatically obtain these inputs via RESPACK.

In this report, as a RESPACK application, I present results for an *ab initio* GW calculation of transition-metal chalcogenides Ta₂NiS₅ and Ta₂NiSe₅ which are actively studied as a

possible candidate of excitonic insulators. Using an *ab initio* GW calculation, we studied low-energy electronic structures, especially for the band gap. These materials have a layered structure stacked loosely by a weak van der Waals interaction, and in each layer, Ni single chains and Ta double chains are running along the *a* axis of the lattice to form a quasi-one-dimensional (1D) chain structure. The observed resistivity shows a semiconducting behavior over a wide temperature range with a quasi-1D anisotropic electron conduction at high temperatures. The experimental band gaps at room temperature are estimated as nearly 0.13 and 0.36 eV for the sulfide and selenide, respectively [6]. The crystal structure is body-centered orthorhombic ($a=3.415 \text{ \AA}$, $b=12.146 \text{ \AA}$, $c=15.097 \text{ \AA}$ for Ta₂NiS₅ and $a=3.496 \text{ \AA}$, $b=15.829 \text{ \AA}$, $c=15.641 \text{ \AA}$ for Ta₂NiSe₅) and contains 16 atoms in the body-centered unit cell. We calculate density functional band structure, maximally localized Wannier functions, dielectric properties, and GW spectral functions to understand the low-energy properties of these compounds.

Density-functional calculations were performed with xTAPP with plane-wave basis sets, where we employed norm-conserving pseudopotentials and the generalized gradient approximation (GGA) for the exchange-correlation potential. Maximally localized Wannier functions were used for the interpola-

tion of the self-energy. The experimental structure obtained by an X-ray measurement at room temperature was adopted in the calculations [6]. The cutoff energies in the wave function and the charge densities are 196 and 784 Ry, respectively, and a $7 \times 7 \times 3$ k-point sampling was employed. The cutoff for the polarization function was set to 4 Ry, and 100 bands were considered. Nickel pseudopotential was constructed under the semicore configuration $(3s)^2(3p)^6(3d)^9$ by employing the cutoff radius 0.8 bohr. It should be noted that in the GW calculation of 3d transition-metal compounds, it is very important in quantitative accuracy to use a pseudopotential parametrized for the semicore configuration.

Figure 1(a) compare the calculated GW spectral function with the density-functional GGA bands (white solid curve) of Ta_2NiS_5 . The GW spectra give clear gap in contrast to the GGA ones being the metallic band structure. We also show in Fig. 1(b) the comparison of the GW (green curve) with GGA (red curve) density of states. The GW gap is estimated as nearly 2 eV.

Figure 2 displays the results of Ta_2NiSe_5 . The view of the figure is the same as that of Fig. 1. Our calculated GGA band structure is in a good agreement with the past results [7]. The GW band gap is near 1 eV and appreciably smaller than the sulfide. In the case of insulators, it would be necessary to solve the Bethe-Salpeter equation for a more quantitative argument for the band gap, which is an important issue for the future study.

For code developments of RESPACK, I acknowledge Yoshihide Yoshimoto, Yoshiro No-hara, Yusuke Nomura, Terumasa Tadano, Mitsuaki Kawamura, and Maxime Charlebois. For making interface with mVMC and $\mathcal{H}\Phi$, I thank to Takahiro Misawa, Kazuyoshi Yoshimi, and Yuichi Motoyama. I also thank to Shinji Watanabe for useful discussions about transition-metal chalcogenide.

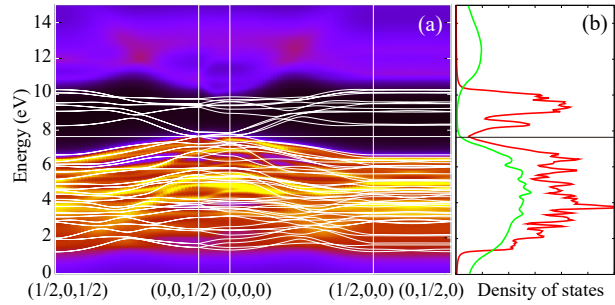


Figure 1: (Color online) (a) Calculated GW spectral function of Ta_2NiS_5 , where the GGA bands are superposed with white solid curves. (b) Comparison between the GW (green) and GGA (red) density of states.

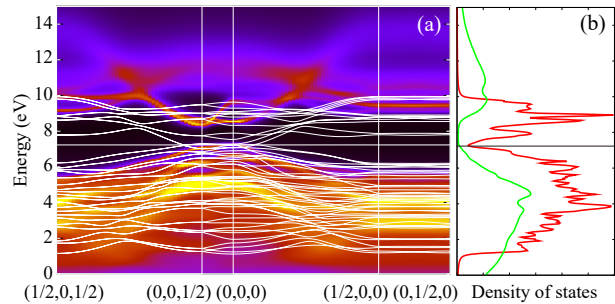


Figure 2: (Color online) (a) Calculated GW spectral function of Ta_2NiSe_5 , where the GGA bands are superposed with white solid curves. (b) Comparison between the GW (green) and GGA (red) density of states.

References

- [1] <https://sites.google.com/view/kazuma7k6r>
- [2] <http://xtapp.cp.is.s.u-tokyo.ac.jp/>
- [3] <http://www.quantum-espresso.org/>
- [4] <https://github.com/issp-center-dev/mVMC>
- [5] <http://issp-center-dev.github.io/HPhi/index.html>
- [6] S. A. Sunshine, J. A. Ibers, *Inorg. Chem.*, **24**, 3611 (1985).
- [7] T. Kaneko, T. Toriyama, T. Konishi, Y. Ohta1, *Phys. Rev. B* **87**, 035121 (2013).

Analysis of Thermoelectric Properties of Clathrate Compounds with Ab Initio Calculations

Masato OHNISHI

Department of Mechanical Engineering, The University of Tokyo

7-3-1 Hongo, Bunkyo, 113-8656

Clathrate compounds are promising candidates for thermoelectric materials in terms of the “electron-crystal phonon-glass” concept. Because of strong anharmonic potential of guest atoms in cage structures of type-I clathrates, guest phonon modes lead to strong phonon scattering. Recently, first-principles simulations of phonon properties of a clathrate have been first demonstrated with using self-consistent phonon (SCP) theory that can include temperature-dependent 4th-order anharmonic interatomic force constants (IFCs) into harmonic IFCs [1]. In this study, we reveal unusual anharmonic effects of phonons by comparing phonon properties of type-I $\text{Ba}_8\text{Ga}_{16}\text{X}_{30}$ ($\text{X} = \text{Si}, \text{Ge}, \text{Sn}$; BGX) as shown in Fig. 1 with first-principles simulations. Figure 2 shows that imaginary (negative) frequencies appeared without including the anharmonicity can be rifted up to positive values with using the SCP method. We have succeeded, for the first time, to calculate temperature-dependent thermal conductivities of BGSn with first-principles approach, which has the minimum thermal conductivity among the reported values of clathrates. Because the selection of atoms composing cage structures, namely Si, Ge, or Sn, manipulates strength of the anharmonicity, we have clearly observed effects of anharmonicity of phonons in clathrates. For example, we have observed an unusual effect of grain boundaries on phonon transport in BGSn; polycrystallization

decreases a thermal conductivity of BGSn more at higher temperature.

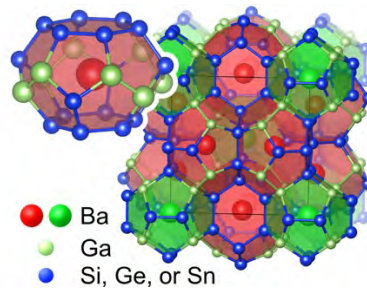


Fig. 1. Type-I $\text{Ba}_8\text{Ga}_{16}\text{Sn}_{30}$ clathrate.

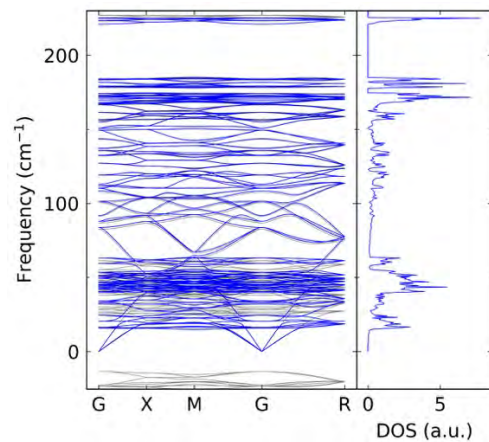


Fig. 2. Phonon dispersion and density of states of type-I BGSn. Blue and grey lines show results, respectively, with and without considering quartic anharmonicity.

References

- [1] T. Tadano and S. Tsuneyuki, *Phys. Rev. Lett.* **120**, 105901 (2018).

Ab initio studies toward functional nanomaterials based on abundant elements

Tetsuya TAKETSUGU

Faculty of Science, Hokkaido University

N10W8, Sapporo, Hokkaido 060-0810

Ab initio studies on various nano materials are crucial to understand and design new functional materials with abundant elements for reducing costs and dependences on precious metals used in many important aspects in our daily lives and therefore toward sustainable society. Heterogeneous catalysts used in automotive gas exhausts control, water gas shifts, fuel cells, as well as combustive decomposition of ammonia rely mostly on the expensive and rare metals such as Pt, Rh, Pd, or Ru. Platinum and palladium are also used for hydrogen based energy strategies. Due to their high cost and limited amounts, to reduce or even replace these metals is emergent issues in industry. To that end, we perform density functional theoretical (DFT) computations under the periodic boundary conditions together with projector augmented wave method with VASP using ISSP supercomputers to gain chemical insights to understand the chemical mechanisms in conventional catalysts as well as to design novel catalysts with abundant elements.

Also important aspect of function of nanomaterials is in its excited states. To utilize electronically excited molecules as a functional materials, the interaction between light and matter should be studied as well as its dynamical behavior. To this end, we studied electronic excitations in real-time using SALMON, which allows us to study a direct electron dynamics and molecular dynamics following the induced electron movements under the framework of the time dependent density functional

theory solved in real-time and real-space algorithm.

Concerning the catalysis, NO and NH₃ decompositions are studied [1-3]. As a preliminary step, we mostly utilized cluster models for these reaction pathway searches. Cu, Ag, and Au are used for NO decomposition and Cu, Ni, and Ru are used for NH₃ adsorption and decompositions. The cluster calculations showed that Cu is a good candidate for abundant catalysts for these reactions. For the surface calculations, we are performing DFT calculations on surfaces under the periodic boundary conditions using VASP, using several surface faces.

On the studying excited states of a molecule, we tested real-time electron dynamics calculations using benzene molecule. We have confirmed from many test calculations that for an accurate and reliable results, a real-space mesh of 0.25 Å and time step of 1 as is required. Parallel calculations using MPI and OpenMP are also tested and it turned out that the balanced combination of these two types of parallelization gives better performance, though the balance depends on the system size, i.e., the number of electrons and atoms.

References [1] T. Iwasa, et al., *J. Phys. Chem. A*, 123, 210-217 (2019). [2] S. Kiritoshi, T. Iwasa, K. Araki, Y. Kawabata, T. Taketsugu, S. Hinokuma, and M. Machida, *RSC Advances*, 8 41491-41498 (2018). [3] S. Hinokuma, K. Araki, T. Iwasa, S. Kiritoshi, Y. Kawabata, T. Taketsugu, and M. Machida, *Catal. Commun.*, 123, 64-68 (2019).

Development of new structural search method and search for new functional materials

Masaaki GESHI

Institute for NanoScience Design,

Osaka University, Machikaneyama, Toyonaka, Osaka 560-8531

We propose an efficient structure search method by using first-principles calculation based on a random search method. What is most costly is calculation of structural optimization. Therefore, we have to reduce the number of first-principles calculations itself. To realize this, we propose a method to perform the structural optimization only on structures selected by enthalpy values calculated by one self-consistent field (SCF) calculation. To do this correctly and effectively, we propose One-Shot Enthalpy used Random Structure Searching (OSE-RSS) method.

The basic concept of the OSE-RSS method is as follows. In a potential energy surface (PES), we can consider physically true that *a certain structure near the ground state must reach the ground state except for a case that a potential energy surface is abnormal*. We cannot prove or guarantee that a certain structure reaches to the ground state after performing the structural optimization. However, the above sentence is considered true, at least physically.

The described idea is explained in Fig. 1. The enthalpy values of the randomly generated initial

structures are distributed on the enthalpy surface.

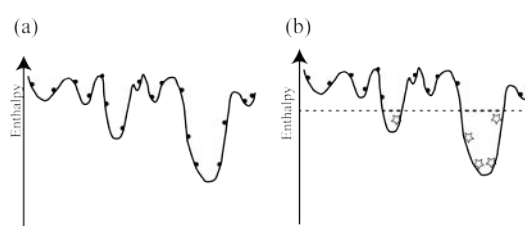


Fig.1 The concept of the OSE-RSS method. (a) The normal RSS method and (b) the OSE-RSS method. The black solid circles and open stars also mean the enthalpy of the generated initial structures. The latter is lower than a given criteria.

In the normal RSS method, all enthalpy values of the randomly generated structures are calculated after performing the full structural optimization as shown in Fig. 1(a). However, in the OSE-RSS method, the full structural optimization is performed only for the selected structures with lower enthalpy values as shown in Fig. 1(b).

This method can significantly reduce the computational cost. We apply this method to Si and H₂S and some materials, and demonstrate the usefulness of this method.

Elucidation of the surface of supported metal catalyst in an electric field

Yasushi Sekine

Sekine Laboratory, Applied Chemistry,

Waseda University, Okubo, Shinjuku, Tokyo 169-8555

We have studied ammonia synthesis using the electric field. Our findings from an earlier study suggested that proton conducting support surface promotes N_2 dissociation in the electric field [1], [2]. In general, N_2 directly dissociates into nitrogen atom over an active metal. In the electric field, however, the H^+ over support reacts with N_2 over active metals, and N_2H is formed. The novel reaction path in the electric field suggests that factors which determines ammonia synthesis rate will be different from the general ones. Therefore, we focused on the optimization of active metals for ammonia synthesis in the electric field [3].

First, the N_2H formation energies for active metals (Ru, Fe, Co, Ni, Pd, Pt) were considered using DFT calculations. We used super computer for this calculation. As a calculation package, VASP-5.4.1 was used, and various models were calculated at the same time. Results suggested that Fe and Ni are suitable for N_2H formation. Based on the findings, ammonia synthesis tests were conducted. Results revealed that, Fe and Ni based catalysts exhibited higher activity than Ru, which is the best metal for the

conventional ammonia synthesis using heterogenous catalysts. Investigating the correlation between the calculated N_2H formation energy and experimental ammonia synthesis rate, we found out the ammonia synthesis rate in the electric field is well scaled by N_2H formation energy over active metals as shown in Fig.1

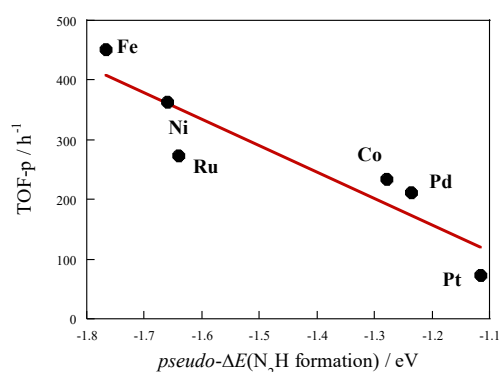


Fig. 1. Correlation between ammonia synthesis rate (TOF-p) and calculated N_2H formation energy (pseudo- $\Delta E(N_2H \text{ formation})$).

References

- [1] R. Manabe *et al*, *Chem. Sci.*, **8**, (2017) 5434-5439.
- [2] K. Murakami *et al*, *Catal. Today*, **303**, (2018) 271-275.
- [3] K. Murakami *et al*, *Catal Today*, *in press*.

Reduction of Rare Metals in Fuel Cell Catalysts and Hydrogen Permeable Membrane

Norihito Sakaguchi

*Center for Advanced Research of Energy and Materials, Faculty of Engineering,
Hokkaido University, Sapporo, Hokkaido 060-8628*

We investigated the catalyst atom adsorption and diffusion properties on non-metal element doped graphene and hydrogen dissolution and diffusion properties in the interfaces of ceramic materials, with the aid of the first principles calculation based on the density functional theory (DFT).

At first, we investigated adsorption and diffusion properties of Pt atoms on non-metal element doped graphene. This year, we focused on the surrounding gas effect on adsorption and diffusion properties of Pt atoms. In order to model the operating environment of fuel cells, we consider the H, H₂, O, O₂, OH as the surrounding gas. We performed the total energy and electronic structure calculations using The Vienna Ab initio simulation package (VASP). We installed parallelized VASP with Intel® MPI Library and Intel® Math Kernel Library. We found that the adsorption energies and diffusion activation barriers of Pt atoms on non-metal element doped graphene decrease by surrounding gas adsorption. This is because the strong covalent bonds between Pt atom and adsorbates form using electron

contributing weak covalent bonds between Pt and atoms and non-metal element doped graphene. However, In the cases of O-, Si, P-doped and monovacant graphene, the adsorption energies and diffusion activation barriers are still larger than 1 eV. Therefore, we concluded that the these dopants in graphene can prevent the detachment and surface diffusion of Pt atoms.[1]

We also investigated the hydrogen dissolution and diffusion properties in the interfaces of TiN. We found that the interface of TiN grains realizes high hydrogen permeability. We also studied hydrogen absorption properties in ceramic materials[2] and optical properties of doped ceramic materials using DFT calculations. [3]

References

- [1] S. Hasegawa, Y. Kunisada, N. Sakaguchi: ACS Omega 4 (2019) 6573.
- [2] T. Watanabe, Y. Kunisada, N. Sakaguchi: ChemPhysChem in press.
- [3] G. Saito, Y. Kunisada, T. Watanabe, X. Yi, T. Nomura, N. Sakaguchi, T. Akiyama: J. Am. Ceram. Soc. 102 (2019) 524.

***Ab initio* molecular dynamics study of static structure of glasses**

Akihide KOURA

Student Affairs Department,

Kumamoto University, Kurokami, Chuo-ku, Kumamoto, 860-8555

We have investigated the static structure of amorphous materials under pressure based on *ab initio* molecular dynamics (AIMD) simulations. In this year, we especially focused on the amorphous Mg-Zn-Y and V₂O₅ alloys.

On the V₂O₅ glass, we have focused on not only the static structure but also the diffusion mechanism, because experimental studies suggest O atoms are desorbed from the V₂O₅ glass, then the composition may become V₂O_{5-x}. However, the desorption mechanism is still unclear. In order to clarify the mechanism, AIMD simulations were carried out. In this study, the generalized gradient approximation was used for the exchange-correlation energy. The dispersion correction by Grimme and the Hubbard correction were also employed. We used a 168-atom system in a cubic supercell. At first, we obtained the bulk amorphous state by cooling from 4000 to 300 K.

In order to make the surface, the supercell size was elongated and the final configuration of the amorphous V₂O₅ was set at the center of the cell as a slab. It was expected that an O₂ molecule desorbed because an O-O bond appeared as soon as starting calculation. However, O₂ molecule desorption from the slab did not occur at 300 K. In order to enhance the desorption, the temperature of system was

increased gradually up to 1700 K, however, the slab become widely spread in whole cell as a bulk system without O₂ desorption. To avoid this change, a larger system which has enough vacuum is required.

We also studied the static structure of amorphous Mg-Zn-Y alloy. Although the main component of the alloy is Mg atoms, fragments of L1₂-type Zn₆Y₈ cluster exist in the amorphous state. These fragments contribute the stability and toughening of alloy because of the strong bonds.

In our calculation processes, F4 queue was mainly used during all calculation processes with using 96 cores. This number of cores is more useful to submit jobs comparing with using larger number of cores. When we used 384 or 576 cores to run a job using more big system, our queuing time become rather long. Therefore, in order to have enough calculation time stably, we had to choose suitable number of cores.

In this year, three studies [1-3] with using ISSP supercomputer were published.

References

- [1] A. Koura and F. Shimojo, *Phys. Status Solidi B* **255** (2018) 1800103.
- [2] S. Hosokawa, *et al.*, *J. Alloys Compd.* **762** (2018) 797.
- [3] M. Inui, *et al.*, *Phys. Rev. B* **97** (2018) 174203.

Prediction of properties of organic ferroelectrics and piezoelectrics by first-principles calculation

Shoji ISHIBASHI

*Research Center for Computational Design of Advanced Functional Materials (CD-FMat),
National Institute of Advanced Industrial Science and Technology (AIST)
Tsukuba, Ibaraki 305-8565*

Organic ferroelectrics and piezoelectrics are promising materials since they contain neither toxic nor rare elements. Recently, we observed the transition from an antiferroelectric (AFE) phase to a ferroelectric (FE) phase under a strong electric field on squaric acid (SQA) and proposed two possible FE phases (FE- α and FE- β) with their molecular arrangements and space groups [1]. The experimentally observed FE phase is thought to be the FE- α phase. On the other hand, the FE- β phase has not yet been experimentally confirmed.

In the present study, by computationally applying a static electric field [2], we simulate the AFE-to-FE transitions in SQA [3]. The calculations are performed using the computational code QMAS. As for the exchange-correlation functional, to reproduce the lattice parameters accurately, the rVV10 functional [4] is used.

Depending on the direction of the electric field, two different metastable ferroelectric (and piezoelectric) phases have been found. One of them corresponds to the experimentally confirmed FE- α phase, whereas the other corresponds to the FE- β phase. The spontaneous polarization values of the phases are 14.5 and 20.5 $\mu\text{C}/\text{cm}^2$, respectively. They are relatively high among those of the existing organic ferroelectrics. Their crystal structures are obtained as a function of the electric field. Significant converse piezoelectric effects are observed for both the phases as shown in Fig. 1 (~ 10 pm/V).

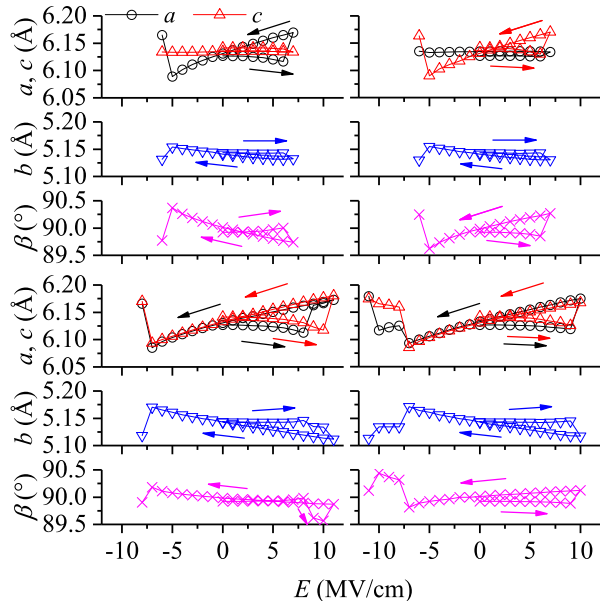


Figure 1: Variation in lattice parameters under electric field. $\mathbf{E} \parallel$ (upper left) \mathbf{x} , (upper right) \mathbf{z} , (lower left) $\mathbf{x}+\mathbf{z}$, and (lower right) $\mathbf{x}-\mathbf{z}$.

References

- [1] S. Horiuchi, R. Kumai, and S. Ishibashi: Chem. Sci. **9** (2018) 425.
- [2] I. Souza, J. Íñiguez, and D. Vanderbilt: Phys. Rev. Lett. **89** (2002) 117602.
- [3] S. Ishibashi, S. Horiuchi, and R. Kumai: Phys. Rev. B **97** (2018) 184102.
- [4] R. Sabatini, T. Gorni, and S. de Gironcoli: Phys. Rev. B **87** (2013) 041108(R).

Topological Analysis and Order Parameter of the System

Kazuto AKAGI

AIMR, Tohoku University, Katahira, Aoba-ku, Sendai, Miyagi 980-8577

We have studied nano-crystallization in highly supercooled Ti-based liquids by MD simulations and experimental measurements [1]. The growth of nano-crystals in MD trajectories can be detected by a conventional CNA (common neighbor analysis), but it was still difficult to see change in structures during the incubation period before the nucleation. This year, we introduced topological data analysis (TDA) based on persistent homology to evaluate local order in the system quantitatively.

Four systems ($\text{Ti}_{75}\text{Ni}_{25}$, $\text{Ti}_{67}\text{Ni}_{33}$, $\text{Ti}_{55}\text{Ni}_{45}$ and $\text{Ti}_{50}\text{Ni}_{50}$; 51,200 atoms) \times 25 different configurations were annealed at 3,000 K for 100 ps, cooled down to 950 K during 200 ps and held at 950 K for 3,000 ps with NPT ensemble using LAMMPS with EAM[2]. “HomCloud” package [3] was used to generate a series of alpha complex from each atomic configuration and calculate persistent homology. The system was divided into $24 \times 24 \times 24$ overlapped cells to evaluate the local order, and “HomCloud” parallelized to treat massive objects was performed on 6 nodes of System B.

The output from “HomCloud” gives the structural information on 1-dim. holes (ring structure) or 2-dim. holes (cavity) as a “persistence diagram (PD)” recording *birth* and

death timing of each hole. Since the growth of *bcc* structure was commonly observed in the PD, we performed MD calculation of a $\text{Ti}_{50}\text{Ni}_{50}$ system with *bcc* structure at 950K to prepare a reference PD. An order-parameter was designed as inner-product between a sample PD and the reference PD via appropriate vectorization. Using this order-parameter, we obtained novel findings such as “increase of *precursor* structure before nucleation” and “correlation with local potential energy (Figure)” to make further statistical analyses.

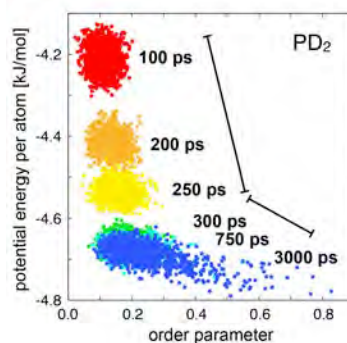


Fig. Change in ordering mode detected by TDA

References

- [1] Z. Wang, C. L. Chen, S. V. Ketov, K. Akagi, A. A. Tsarkov, Y. Ikuhara, and D. V. Louzguine-Luzgin, *Materials & Design* **156** (2018) 504.
- [2] L. Ward, A. Agrawal, K.M. Flores and W. Windl, <https://arxiv.org/abs/1209.0619>.
- [3] HomCloud, https://www.wpi-aimr.tohoku.ac.jp/hiraoka_lab/homcloud/

Developments of new materials using materials informatics

Tomoki YAMASHITA

*Research and Services Division of Materials Data and Integrated System (MaDIS),
National Institute for Materials Science (NIMS)
1-2-1 Sengen, Tsukuba, Ibaraki 305-0047*

We have developed a crystal structure prediction method based on Bayesian optimization [1] and published a crystal structure prediction tool, CrySPY as an open source software [2]. CrySPY is interfaced with VASP[3], Quantum ESPRESSO[4], soiap[5], and LAMMPS code for structure optimization. Crystal structure prediction with Bayesian optimization can efficiently select the most stable structure from a large number of candidate structures with a lower number of searching trials using a machine learning technique. In the field of crystal structure prediction, there is a very popular algorithm, evolutionary algorithm [6, 7, 8]. Evolutionary algorithm is one of the structure generation methods, while Bayesian optimization is classified into a selection-type algorithm. The key point here is that a selection-type algorithm is not exclusive with evolutionary algorithm.

First we have implemented evolutionary algorithm into our CrySPY code, and carried out test simulations using VASP, Quantum ESPRESSO, and soiap. Then we compared searching efficiency among RS, EA, and BO in the small system of Si16. In each algorithm, a hundred structures were searched. A hundred structures were selected from randomly generated five hundred structures particularly in BO. The success rates to find the most stable structure were 60%, 60%, and 50% for RS, EA, and BO, respectively. The importance of random generation is found compared with evo-

lutionary operations even in EA. RS could be the most efficient for small systems. For the system of Si32, the success rates were 40%, 70%, and 40% for RS, EA, and BO, respectively. When the system becomes complicated, the efficiency of random structure generation gets worse. EA is a better algorithm for structure generation in large systems.

References

- [1] T. Yamashita, N. Sato, H. Kino, T. Miyake, K. Tsuda, and T. Oguchi, *Phys. Rev. Materials* **2**, 013803 (2018).
- [2] <https://github.com/Tomoki-YAMASHITA/CrySPY>.
- [3] G. Kresse and J. Furthmüller, *Phys. Rev. B* **54**, 11169 (1996).
- [4] P. Giannozzi et al., *J.Phys.:Condens.Matter* **21**, 395502 (2009).
- [5] <https://github.com/nbsato/soiap>.
- [6] A. R. Oganov and C. W. Glass, *J. Chem. Phys.* **124**, art. 244704 (2006).
- [7] A. R. Oganov, A. O. Lyakhov and M. Valle, *Acc. Chem. Res.* **44**, 227 (2011).
- [8] A. O. Lyakhov, A. R. Oganov, H. T. Stokes, and Q. Zhu, *Comp. Phys. Comm.* **184**, 1172 (2013).

Development of an efficient electron-transport simulator for atomic-layered materials

Yoshiyuki EGAMI

*Division of Applied Physics, Faculty of Engineering, Hokkaido University
Kita 13, Nishi 8, Kita-ku, Sapporo, Hokkaido 060-8628*

Recently, due to the improvement of computing power and the diffusion of massively parallel computers, obstacles for performing calculations with large computational costs, such as numerical simulation of large-scale models and pursuit of computational accuracy using first-principles calculations, are reduced. However, in order to use limited computer resources effectively, it is essential to develop an algorithm with low computational costs.

In the electron-transport property calculations for nanoscale materials suspended semi-infinite electrodes, the self-energy matrices in the electrodes are required. The computational cost for obtaining the self-energy matrices are generally proportional to the cube of the electrode length of the lateral direction perpendicular to the transport direction. This prevent us to perform the transport calculations for two-dimensional systems with a large surface. So far, I developed first-principles electron-transport property simulators[1, 2, 3] based on the real-space finite-difference approach[4], and clarified the transport properties of nanoscale materials[5, 6].

In this subject, the procedure for preparing the self-energy matrices was improved to carry out the transport property calculations of a large-scale system with low calculation cost without deterioration of calculation accuracy. In the procedure, the self-energy matrices of the large electrode unit cell, where the primitive unit cell is repeated in the directions parallel to the electrode surface, can be accurately

reproduced from those of the small primitive unit cell without accuracy deterioration.

For demonstration of the proposed method, electron transport properties of a fluorinated graphene were examined, where graphene surface is terminated by fluorine atoms. We discussed the controllability of transport properties by chemical modification, and clarified the influence of the density and the structural symmetry of adatoms on the transport properties. In particular, the changes in transmission due to the difference in the structural symmetry are so small that it is difficult to observe them if the self-energy matrices cannot be calculated accurately. The procedure can accurately and efficiently evaluate such slight changes that may be buried in numerical errors. These works have been performed on System B and System C.

References

- [1] Y. Egami, K. Hirose and T. Ono: Phys. Rev. E **82**, 56706 (2010).
- [2] Y. Egami and K. Hirose: JPS Conf. Proc. **1**, 016012 (2014).
- [3] Y. Egami, S. Iwase, S. Tsukamoto, T. Ono and K. Hirose: Phys. Rev. E **92**, 033301 (2015).
- [4] K. Hirose *et al.*: *First-Principles Calculations in Real-Space Formalism*, (Imperial College Press, London, 2005).
- [5] Y. Egami and H. Akeru: Physica E **88** (2017) 212.
- [6] Y. Egami and M. Taniguchi: Jpn. J. App. Phys. **57** (2018) 021601.

Ab-initio simulations of high-order harmonic generation from crystalline solids

Yasushi SHINOHARA

Photon Science Center,

The University of Tokyo, Hongo, Bunkyo-ku, Tokyo 113-8656

State-of-the-art coherent light sources allow us to induce nonequilibrium electron dynamics beyond the perturbative regime [1]. One of the simplest phenomena in the photo-induced electron dynamics is high-order harmonic generation (HHG), photon emission peaked at multiple photon energies of driving field frequency. Intensity distribution and angle dependence of the emitted HHG spectra are expected to have information on electronic structures of materials.

We have developed an *ab-initio* theoretical framework to describe electron real-time dynamics for crystalline solids [2]. The theoretical framework is based on electronic structures derived by density-functional-theory (DFT). The DFT calculation is performed by Elk FP-LAPW code [3]. Eigenvalues and momentum operator matrix elements based on local-density approximation are taken from Elk output files. We perform real-time evolution of a quantum system with the eigenvalues and matrix elements under applied vector potential because we employ the velocity gauge for electron-light interaction. We have already applied our code to HHG from GaSe and compared it with

experimental results [2].

This year, we work on theoretical development and its application related to relaxation, and another application of our codes.

When photon energy is close to the band gap of materials, intense HHG yield above band gap is realized. Interband contribution to the yield is expected to be stronger for this situation because induced dipole due to electron-hole excitation can generate photon for this photon energy range. Fast relaxation for interband density-matrix is reported to realize well-peaked spectra on the multiple photon energies rather than a broad spectral feature. The relaxation was defined by field-free Hamiltonian. A way to introduce the relaxation depends on whether gauge we choose, the length- or the velocity-gauge, apart from the choice of the actual equation of motion. We employ a length-gauge-based-relaxation formula [4], while we use the velocity-gauge for the equation motion. This formula is derived via a gauge transformation from the length-gauge equation of motion with the relaxation term. The transformed equation motion has a physically natural interpretation that the relaxation happens only for components of instantaneous

eigenfunction meaning no-relaxation for the adiabatically evolved system. This formula is installed in our previous code. Simulations with the relaxation are performed to GaSe but higher driving photon frequency than previous investigations. In addition to the relaxation role in the HHG that peaked structure, our simulation shows fast relaxation leads to expected crystal symmetry of HHG spectra which is consistent with experimental results [4].

We apply our framework, without the relaxation, to HHG from perovskite CsPbCl₃ compared with experimental results [6]. The total yield of HHG spectra is dominated by the intraband contribution from our simulation. We perform further decomposition of the intraband contribution to each band contribution. Our results show the most prominent part is from valence top bands rather than conduction bands.

References

- [1] F. Krausz and M. Ivanov, *Rev. Mod. Phys.* **81** (2009) 163.
- [2] K. Kaneshima, Y. Shinohara, K. Takeuchi, N. Ishii, K. Imasaka, T. Kaji, S. Ashihara, K.L. Ishikawa, and J. Itatani, *Phys. Rev. Lett.* **120** (2018) 243903.
- [3] <http://elk.sourceforge.net>
- [4] Y. Shinohara, in preparation.
- [4] K. Imasaka, T. Kaji, Y. Shinohara, K.L. Ishikawa, S. Ashihara, in preparation.
- [6] Hideki Hirori, Peiyu Xia, Yasushi Shinohara, Tomohito Otobe, Yasuyuki Sanari, Hirokazu Tahara, Nobuhisa Ishi, Jiro Itatani, Kenichi L. Ishikawa, Tomoko Aharen, Masashi Ozaki, Atsushi Wakamiya, Yoshihiko Kanemitsu, *APL Materials* **7**, 041107 (2019).

Thickness dependence of strain in β -FeSi₂(100) nano-sheet

Ken HATTORI

*Graduate School of Science and Technology, Nara Institute of Science and Technology
Takayama, Ikoma, Nara 630-0192*

Using in-plane two-dimensional (2D) X-ray diffraction (XRD), author's group has been studied the strain of β -FeSi₂(100) nano-films on Si(001) [1] prepared in ultra-high vacuum. The thickness of the film was approximately 1.5 nm, corresponding three quintuple layers (QL). Here unity QL has stacking layers of Si (8 atoms in a b - c unit)/Fe (2)/Fe (2)/Si (8)/Fe (4) with a Si (8) bottom layer, as shown in Fig. 1 [2].

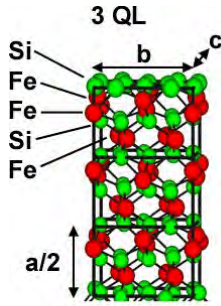


Figure 1: A model of β -FeSi₂(100) with 3 QL in thickness. 1 QL corresponds to half of lattice constant a .

Since the lattice mismatch of β -FeSi₂(100) to Si(001) is +1.4% in the b axis and +2.0% in the c axis, we expect the compressive strain of -1.4% and -2.0% of β -FeSi₂ from the bulk lattice constants b (7.791 Å in experiment) and c (7.833 Å), respectively, when the complete epitaxial growth. 2D XRD peak-fitting analyses for β -FeSi₂ diffraction spots indicated, however, that the strain were 0.0% and -0.3%, respectively. High-resolution transmission electron microscopy (HR-TEM) also showed uncompressed β -FeSi₂. This implies that the interaction of β -FeSi₂ to Si substrate is weak, and that β -FeSi₂ acts as a strain-free and free-standing nano-film. This is a quite curious behaviour of the nano film; the film is not epitaxially grown.

In addition, the XRD results also indicate anisotropic strain between b and c (0.0% and -0.3%), which implies the deformation of the rectangular unit (7.79 Å × 7.83 Å) to square-like unit (7.79 Å × 7.81 Å) in the nano film. In order to confirm the deformation behaviour, we calculated strain of free-standing β -FeSi₂(100) as a function of thickness using Simulation Tool for Atom TEchnology (STATE)-Senri [3] under the super computing system in the institute for solid state physics.

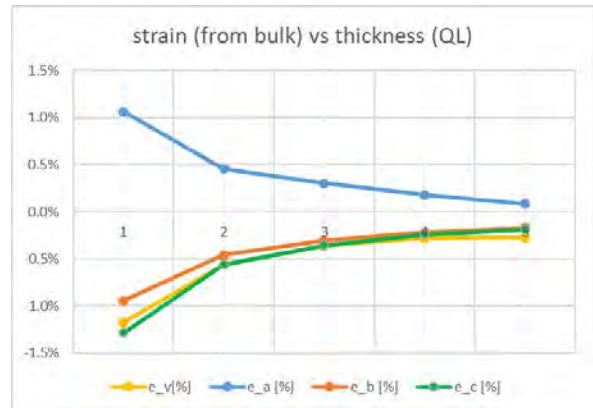


Figure 2: Strain of a (blue), b (brown), c (green) axes, and volume (yellow) from the bulk values in the free-standing β -FeSi₂(100), as a function of thickness (QL unit).

The models with 1, 2, 3, 4, and 5 QLs have total 32, 56, 80, 104, and 128 atoms with slabs of 5.0, 10.0, 14.9, 19.9, and 24.8 Å and vacuums of 5.6, 11.2, 16.9, 22.5, and 28.2 Å, respectively. The $4 \times 4 \times 1$ k-point mesh was used. The total energy was calculated as a function of in-plane lattice constants b and c , where the bottom Si atoms were fixed to positions proportional to the calculated bulk positions. The strain in b and c directions, and also a direction from

the bulk values were estimated from the lattice constants satisfying the energy minimum.

Figure 2 shows the strain of a , b , and c axes as a function of thickness. The strain of b and c decrease and of a increase with decreasing thickness. This implies shrinking in-plane lattice constants and expanding out-of-plane lattice constant in the complete free-standing nano-films. In addition, we notice that strain of c is more compressed than strain of b . This tendency supports our XRD results

The authors thank Profs. Morikawa, Hamada, and Inagaki in Osaka University, and Prof. Yanagisawa in Ryukyu University for their great support in STATE-Senri calculations.

References

- [1] S. Takemoto, K. Hattori, et al., (unpublished).
- [2] O. Romanyuk, K. Hattori, M. Someta, and H. Daimon, Phys. Rev. B **90** (2014) 155305.
- [3] Y. Morikawa, Phys. Rev. B **63** (2001) 033405, and references therein.

Theoretical Study of Industrial Enzyme and Drug Target Protein using the Forth Revolution

Yuta Yamamoto¹, Shogo Nakano², Vladimir Sladek and Hiroaki Tokiwa¹

¹*Rikkyo University, 3-34-1 Nishi-Ikebukuro, Toshima, Tokyo 171-8501*

²*University of Shizuoka, 52-1 Yada, Suruga-ku, Shizuoka 422-8526*

In order to improve stability and bioactivity of the target industrial enzyme, we could rationally design artificial enzyme proteins based on the expansion of protein sequence databases, such as full-consensus design (FCD) and ancestral-sequence reconstruction (ASR). Artificial enzyme with enhanced activity levels compared with native ones can potentially be generated by such methods, but successful design is rare because preparing a sequence library by curating the database and selecting a method is difficult. Utilizing a curated library prepared by reducing conservation energies, we successfully designed several artificial l-threonine 3-dehydrogenases (SDR-TDH) with higher activity levels than native SDR-TDH, FcTDH-N1, and AncTDH, using FCD and ASR, respectively.[1] Structural molecular dynamics (MD) simulations and *ab initio* quantum chemical calculations using the fragment molecular orbital (FMO) method for the SDR-TDHs systems revealed that only the flexibility at specific regions was changed, suggesting that multiple mutations introduced in the artificial SDR-TDHs altered their flexibility and thereby

affected their enzymatic properties. Benchmark analysis of the SDR-TDHs indicated that both FCD and ASR can generate highly functional proteins if a curated library is prepared appropriately.

We, furthermore, develop the 3D-visualization of interaction energies in protein system (3D-VIEP) method; the toolkit AnalysisFMO, which should enable a more efficient and convenient workflow with FMO data generated by quantum-chemical packages such as GAMESS, PAICS, and ABINIT-MP programs for the theoretical evaluation of activity of a pharmaceutical candidate complied with certain expectations. [2]

Reference

- [1] S. Nakano, T. Motoyama, Y. Miyashita, Y. Ishizuka, N. Matsuo, H. Tokiwa, S. Shinoda, Y. Asano, S. Ito, *Biochemistry*, **57(26)**, 3722-3732 (2018) DOI: 10.1021/acs.biochem.8b0033.
- [2] T. Tokiwa, S. Nakano, Y. Yamamoto, T. Ishikawa, S. Ito, V. Sladek, K. Fukuzawa, Y. Mochizuki, H. Tokiwa, F. Misaizu, Y. Shigeta, *J. Chem. Inf. Model.*, **59 (1)**, 25–30 (2019) DOI: 10.1021/acs.jcim.8b00649.

Theoretical Design of Energy Harvesting and Storage Device Materials by First-Principles Calculations

Hiroyoshi MOMIDA, Motoyuki HAMAGUCHI, Hiroshi KATSUMOTO

Institute of Scientific and Industrial Research, Osaka University

8-1 Mihogaoka, Ibaraki, Osaka 567-0047

By using the first-principles calculations, we have investigated piezoelectric properties of wurtzite materials as the energy harvesting device materials and electrode properties of transition metal oxide materials for the lithium-ion secondary batteries as the energy storage device materials. The calculations are done using HiLAPW and Quantum Espresso codes.

Piezoelectricity of nano-structures of wurtzite materials: The wurtzite materials can have piezoelectric properties because of the lack of inversion symmetry [1]. Recently, nano-structured ZnO have been attracted great interest because of their high piezoelectric performance. In this study, we have studied the piezoelectric properties of nano-film and nano-tube structures of wurtzite ZnO by means of the first-principles calculations. In the nano-film structure of ZnO(0001), we find that the significant thickness dependence of atomic structures. The wurtzite-type atomic structures are kept for thicker films, but the flatter atomic structures are more stable for thinner films. We also perform the first-principles calculations for ZnO [0001] nano-tubes with $\{10\bar{1}0\}$ facet. The calculated result shows that the ZnO nano-tubes with small diameter can have higher piezoelectric properties compared with the bulk values.

Electrode properties of Li-ion secondary battery materials: The so-called cation-disordered rock-salt structure materials including Li_2MTiO_4 ($M =$ transition-metal elements) have been expected to be a candi-

date cathode material for future Li-ion secondary batteries [2]. Recently, it has been experimentally reported that the battery performance of $\text{Li}_2\text{MnTiO}_4$ can be improved by increasing the composition ratio of Li as to be $\text{Li}_{2+2x}\text{Mn}_{1-x}\text{Ti}_{1-x}\text{O}_4$ ($x \sim 0.2$). To clarify microscopic origin of the improvement, we have performed the first-principles calculations of $\text{Li}_{2+2x}\text{Mn}_{1-x}\text{Ti}_{1-x}\text{O}_4$ models with several excess amounts of Li (x) ranging from 0 to 0.5. From the energy analyses, we evaluate the theoretical voltage-capacity profiles of the materials, showing that the calculated voltage values are consistent with the experimental values. The calculated electronic structures show that the redox reactions of Mn are the primary mechanism for the battery reactions especially in the early discharge process, and that the redox reactions of O becomes important in the latter discharge reaction process. We have also studied material properties of SnS anode materials for Na-ion batteries [3].

References

- [1] H. Momida and T. Oguchi: Appl. Phys. Express **11** (2018) 041201/1-4.
- [2] M. Hamaguchi, H. Momida, and T. Oguchi: J. Phys. Soc. Jpn. **87** (2018) 044805/1-8.
- [3] H. Kotaka, H. Momida, A. Kitajou, S. Okada, and T. Oguchi: J. Comput. Chem. Jpn. **18** (2019) 78-83.

First-principles Thermodynamics and Statistical Mechanics Simulations of Catalytic Reactions at Solid Surfaces

T. N. PHAM, S. A. WELLA, S. E. M. PUTRA, F. MUTTAQIEN, K. INAGAKI,
Y. HAMAMOTO, I. HAMADA, and Y. MORIKAWA

*Department of Precision Science and Technology, Graduate School of Engineering,
Osaka University, 2-1 Yamada-oka Suita, Osaka 565-0871*

In this project, we have studied atomic geometries, electronic properties and chemical reactions at surfaces and interfaces, especially, we focused on etching processes of SiC in water using Pt catalysts [1], dopants in semiconductors [2], NO dissociation by hydrogen bonding on Cu(110) [3], metal-insulator transition at LaNiO₃ thin-films on SrTiO₃ substrate [4], bonding states of single-atom Pt at graphene edges [5], the origin of the change in the absorption spectra upon oxidation and reduction in Ru-complexes [6], and formic acid adsorption on Cu(111) [7]. In the present report, we discuss the enhancement of the NO dissociation by hydrogen bonding [3].

Nitric oxide (NO) emission from the exhaustive gas of combustion process has caused negative impacts on the environment, e.g, acid rain, photochemical smog, and ozone depletion. Therefore, NO reduction to harmless substances is an important task to mitigate the environmental pollution. The catalysts of expensive precious metals such as Pt, Rh, and Pd are often employed to remove NO as well as CO and unburned hydrocarbon gases simultaneously from the exhaust gas. However, the practice requires that the catalysts must be abundant, low cost, and high catalytic activity. Among various alternative materials, copper-based catalysts are very promising owing to their excellent performances for the NO reduction.

As essential steps for the NO reduction, the NO adsorption and dissociation to N and O on the copper surfaces have been intensively studied by both experiment and theory. On low-index Cu surfaces, i.e., Cu(100), Cu(110), and Cu(111), NO is molecularly adsorbed at rather low temperature followed by formations of dimeric (NO)₂ and N₂O species with further gas exposure. Recently, Shiotari and co-workers experimentally studied the NO adsorption and dissociation on the Cu(110) surface at low-coverage region using scanning tunneling microscopy (STM), reflection absorption infrared spectroscopy, and electron energy loss spectroscopy [8].

Herein we present a DFT calculation to clarify the role of water molecules and the mechanism of the hydrogen bonding induced NO dissociation on the Cu(110) surface.

The calculations were carried out by using the simulation tool for atom technology (STATE) package [9, 10]. The Vanderbilt's ultrasoft pseudopotentials were used to describe the electron-ion interactions. Wave functions and augmented charge density were expanded by a plane wave basis-set with cut-off energies of 36 and 400 Ry, respectively. In this study, we compared results obtained by the Perdew-Burke-Ernzerhof (PBE) generalized gradient approximation (GGA) exchange-correlation functional to those obtained by van der Waals density functionals (vdW-DFs),

which take into account the dispersion interaction. We used vdW-DF1, optB86b-vdW, and rev-vdW-DF2[11] functionals as implemented in the STATE code[10].

After optimizing possible initial NO/Cu(110) configurations, we obtained two types of favorable adsorption configurations: (1) an upright NO in which N binds to the surface (N^*O) and (2) a side-on NO connecting two short-bridge sites (N^*O^*) along [001] direction. The van der Waals corrected functionals such as rev-vdW-DF2 and optB86b-vdW successfully reproduce the side-on configuration of adsorbed NO, which is an important precursor for the NO dissociation. The NO dissociation without water requires an activation energy of 0.76 eV. We find that hydrogen bonds efficiently reduce the activation energy of NO dissociation down to 0.34 eV and 0.27 eV with a water dimer and two water dimers near N^*O^* , respectively. Our study reveals the promotion effect of the water molecules is only dominant when one of the water molecules in a water dimer donates a hydrogen bond to O of side-on NO (see Fig. reffig:fig1. The N-O bond is weakened as the results of the enhanced back donation by the hydrogen bond between the water dimer and side-on NO. Our present results provide a physical insight of the role of hydrogen bonds from water, which may be helpful to practical applications of copper surface in NO reduction as well as the design of novel catalysts for this purpose.

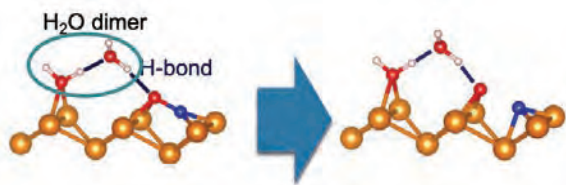


Figure 1: Hydrogen-bond enhanced N-O dissociation on Cu(110).

References

- [1] P. V. Bui, D. Toh, A. Isohashi, S. Matsuyama, K. Inagaki, Y. Sano, K. Yamauchi, and Y. Morikawa: *Jpn. J. Appl. Phys.* **57** (2018) 055703.
- [2] Y. Takano, N. Kobayashi, and Y. Morikawa: *J. Phys. Soc. Jpn.* **87** (2018) 061013.
- [3] T. N. Pham, M. Sugiyama, F. Muttaqien, S. E. M. Putra, K. Inagaki, D. N. Son, Y. Hamamoto, I. Hamada, and Y. Morikawa: *J. Phys. Chem. C* **122** (2018) 11814.
- [4] H. D. Nguyen, B. T. Cong, and Y. Morikawa: *J. Phys. Soc. Jpn.* **87** (2018) 114704.
- [5] S. A. Wella, Y. Hamamoto, Suprijadi, Y. Morikawa, and I. Hamada: *Nanoscale Adv.* **1** (2019) 1165.
- [6] S. S. Tan, S. Yanagisawa, K. Inagaki, M. B. Kassim and Y. Morikawa: *Phys. Chem. Chem. Phys.* **21** (2019) 7973.
- [7] S. E. M. Putra, F. Muttaqien, Y. Hamamoto, K. Inagaki, I. Hamada, and Y. Morikawa: *J. Chem. Phys.* **150** (2019) 154707.
- [8] A. Shiotari, T. Mitsui, H. Okuyama, S. Hatta, T. Aruga, T. Koitaya, and J. Yoshinobu: *J. Chem. Phys.* **140** (2014) 214706.
- [9] Y. Morikawa: *Phys. Rev. B* **51** (1995) 14802.
- [10] Y. Hamamoto, I. Hamada, K. Inagaki, Y. Morikawa: *Phys. Rev. B* **93** (2016) 245440.
- [11] I. Hamada: *Phys. Rev. B* **89** (2014) 121103.

Analysis on atomic and magnetic structure in magnetic molecular complex, crystal and interface and investigation of electron correlation effect

Masao OBATA^{1,2}, Mega CHRISTIVANA², and Hasan Al RASYID²

Institute of Science and Engineering, Kanazawa University, Kanazawa, Ishikawa 920-1192

Graduate School of Natural Science and Technology, Kanazawa University, Kanazawa,

Ishikawa, 920-1192

We have investigated the weak-bound magnetic material systems such as magnetic molecular crystal and two-dimensional layered material. They have received a lot of attention due to their unique physical properties such as its magnetization and crystal structure which could be controllable by external field. However, the current density functional theory (DFT)-based first-principles approach are not suitable for investigating these material accurately due to omission of some physical interactions, e.g. van der Waals (vdW) interaction and magnetic dipole-dipole (MDI) energy. Therefore, we developed computational method to evaluate these contributions.

1) MDI energy estimation of magnetic crystal

We have developed computational approach to employ MDI energy, which is one origin of magnetic anisotropy and diamagnetic field. It may be calculated with using spatial spin density $\mathbf{m}(\mathbf{r}) = (m_x, m_y, m_z)$ obtained from DFT calculation as follows:

$$E_{\text{MDI}} = \sum_{\alpha\beta} \iint d\mathbf{r}d\mathbf{r}' m_{\alpha}(\mathbf{r})f(\mathbf{r} - \mathbf{r}')m_{\beta}(\mathbf{r}'),$$

where $f(\mathbf{r}) = \frac{1}{8c^2} \frac{r^2 \delta_{\alpha\beta} - 3r_{\alpha}r_{\beta}}{r^5}$ and c is speed of

light in Hartree unit. We applied this approach to antiferromagnetic molecular crystal (monoclinic crystal solid oxygen α phase: α -O₂). The obtained magnetic anisotropy energy of α -O₂ shows that the b -direction of monoclinic structure is the easy axis of molecular spin moment [1], supporting the experimental result.

2) Implementation and application of vdW-DF approach with non-collinear magnetism

We extended vdW-DF [2] — which is able to estimate nonlocal correlation energy without empirical parameter — to non-collinear magnetism. As a demonstration, we applied it to a triangle magnetic lattice of β -phase solid oxygen. Our method could predict crystal structure more accurately compared to a standard generalized gradient approximation.

References

- [1] M. Obata et al., AIP Adv. **8**, 10149 (2018).
- [2] M. Dion et al., Phys. Rev. Lett. **92**, 246401 (2004).

First-Principles Study on Hydrogen Adsorption and Desorption of Germanene

M. ARAIDAI^{1,2,3}, M. KUROSAWA^{2,3}, A. OHTA^{2,3}, and K. SHIRAISHI^{1,2}

¹*Institute of Materials and Systems for Sustainability,*

²*Graduate School of Engineering,*

³*Institute for Advanced Research,*

Nagoya University, Furo-cho, Chikusa-ku, Nagoya, Aichi 464-8601

Two-dimensional crystals consisting of group IV element heavier than carbon, such as silicene, germanene, and stanene, are supreme thin-film materials. They have been theoretically predicted to possess high carrier mobility and some intriguing functions such as band-gap control and topological insulator [1,2]. They have been recently synthesized on metallic substrates [3-6]. However, it has been reported that the electronic state of silicene on a metallic substrate are dramatically modified by the strong interactions with the surface atoms [7,8]. On the other hand, a hydrogenation of CaSi_2 [9] or CaGe_2 [10] crystal is one of the most promising methods to fabricate single layer Si or Ge crystal. A hydrogenated silicene (silicane) or germanene (germanane) crystal can be obtained by the hydrogenation and we can easily exfoliate the free-standing one from the crystal. In this study, we theoretically investigate whether hydrogen atoms can be desorbed from the germanane by controlling hydrogen atmosphere; that is, a free-standing germanene can be created from a germanane.

To discuss the hydrogen adsorption and desorption property of germanane, we calculate the free energies of reactant and products. The difference ΔG determines the direction of this reaction. If ΔG is negative, germanene is created. If positive, germanane is created. The free energy consists of two parts: contributions of electrons and lattice vibration. We used VASP code [11] to calculate the electronic contributions and ALAMODE code [12] to calculate the vibrational contributions.

Figure 1 shows the phase diagram for

germanene formation. The horizontal axis is temperature, and the vertical axis is hydrogen pressure. The color contour indicates ΔG . We can see that the boundary between positive and negative regions is the left upper corner of the diagram. We observe from Fig. 1 that ΔG is negative over a wide area. Therefore, germanene can be created from germanane at ordinary temperatures and pressures. On the other hand, we have found that silicene cannot be created from silicane at ordinary temperatures and pressures.

References

- [1] K. Takeda and K. Shiraishi, *Phys. Rev. B* **50**, 14916 (1994). [2] M. Ezawa, *New J. Phys.* **14**, 033003 (2013). [3] A. Fleurence, et al., *Phys. Rev. Lett.* **108**, 245501 (2012). [4] P. Vogt, et al., *Phys. Rev. Lett.* **108**, 155501 (2012). [5] L. Li, et al., *Adv. Mat.* **26**, 4820 (2014). [6] F.-F. Zhu, et al., *Nat. Mater.* **14**, 1020 (2015). [7] Z.-X. Guo, et al., *J. Phys. Soc. Jpn.* **82**, 063714 (2013). [8] M. X. Chen and M. Weinert, *Nano Lett.* **14**, 5189 (2014). [9] H. Nakano and T. Ikuno, *Appl. Phys. Rev.* **3**, 040803 (2016). [10] E. Bianco, et al., *ACS Nano* **7**, 4414 (2013). [11] G. Kresse and D. Joubert, *Phys. Rev. B* **59**, 1758 (1999). [12] T. Tadano, et al., *J. Phys.: Condens. Matter* **26**, 225402 (2014).

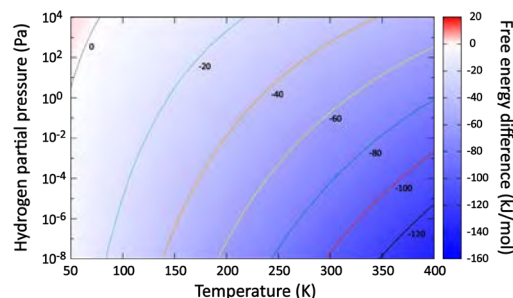


Fig. 1: Phase diagram on hydrogen adsorption and desorption of germanene.

Ab initio Molecular Dynamics Simulation of Sustained Chemical Reaction Processes in Deep-sea Hydrothermal Vents

Kohei Shimamura

Graduate School of System Informatics,

Kobe University, 1-1 Rokkodai, Nada-ku, Kobe 657-8501

We have investigated ocean impact events of meteorites during late heavy bombardment period lasting about 3.8 billion years ago by *ab initio* molecular dynamics (AIMD) simulation based on density functional theory (DFT). The impact energy and the reductive action of metallic iron contained in the meteorites would have resulted in a large amount of reductive molecules on a global scale, providing an environment that was easy to maintain life activity. We therefore have investigated the reaction processes in which reductive carbon source molecules were produced from carbon dioxides by imitating oceanic collision of the iron bearing-meteorites, where hydrocarbons and carboxylic acids were produced and their production processes were clarified in detail at the atomistic level [1].

However, it is questionable whether the impact events were directly involved in the birth of life although the events may have changed the ancient Earth's environment to reductive one. This is because the events cannot supply reductive molecules continuously. For this reason, we have focused on the alkaline

deep-sea hydrothermal vent environment. In this environment, a reducing agents such as hydrogen are constantly supplied, and a sustained chemical reaction system can be constructed on the precipitated film-like or vesicle-like iron sulfides. We have simulated this environment and have already confirmed by simulation that a carboxylic acid was produced from a carbon dioxide on the sulfide surface. However, due to the large calculation cost of AIMD, it was not possible to make the calculation system large enough to confirm the sustained chemical reaction.

In order to achieve our goal, we need to employ lower computational cost methods that can represent chemical reactions. Therefore, we attempt to solve this problem by using two methods, that is, molecular dynamics simulation using density functional tight binding (DFTB) and an empirical interatomic potential based on and artificial neural network (ANN).

Reference

[1] K. Shimamura, F. Shimojo, A. Nakano, and S. Tanaka: *J. Comp. Chem.* **40**, 349 (2019).

Modulation of phonon modes originate from impurities in GaN

Masato Oda

Department of Applied Physics,

Wakayama University, 930, Sakaedani, Wakayama, 640-8510

GaN is one of the most important materials in devices such as light-emitting diodes (LEDs) and laser diodes. However, defects in the GaN structure may result in degradation in the active regions of such devices. Yet, it remains unknown how these defects originate. Thus, we quantitatively investigated the electron-phonon interactions that occur around Ga vacancies (V_{Ga}) in GaN by carrying out first-principles calculations.

We show that, the conditions required for the phonon-kick mechanism in the neutral state [1] are also valid in the positively charged state [2]. Moreover, the defect reactions via the phonon-kick mechanism are likely to occur around V_{Ga} due to the higher-amplitude localized modes, which should cause N atoms to migrate toward the V_{Ga} and form a $N_{\text{Ga}}-V_{\text{N}}$ complex defect.

These findings are an important

contribution to our basic knowledge of the origin of defects in GaN and have practical applications in the development of light-emitting diodes and transistors that offer longer lifetimes and higher efficiencies.

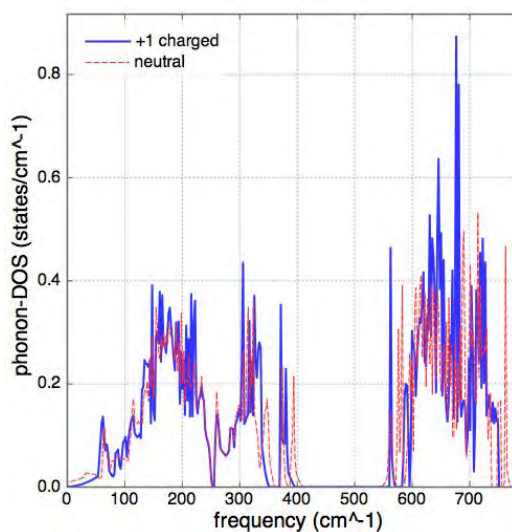


Fig. 1 Phonon DOS of V_{Ga} in GaN in the positively charged and the neutral states.

References

- [1] T. Tsujio, M. Oda, and Y. Shinozuka: *Jpn. J. Appl. Phys.* 56, 091001 (2017).
- [2] M. Oda: *Jpn. J. Appl. Phys.*, in press

Vibrational properties of crystalline organic semiconductors from first-principles

Susumu Yanagisawa

*Department of Physics and Earth Sciences, Faculty of Science, University of the Ryukyus
1 Senbaru, Nishihara, Okinawa 903-0213*

These years, impacts of the crystal geometry and configuration between neighboring molecules upon electronic properties of organic semiconductor crystals have been demonstrated[1], and the importance of accurately describing the van der Waals (vdW) interaction in molecular solids from first-principles has been realized. Thanks to the development of reliable vdW-inclusive methods, prediction of crystal geometries of organic crystals in quantitative agreement with experiments is becoming possible. The author has theoretically demonstrated subtle interplay between the crystal geometries and the intermolecular transfer integrals[2]. Description of the vdW interaction between the molecular adsorbate and the metal substrate clarified the impact of the slight molecular geometry relaxation upon the interface electronic structure[3].

First-principles calculations have been used for gaining insights into not only the electronic properties at low temperature, but also those at room temperature. However, such approaches may not be valid in case of organic crystals, whose structural configurations or conformations can be significantly fluctuated, depending on the ambient temperature. In such cases, the electron-phonon coupling effect upon the electronic band structure at finite temperature may be non-negligible[4]. In this study, to gain insights into the electron-phonon coupling and resulting modification of the crystalline band structure of organic semiconductor crystals from first-principles, we conducted

calculation of phonon dispersion of some typical organic semiconductor crystals such as naphthalene and rubrene.

To calculate the phonon dispersion, we employed the Quantum Espresso v6.3[5]. To obtain as accurate force constants and phonon frequencies as possible, we set tight convergence thresholds on total energy, force, and pressure, and for self-consistency during crystal geometry optimization. Optimized norm-conserving Vanderbilt (ONCV) pseudopotentials[6] were used, and the plane wave cutoff energy was 240 Ry. The dynamical matrices were treated within the density functional perturbation theory (DFPT)[7], as implemented in the Quantum Espresso program. The \mathbf{q} -point set within the Brillouin zone at which the second-order energy is calculated was $4\times 4\times 4$ ($2\times 2\times 2$) for naphthalene (rubrene). Throughout the calculation, a variant of the vdW density functional[8, 9, 10] was used. The lattice constants of the equilibrium structures obtained were in agreement with experiments measured at low temperature, with the mean absolute deviation from the experimental values being within 1 %. All the calculations were done on system B of the supercomputer center in ISSP, and the number of cores used in the flat MPI calculation ranged from 384 to 576.

As a test case, the phonon dispersion of crystalline naphthalene was calculated (see Figure 1). The calculated phonon dispersion curve is characterized by the phonon modes

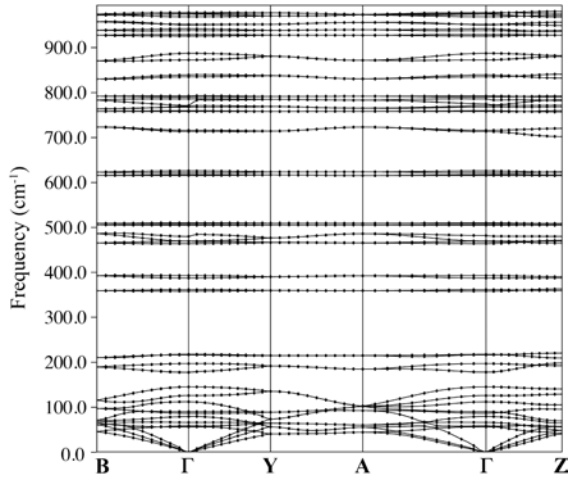


Figure 1: Calculated phonon dispersion curve of crystalline naphthalene

Table 1: Phonon frequencies at Γ point of crystalline rubrene. Units are cm^{-1} .

modes	frequency
B_{1u}	20.6 <i>i</i>
B_{3u}	20.0
B_{2u}	36.8
B_{1u}	42.8
B_{3g}	43.6
B_{1g}	45.3

whose frequencies are below 150 cm^{-1} , that are dominated by the intermolecular vibrational modes. The dispersion curve is in agreement with the previous result obtained with similar level of theory, and in fair agreement with experiments[11]. In case of rubrene, however, as shown in Table 1, one of the phonon frequencies became an imaginary frequency. The erroneously imaginary phonon frequency may come from accumulation of the numerical errors in the calculated forces. The three lowest phonon frequencies corresponding to lattice translation should be zero due to the acoustic sum rule. There may some room for improvement on the numerical treatment for imposing the acoustic sum rule[12], and further test is in progress.

The author would like to thank Ikutaro

Hamada for providing me with theoretical crystal geometries which can be used as initial geometries of the calculation and for advice on the phonon calculation.

References

- [1] J.-L. Brédas, J. P. Calbert, D. A. da Silva Filho, and J. Cornil, Proc. Natl. Acad. Sci. U. S. A. **99** (2002) 5804.
- [2] S. Yanagisawa, K. Yamauchi, T. Inaoka, T. Oguchi, and I. Hamada, Phys. Rev. B **90** (2014) 245141.
- [3] K. Yonezawa, S. Yanagisawa, and S. Kera, in preparation for publication.
- [4] S. Ciuchi, R. C. Hatch, H. Höchst, C. Faber, X. Blase, and S. Fratini, Phys. Rev. Lett. **108** (2012) 256401.
- [5] P. Giannozzi et al., J. Phys. Condens. Matter **21** (2009) 395502; P. Giannozzi et al., J. Phys. Condens. Matter **29** (2017) 465901.
- [6] D. R. Hamann, Phys. Rev. B **88** (2013) 085117.
- [7] S. Baroni, S. de Gironcoli, A. Dal Corso, and P. Giannozzi, Rev. Mod. Phys. **73** (2001) 515.
- [8] I. Hamada, Phys. Rev. B **89** (2014) 121103(R).
- [9] T. Thonhauser et al., Phys. Rev. Lett. **115** (2015) 136402; T. Thonhauser et al., Phys. Rev. B **76** (2007) 125112.
- [10] R. Sabatini et al., J. Phys.: Condens. Matter **24** (2012) 424209.
- [11] F. Brown-Altvater, T. Rangel and J. B. Neaton, Phys. Rev. B **93** (2016) 195206.
- [12] X. Gonze and C. Lee, Phys. Rev. B **55** (1997) 10355.

Magnetic properties of Fe/Pd(001) bilayer affected by quantum-well states in Pd layer

Kousuke Mochihara¹, Hiroyuki Kageshima², and Tetsuya Sato¹

1Department of Applied Physics and Physico-Informatics, Keio University, 3-14-1 Hiyoshi, Kohoku-ku, Yokohama 223-0061, Japan

2Interdisciplinary Graduate School of Science and Engineering, Shimane University, 1060 Nishikawatsu-cho, Matsue 690-8504, Japan

It is known that at interface between 3d transition metal and (Pd, Pt), strong magnetic anisotropy is generated. We found experimentally that the magnetic anisotropy and magnetic moment of Fe/Pd depend on the thickness of Pd layer [1]. In order to clarify the magnetization change, we performed first-principles calculation using the PHASE/ 0 program.

We used the pseudopotential method and LDAPW92 to the exchange and correlation interactions. A slab of vacuum (two monolayers) /Fe (three monolayers) /Pd (N monolayers) /vacuum (three monolayers), $59 \times 59 \times 1$ k-points, and 36Ry of cut-off energy were used.

We calculated lattice constant which obtains the lowest energy. Using the obtained lattice constant, we calculated Pd layer thickness dependency of the magnetic moment of Fe / Pd slab. As a result, magnetic moment of Fe/Pd changed in oscillatory manner with Pd 6 MLs period, which was in agreement with the experiment. It is known that quantum well

states formed in Pd layer changes the electronic state near the Fermi energy in a 6 MLs period [2]. The change of the electronic state based on the Pd quantum well states is considered to be the cause of the change of magnetic moment of Fe/Pd.

We also calculated the energy difference between when the magnetic moment was directed in the out-of-plane direction and when it was directed in the in-plane direction. The energy difference changed depending on Pd layer thickness. In order to investigate the mechanism, electronic band dispersions were calculated. As a result the electronic state near Fermi energy changes depending on the thickness of Pd layer. The magnetic anisotropy is considered to have changed because they depend on electronic states near the Fermi energy.

References

- [1] K. Mochihara *et al.*: ICM2018, Moscone center, San Francisco (2018)
- [2] S. Sakuragi *et al.*: Phys. Rev. B **97**, 214421 (2018)

Effects of light elements on transport properties of liquid Fe alloy under ultrahigh pressure condition : ab initio molecular-dynamics simulations

Satoshi OHMURA

Research Center for Condensed Matter Physics / Department of Environmental and Civil Engineering

Hiroshima Institute of Technology, Saeki-ku, Hiroshima, 731-5143

We have studied effects of light elements on transport properties of liquid Fe alloy under ultrahigh pressure conditions using ab initio molecular-dynamics simulations. Liquid Fe is a main component of earth's outer core. However, light element (LE) such as hydrogen, carbon, oxygen, silicon and sulfur are expected to be also present in the core. The LE are known to have a strong influence on structural and transport properties of liquid iron under high pressure. However, there are still many uncertainties as to the influence of these LE. Under this circumstance, we have performed ab initio molecular-dynamics simulations for liquid Fe with H, C, O, S and Si at various concentrations from 0 to 30 at% under high pressure. The simulation clarified that H, C and O which are relatively lighter element compared with Si and S are incorporated into the liquid interstitially while Si and S are "substitutional" -type impurities for liquid Fe. In terms of transport property, "substitutional"-type light elements such as Si

and S have more influence on electrical conductivity than "interstitial"-type light elements such as H, C and O.

In addition to liquid FeS mixture, we have investigated the structural properties of liquid S (single material). The static structures of liquid S under high pressure obtained by our simulation indicate the existence of a covalent-like interaction even in the metallic state and the covalent-like interaction gradually decreases with increasing pressure. By analyzing the static structure factor, it is found that the covalent-like interaction still remains at approximately 200 GPa, and liquid S has a simple liquid structure at 320 GPa and higher pressures. These results indicate that the covalent-like interaction disappears at a pressure between 200 and 320 GPa [1].

References

- [1] S. Ohmura and F. Shimojo, *J. Phys. Condens. Matter* **31**, (2019) 215101.

Theoretical analysis of dynamical effects of nanographene

Koichi KUSAKABE

*Graduate School of Engineering Science, Osaka University
1-3 Machikaneyama, Toyonaka, Osaka 560-8531*

1. Switching of edge states at an armchair graphene edge

Introduction of a coherent TO-phonon mode at the armchair edge can cause deformation of the atomic arrangement in the graphene. This mode induces an edge state (Fig. 1) around the Dirac point. Realization of coherent-phonon-induced edge states is within an experimentally feasible condition,[1] which are dynamically induced edge states at the a_{11} arm-chair edge different from the static edge states at a_{21} edges by chemical modification.[2]

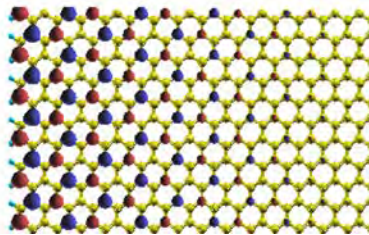


Figure 1: An armchair edge state.

2. Magnetically controlled gap at the Dirac cone in Ni/graphene/Ni

When a local Ni/graphene/Ni sandwiched structure is in the ground state having the antiparallel configuration of spin moments in the upper and lower Ni slabs, the spin-dependent potential causes gap opening of the Dirac cone by the broken chiral symmetry for each of spin components. Since switching to the parallel configuration recovers the symmetry, closed Dirac cones appear. Using this function, we proposed a magnetically controlled Dirac cone for spin-electronic applications.[3]

3. Simulation of excited TNT molecules

The electron transfer among TNT molecules can cause the weakened CH bonds as well as rotational motion of nitro groups. The explored adiabatic potential surfaces are tested for possible correlation effects when the local short-range correlation is added by the U term. Although the effect is not big, we have proposed relevance of an electron correlation effect promoting localization of catalytic electrons for the enhanced oxidative dehydrogenation promoting production of nanographene.

4. Development of simulation tools

Owing to the correlation-induced redistribution of holes in multi-layer cuprates,[4] relevance of the correlation effects for the multi-layer cuprate superconductors is shown using a TPSC approach.[5] In this respect, development of self-consistent simulation tools are under development, where a unified picture by the super processes can be a solution.[6]

Acknowledgement

This work was partly supported by KAKENHI (Nos. 16H00914 and 18K03456).

References

- [1] K. Kusakabe, *et al.* J. Phys. Soc. Jpn. **87**, 084716 (2018). [2] M. Ziatdinov, *et al.* Phys. Chem. Chem. Phys. **19**, 5145-5154 (2017). [3] Y. Wicaksono, *et al.* CARBON, **143**, 828-836 (2018). [4] K. Nishiguchi, *et al.* J. Phys. Soc. Jpn. **86**, 084707 (2017). [5] K. Nishiguchi, *et al.* Phys. Rev. B. **98**, 174508 (2018). [6] S. Teranishi, *et al.* J. Phys. Soc. Jpn. **87**, 114701 (2018).

Exploration of surface reactions on model real catalyst

Wataru MIZUKAMI

*Department of Advanced Materials Science and Engineering, Faculty of Engineering Sciences
Kyushu University, 6-1 Kasuga Park, Fukuoka, 816-8580, Japan*

This year, we studied two chemical reactions on inorganic surfaces using density functional theory (DFT) utilizing parallel computational resources of ISSP's supercomputer system: Alkylation of Ziegler–Natta catalyst; diffusion of an organic semiconductor molecule 3,4,9,10-perylene-tetracarboxylic dianhydride (PTCDA) on Ge(001) surface. We used the Vienna Ab initio Simulation Package (VASP) version 5.4.4 for DFT calculations. Transition states of those reactions were located using the nudged elastic band (NEB), climbing-image NEB and dimer method successively.

The first system, Ziegler–Natta catalyst, was based on titanium chlorides supported by MgCl_2 . It has been industrially widely used for olefin polymerization. Despite its popularity and long history, its detailed reaction mechanisms have not been fully understood yet owing to the difficulty in studying chemical reactions of inhomogeneous catalyst. We studied the alkylation process, which occurs prior to polymerization process and activates titanium chlorides on MgCl_2 surface. The reaction profiles of the process were computed for TiCl_n on $\text{MgCl}_2(100)$ surface. Our calculations validated that not a single but two alkyl aluminum molecules are involved in the alkylation process and form a transition state with a titanium chloride. Additionally, it was found that the consideration of dispersion interactions is vital to estimate reaction energies for this system; DFT calculations with dispersion corrections

indicated that the reaction is exothermic, while it is endothermic without the corrections.

Secondly, we studied the diffusion process of PTCDA on the Ge(001) surface. Organic-inorganic hybrid semiconductors have attracted attention as future electronic materials. It is, therefore, important to know the basic properties of interfaces between organic and inorganic semiconductors. PTCDA is an organic molecule and n-type organic semiconductor, while germanium is a well-known inorganic semiconductor; PTCDA on Germanium can be looked as a model system to investigate interfaces of organic-inorganic semiconductors. Recently, STM experiments observed that PTCDAs on Ge(001) take only a single configuration and they can order on a semiconductor surface at high temperatures[1, 2] The estimated activation energy was larger than 30kcal/mol. Such a high activation barrier explains why the self-ordering of chemisorbed PTCDA occurs only at high temperatures.

References

- [1] P. Kocan, Y. Yoshimoto, K. Yagyu, H. Tochiwara, T. Suzuki, *J. Chem. Phys. C* 121, 3320-3326 (2017).
- [2] P. Kocan, B. Piczyrak, L. Jurczyszyn, Y. Yoshimoto, K. Yagyu, H. Tochiwara, T. Suzuki, *Phys. Chem. Chem. Phys.* *in press.*

van der Waals density functional study of organic-metal interfaces

Yuji HAMAMOTO

*Department of Precision Science and Technology, Graduate School of Engineering,
Osaka University, Yamada-oka, Suita, Osaka 565-0871*

Atomic force microscopy (AFM) [1] is a powerful experimental technique that does not only to visualize the structure of molecules adsorbed on solid surfaces with high resolution, but also enables real-time imaging of chemical reactions of surface-adsorbed molecules. Recently, Shiotari and coworkers have demonstrated that a polycyclic aromatic hydrocarbon adsorbed on the copper (100) surface undergoes an unprecedented dehydrogenation reaction with mechanical stimuli from the AFM tip. While almost all the details of the reaction path have been elucidated by the AFM measurements, the molecular structure of a non-planar intermediate state remains unidentified, since the application of AFM imaging is limited to planar structures.

The purpose of the present study is to fill in the gap in the mechano-chemical reaction path using the van der Waals density functional method [3] as implemented in the STATE code [4-6]. As a starting point of the reaction path analysis, we here investigate the adsorption structures of the initial and final molecules of the reaction referred to as DAPh and DAPyr, respectively. To determine the adsorption

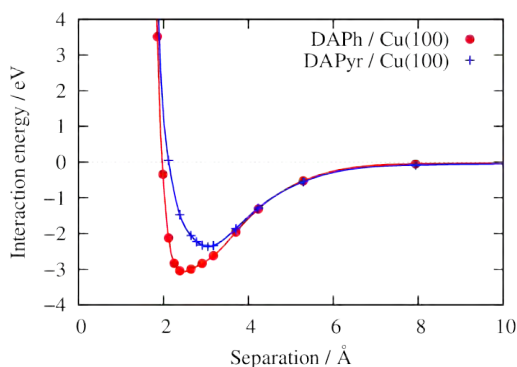


Fig. 1: Interaction energy between planar DAPh and DAPyr molecules and the Cu(100) surface.

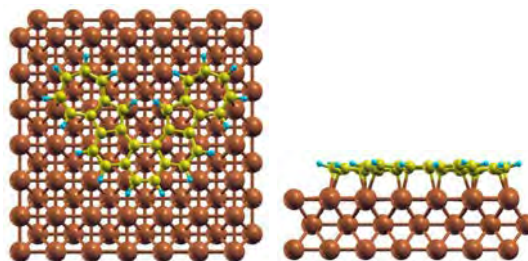


Fig. 2: Relaxed adsorption structure of a DAPh molecule on the Cu(100) surface.

structures, we first calculate interaction energies between planar DAPh and DAPyr molecules on the Cu(100) surface plotted as a function of the molecule-surface separation as shown in Fig. 1. We further relax the structure near the bottom of each energy curve, and depict the relaxed structure of e.g. DAPh/Cu(100) in Fig. 2, which reveals that the DAPh molecule is slightly

distorted and weakly chemisorbed on the surface. The analysis of the reaction path between these two adsorption structures is left to future calculations.

References

- [1] L. Gross, F. Mohn, N. Moll, P. Liljeroth, and Gerhard Meyer, *Science* **325**, 1110 (2009).
- [2] A. Shiotari, T. Nakae, K. Iwata, S. Mori, T. Okujima, H. Uno, H. Sakaguchi and Y. Sugimoto, *Nat. Commun.* **8**, 16089 (2017).
- [3] M. Dion, H. Rydberg, E. Schröder, D. C. Langreth, and B. I. Lundqvist, *Phys. Rev. Lett.* **92**, 246401 (2004).
- [4] Y. Morikawa, K. Iwata, and K. Terakura, *Appl. Surf. Sci.* **169-170**, 11 (2001).
- [5] Y. Hamamoto, K. Inagaki, I. Hamada and Y. Morikawa, *Phys. Rev. B* **93**, 245440 (2016).
- [6] S. A. Wella, H. Sawada, N. Kawaguchi, F. Muttaqien, K. Inagaki, I. Hamada, Y. Morikawa, and Y. Hamamoto, *Phys. Rev. Materials* **1**, 061001(R) (2017).

First-principles study of electronic properties of graphene layers

Yoshitaka FUJIMOTO

Department of Physics, Tokyo Institute of Technology

Oh-okayama, Meguro, Tokyo 152-8551

Graphene is an attractive sensing device material for gas sensors owing to its unique and excellent properties such as large surface-to-volume ratio, strong sensitivity, and high carrier mobility at room temperatures.

Here, we report atomic geometries, energetics, and electronic transport properties of various gas molecules including environmentally polluting and toxic gas molecules (NO, NO₂, CO, CO₂, O₂, and N₂) adsorbed on the B-doped and N-doped graphenes and examine the possibilities of sensor applications of doped graphene for detecting toxic molecules [1, 2].

Table 1 shows the adsorption energies and the distances between the doped graphene and the adsorbed molecules for various gas molecules adsorbed on the B-doped and the N-doped graphenes. For B-doped graphene, only NO and NO₂ molecules can bind chemically with short distances and large adsorption energies, while the remaining four molecules are not chemically but physically adsorbed with relatively long distances and small adsorption energies. For N-doped graphene, all six types of molecules are not chemically adsorbed. It is thus found that the B-doped graphene can chemically bind with only NO and NO₂ molecules in air.

The adsorptions of NO and NO₂ molecules could change the electrical conductances of the graphene. Therefore, the variation of the transport properties could be detected and would be utilized for sensor applications. We here examine the electron transport properties of the graphenes with and without NO and NO₂ molecules. The conductances of the undoped graphene show a linear dispersion as in the experimental observations. For the B-

Table 1: Adsorption energy E_a (eV) and distance d (Å) between molecule and B(N) atom for each gas molecules adsorbed on B(N)-doped graphene.

	B-doped		N-doped	
	E_a	d	E_a	d
NO	-1.23	2.15	-0.35	2.62
NO ₂	-1.16	1.59	-0.74	2.66
CO	-0.12	2.89	-0.14	2.94
CO ₂	-0.03	2.84	-0.11	2.73
O ₂	-0.20	1.83	-0.32	2.69
N ₂	-0.27	2.93	-0.30	2.87

doped graphene, electrons are scattered by the B-atom impurity in graphene, which reduces the conductances (~ 30 %) compared with those of pristine graphene at the energy $E = 0.5$ eV. For the NO₂ molecule adsorbed on the B-doped graphene, the conductances decrease by ~ 40 %. For the adsorption of the NO molecule on the B-doped graphene, the conductances reduce by ~ 50 %. For the energy $E = -0.5$ eV, the conductance of the B-doped graphene without any adsorbates decreases by ~ 30 % compared with that of the pristine graphene, and its reduction rate is almost the same as that at the energy $E = 0.5$ eV. The conductance for the adsorption of the NO₂ molecule decreases by above 50 %, while for the adsorption of the NO molecule, the reduction of the conductance occurs by ~ 35 %. The adsorptions of molecules could change the conductances of the graphenes, and the variation of the conductances depends on the types of the adsorbates. The variation of the con-

ductances induced by the adsorptions of NO and NO₂ molecules could be useful for sensor applications.

In summary, we have studied the adsorption effects of the various molecules including environmentally polluting gases on the B-doped and the N-doped graphenes using first-principles density-functional calculations. Only the NO and NO₂ molecules can chemically bind on the B-doped graphene. The adsorptions of NO and NO₂ molecules could change the conductances of the graphene, and the variation of such electrical signals induced by molecular adsorptions could be detected by using sensor devices such as field-effect transistors and so on.

References

- [1] Y. Fujimoto and S. Saito, Chem. Phys. **478**, 55 (2016).
- [2] Y. Fujimoto and S. Saito, Jpn. J. Appl. Phys. **58**, 015005 (2019).

Theoretical analysis of catalytic surface reaction with proton conductors

Fumiya Murase, Junichiro Otomo

*Department of Environment Systems, Graduate School of Frontier Science,
The University of Tokyo, Kashiwa-no-ha, Kashiwa, Chiba 277-8581*

Ammonia has attracted interest as an energy carrier for the storage and transport of renewable energies. Recently, electrochemical ammonia synthesis using proton conducting electrolysis cell have been studied. The rate-determining step of Ammonia synthesis were found to be N_2 dissociation. N_2 dissociation are assumed to be contributed by back-donation of electrons.

In this study, to clarify the mechanism of N_2 dissociation in electrochemical ammonia synthesis using proton conducting electrolysis cells, we investigated the effect of adsorption of N_2 on metal surfaces. We used Fe and Ru slab models as catalysts. The calculated models are shown in Fig.1. Each slab consists of 12 atomic layers and there is a vacuum region between the slabs of length over 15 Å. In the models, N_2 was far enough from metal surfaces and adsorbed on Fe (110) or Ru (1110) facets.

The calculations in this work were conducted by the density functional theory (DFT) using the Vienna ab initio simulation package (VASP) 5.3.3. [1]. Core-valence effects were included with the projector -augmented wave (PAW) method [2] with plane waves up to a cut-off energy of 500 eV.

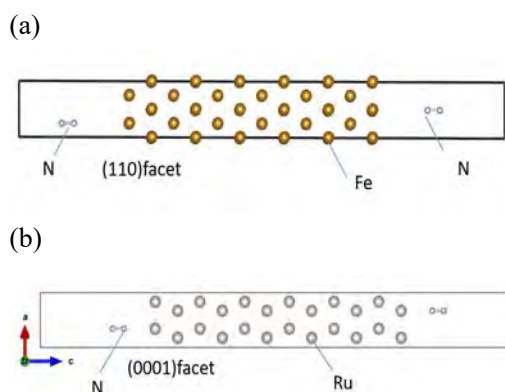


Fig. 1: Structure of calculated slab models

Partial densities of states (pDOS) were calculated to clarify the effect of N_2 adsorption on N_2 dissociation. Fig.2 shows pDOS of N_2 and Ru, and Fig.3 shows pDOS of N_2 and Fe. Both figures suggest that peaks of antibonding orbitals from N 2p broaden and small peaks appear where $E-E_f$ is under 0 eV when N_2 is adsorbed on a metal surface. The results suggest a back-donation of electrons from d-orbitals to unoccupied N 2p. It is assumed that occupied orbitals under 0 eV have an effect on N_2 dissociation.

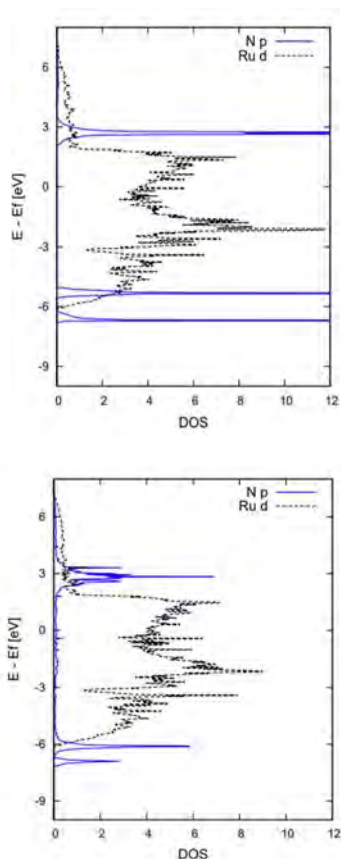


Fig.2: Partial densities of states of the N₂ and Ru (above: N₂ molecule, below: N₂ adsorbed on the on-top)

In the future plan, electric field on ammonia synthesis will be investigated. In addition, not only N₂ dissociation but also H association mechanism will be examined. Furthermore, to study the reaction path, we will use the nudged elastic band (NEB) [3].

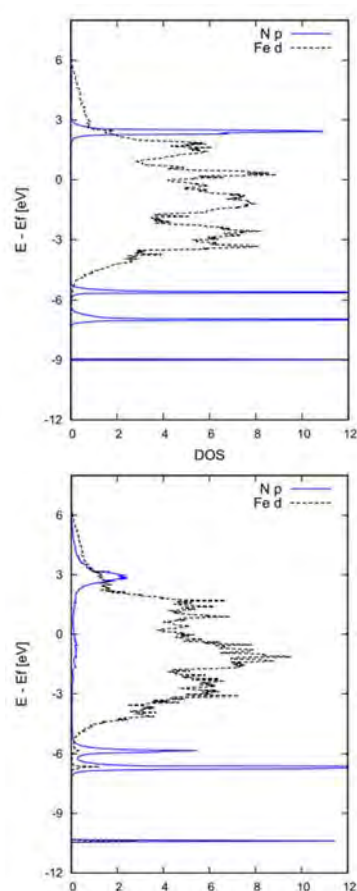


Fig.3: Partial densities of states of N₂ and Fe (above: N₂ molecule, below: N₂ adsorbed on the on-top)

References

- [1] Kresse, G. and Hafner, J.: Phys. Rev. B. **43** (1993) 558-561.
- [2] Blöchl, P.: Phys. Rev. B. **50** (1994) 17953
- [3] Henkelman, G.: J. Chem. Phys., **113** (22) (2000) 9901-99

Ab-initio Metaheuristics for Functional Design of Nanocarbon

Kenji TSURUTA, Keiichi MITANI, Kyosuke SATO, Md. Abdullah Al ASAD, and

Satoshi OHMURA^a

Graduate School of Natural Science and Technology, Okayama University, Okayama 700-8530

^a *Department of Civil and Environmental Engineering, Hiroshima Institute of Technology, Hiroshima 731-5193*

Materials design/development often requires extra-long human effort to find optimum condition for targeted properties. Recently various metaheuristic algorithms have been proposed and utilized vastly to identify optimum structures/processes in complex matters such as protein structures, drug designs, multi-element composition of functional materials, and chemical reaction processes. Many of these are based on the objectives to minimize modeled by empirical interactions and/or reaction rates. There are, however, only a few examples [1] where the methodology has been developed from first principles and applied successfully to predicting transport properties of materials.

In the present work, we have developed a metaheuristic optimization algorithm (MOA) combined with an *ab-initio* evaluation of diffusion paths and their energy barriers for an atom to migrate in a given environment [2]. Using this methodology, we searched for optimum doping conditions for inserting a lithium atom into edges of layered nanographenes. This optimization search provides computational prediction of charge/discharge performance of Li ion battery with nano-carbon based anodes.

Our combined approach consists of two data/operation streams in the computation; the MOA loop on the “master node”, and the *ab-initio* calculation task on the “*ab-initio* cluster”. We employ the genetic algorithm (GA) as a MOA and the energy barrier for the Li insertion is estimated with the Nudged Elastic Band (NEB) method with the Density-Functional-Theory (DFT). The *ab-initio* NEB calculation estimates a minimum-energy path of Li atom for a given set of parameters (species, number, and positions of dopant, the initial and the final state of Li atom insertion) selected by the MOA (GA).

In the GA search, we started with setting the parameter range as follows: Dopant species, the maximum number of dopants, the number of

substitutional sites are N, 7, 20 respectively. After eleven iterations, the energy deviation was converged within 0.2 eV. It has thus been predicted that substitutional doping of two N atoms into graphitic sites is the most optimum conditions for Li insertion, followed by two pyridinic doping as the second minimum. Figure 1 illustrates the predicted insertion path under the two graphitic doping condition. The detailed path depicted in the figure implies that Li atom is likely migrating through a window between two N dopants with an energy barrier of 0.14 eV as predicted by the NEB result [2]. A preliminary experiment for a half-cell anode of LIB indicated that the effect of N doping into nanocarbon-based anode [3] could indeed improve a rapid charging property.

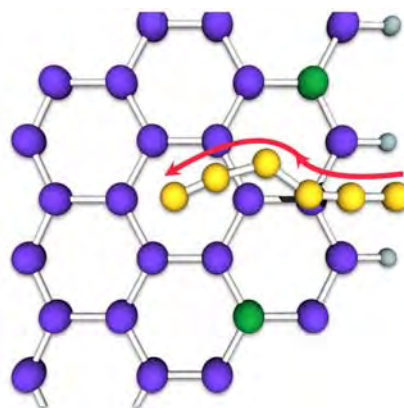


Fig. 1: The insertion path of Li in the GA predicted most optimum doping conditions.

References

- [1] A. Supady, V. Blum, and C. Baldauf, *J. Chem. Inf. Model* **55**, 2338 (2015).
- [2] K. Tsuruta, K. Mitani, Md.A.A. Asad, Y. Nishina, K. Gotoh, and A. Ishikawa, *Mater. Sci. Forum* **941**, 2356 (2018).
- [3] Y. Nishina in *Molecular Technology, Volume 4: Synthesis Innovation 2019*, p.31 (2019).

The Elucidation of Reaction Mechanism of Polyalcohol Dehydration in High Temperature Water with Metadynamics Calculations

Chang Yong Lik¹, Takehiko Sasaki¹, Motoyuki Shiga²

¹ Department of Complexity Science and Engineering, Graduate School of Frontier Sciences,

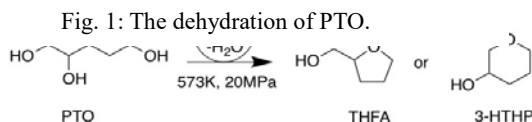
The University of Tokyo, Kashiwa-no-ha, Kashiwa, Chiba 277-8561

² Center for Computational Science and E-Systems, Japan Atomic Energy Agency

148-4 Kashiwanoha Campus, 178-4 Wakashiba, Kashiwa, Chiba, 277-0871

1 Introduction

Recently, high-temperature water (HTW) is recognized as a reaction medium in green chemistry. The dehydration reaction of 1,2,5-pentanetriol (PTO) to tetrahydrofurfuryl alcohol (THFA) and 3-hydroxytetrahydropyran (3-HTHP) in HTW with pressurized CO₂ was reported by Yamaguchi et al. [1]. In order to elucidate these reaction mechanisms we conducted Metadynamics calculations corresponding to the experimental conditions. The free energy surface (FES) analysis was carried out to study the reaction mechanism behind the dehydration



process, and compare it with the previous experimental study [1].

The dehydration reaction pathways of PTO are labeled as 5PTO2, 5PTO5, 6PTO1 and 6PTO5 as shown in Figure 2.

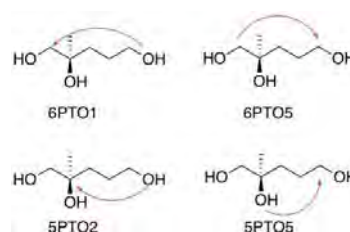


Fig. 2: The dehydration reaction pathways of PTO.

2 Method

By using PIMD[2] (Metadynamics software) developed by one of the coauthor M. Shiga associated with DFTB3 [3] or VASP [4], we analyzed the Free Energy Surfaces by Metadynamics and examined the dehydration reaction to obtain the energy barrier of the transition state from the free energy analysis and estimate the number of calculation steps and required time for the reaction to happen.

In Metadynamics, the FES of the system is sampled based on the reaction coordinates (Collective Variables: CV) of the system, then a positive Gaussian function potential was added to the actual FES to bias the reaction. The definition of CV is shown in Figure 3.

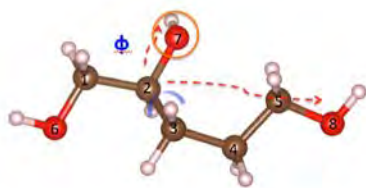


Fig. 3: The definition of CV [5PTO2]: Dihedral angle Φ (C2-O7&C3-C4), the difference in bond length r ($d=r_{28}-r_{27}$), coordination number n_2 (the number of hydrogen attached to O7).

3 RESULTS and DISCUSSION

The free energy of (R)-PTO was calculated with Metadynamics by adding a Gaussian function potential of height=100 K and width= $\{\Phi = 12.0^\circ, r = 0.20, n = 0.066\}$. 6PTO1, 6PTO5 via S_N2 yielded 3-HTHP, while 5PTO2, 5PTO5 via S_N2 yielded THFA. Typical FES results are shown in Fig. 4. The free energy of each reaction pathway was calculated with DFTB and VASP. The free energy barrier of THFA was lower than that of 3-HTHP. This is in line with the experimental results whereby THFA and 3-HTHP are the main and by-products respectively. MTD simulations have provided insights on the mechanism behind the PTO dehydration reaction. It is understood from the free energy profile obtained from MTD simulations that the proton-assisted S_N2 process is the dominant mechanism. No minima are found in the protonated region ($n \approx 2.0$) before the C-O bond exchange on the free energy profile of all reaction pathways, therefore the protonation of hydroxyl group and the C-O bond exchange has to occur in a single step.

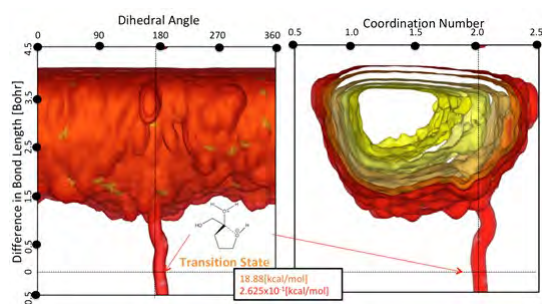


Fig. 4. Free energy surface of 5PTO2 reaction pathway

As the proton-assisted S_N2 process is seen in this study and the previous work [1] this reaction mechanism is believed to be common in polyalcohol dehydration in HTW under acidic condition. The proton is passed around in a network of hydrogen bond network between the water molecules or between the water molecules and polyalcohol. The acidity of HTW facilitates the protonation of the hydroxyl group essential for the reaction. This explains why the polyalcohol dehydration is accelerated with the presence of carbon dioxide in HTW. These results are published recently [5].

References

- [1] A. Yamaguchi, N. Hiyoshi, O. Sato, K.K. Bando, M. Shirai, *Green Chem.*, 2009, 11, 48-52.
- [2] PIMD. <https://ccse.jaea.go.jp/ja/download/pimd/index.jp.html>.
- [3] Density Functional Theory based Tight Binding. <https://www.dkb.org>.
- [4] VASP. <https://www.vasp.at/>.
- [5] Y.L. Chang, T. Sasaki, J. Ribas-Arino, M. Machida, M. Shiga, *J. Phys. Chem. B* 123 (2019) 1662.

Density functional calculations of the catalytic site of fuel cell and photocatalyst

Kazume NISHIDATE

Faculty of Science and Engineering, Iwate University

Ueda 4-3-5, Morioka, Iwate 020-8551

A proton exchange membrane fuel cell (PEMFC) is an energy device in which chemical energy is directly converted into electric energy through the oxygen reduction reaction (ORR). This reaction offers a promising technology to develop efficient and clean power sources for electric vehicles. However, the most effective catalysts currently used for the ORR are platinum group metals (PGM) and their scarcity and expensiveness have been main obstacles to large-scale commercialization. Therefore, it is very important to develop inexpensive and yet efficient non-PGM catalysts for the mass production of fuel cell devices. Meanwhile, a pioneering work [1] has been reported on the ORR activity of Fe(Co)-N₄ macrocyclic molecule adsorbed on carbon materials. Ever since this discovery, a class of Metal-Nitrogen-Carbon (M-N-C) ORR active sites have been extensively studied. Although the energetics have been analyzed in these studies, electronic structure and electron transfer dynamics during the ORR have not been clarified.

We have studied the ORR of FeN₄ embedded in graphene (Gr) and carbon nanotube (CNT) with the first-principles DFT calculations using Vienna Ab initio Simulation Package (VASP). [2] We evaluate the electron transfer between an O₂ molecule and the FeN₄ catalytic site, where O₂ was adsorbed on Fe with end-on bent geometry. Two carbon systems are considered. The first is the 5 × 5 Gr sheet which forms a 12.3 Å × 12.3 Å equilateral par-

allelogram. The second is the (10, 0) CNT which is put in a standing position on 20 Å × 20 Å square plane. The CNT unit is stacked three times in the axial direction and its dimension corresponds to 12.8 Å. The diameter of CNT is 7.9 Å. Cyclic boundary conditions are imposed on Gr as well as on CNT supercells. Throughout the calculations, an O₂ molecule is easily adsorbed on the top of the Fe with the end-on bent atomic configuration. On adsorbing hydrogen atoms, a H₂O molecule is formed and is immediately desorbed from the surface. The overall electronic configurations of the FeN₄ center in Gr during the ORR is essentially the same as those in CNT, demonstrating an universal nature of the reaction mechanism. However, we also found a difference in atomic structure in the ORR. The height of Fe on Gr increases up to 0.344 Å during the ORR while the Fe height on CNT is only 0.217 Å due to the mechanical surface tension, which also affects the energy landscape of ORR. After the ORR, the FeN₄ centers on Gr and CNT recover their initial in-plane configurations and are capable of subsequent ORR.

References

- [1] R. Jasinski: *Nature* **201** (1964) 1212.
- [2] S. Aoyama, J. Kaiwa, P. Chantngarm, S. Tanibayashi, H. Saito, M. Hasegawa, and K. Nishidate: *AIP Advances* **8** (2018) 115113 (9 pages).

Study on physical properties of structural elementary excitations of semiconductor surfaces and interfaces

Hiroyuki KAGESHIMA

*Graduate School of Natural Science and Technology, Shimane University
1060 Nishi-Kawatsucho, Matsue, Shimane 690-8504*

Our project has been focused on the physical properties of structural elementary excitations of semiconductor surface and interfaces. We have performed two topics in this year. One is physical properties of vacancies in two-dimensional material MoS₂ [1]. The other is physical properties of SiO interstitials in SiO₂ at the interface with Si [2, 3, 4]. The calculations were performed based on the first-principles calculation. Program package VASP was employed.

In the first topic, we focus on the supporting effect on vacancy formation in monolayer MoS₂. Vacancy formation is generally more suppressed for the supported cases than the freestanding case in non-negatively-charged conditions. These are the results of difference in charging of vacancies. We can thus propose that MoS₂ should be processed in the S-rich and non-negatively-charged conditions to prevent the formation of vacancies. We can also propose that the choice of supporting substrate is important to process MoS₂ to obtain better quality electronic devices.

In the second topic, we focus on the pressure effect on SiO₂ with SiO interstitials. It is known that the SiO interstitials are injected into the oxide when the Si is thermally oxidized. In addition, for the Si pillar oxidation, it is known that a large compressive pressure as high as 5 GPa is induced in oxide. We therefore study the pressure effect on the dynamical property of SiO₂ with SiO interstitials. Analyzing calculated results, we found that the Si

dynamical property is enhanced by the pressure at 3000 K, while it is slightly diminished at 6000 K. This indicates that Si dynamical property is more enhanced by the pressure at the experimental oxidation temperature such as 1000 K. We also fit the pressure dependence of Si diffusion coefficients by the Lorentz type function of pressure (at 3000 K) or parabolic function (at 6000 K). Then we evaluate the activation volume as the function of SiO density. The results show that the activation volume is negative in low SiO density, but its absolute value decreases with the SiO density. This suggests that the SiO interstitials suppress the pressure effects on Si dynamical property.

References

- [1] S. Urasaki and H. Kageshima, *Jpn. J. Appl. Phys.* **57** (2018) 125202.
- [2] Y. Yajima, K. Shiraishi, T. Endoh, and H. Kageshima, *Jpn. J. Appl. Phys.* **57** (2018) 06KD01.
- [3] Y. Yajima, K. Shiraishi, T. Endoh, and H. Kageshima, 2018 International Conference on Solid State Devices and Materials (SSDM2018), Tokyo, Japan, PS-1-04 (2018).
- [4] Y. Yajima, K. Shiraishi, T. Endoh, and H. Kageshima, 14th International Conference on Atomically Controlled Surfaces, Interfaces, and Nanostructures (ACSIN-14), Sendai, Japan, 22P118 (2018).

Ab Initio Band Structure Calculation of InSb Using VASP

Hiroki FUJISHIRO

Department of Applied Electronics,

Tokyo University of Science, Niijuku, Katsushika, Tokyo 125-8585

High electron mobility transistors (HEMTs) are one of the most promising devices for future terahertz electronics. InSb is suitable for use in the channel layer of high-speed HEMTs since InSb has the lightest electron effective mass in III-V semiconductors. However, there are no lattice-matched barrier materials for InSb channel HEMTs. As a result, InSb channel is compressively strained in HEMTs. On the other hand, Monte Carlo (MC) simulations are the powerful tool to predict performance of HEMTs. For MC simulations, accurate band parameters are strongly required. In this work, we carried out ab initio band structure calculations of unstrained and compressively strained InSb using Vienna Ab initio Simulation Package (VASP) based on the method in the local density approximation to obtain band parameters.

As for the band parameters of InSb, several papers have already been published [1, 2]. Table 1 summarizes the band parameters of InSb. In our previous work [2], we calculated the unstrained and the strained band structures of InSb by the empirical pseudopotential method.

We could not obtain the values of the band gap energy E_g . To overcome this problem, we carried out the band structure calculations of unstrained and compressively strained InSb using VASP. In Table 1, our present calculation results are also shown. We obtained the E_g of 0.34 and 0.48 eV for unstrained (0%) and compressively strained (-1.32%) InSb, respectively. The E_g value in this work is larger than that in [1]. The electron effective mass in the Γ valley m_{Γ}^* is almost same as the values in the previous papers [1, 2]. The increase in the value of m_{Γ}^* was observed for the -1.32% compressively strained InSb, which is the same as our previous result [2].

Using the obtained band structures, we'll carry out more rigorous MC simulations of InSb channel HEMTs.

References

- [1] H. Rodilla, T. González, D. Pardo, and J. Mateos: *J. Appl. Phys.* **105** (2009) 113705.
 [2] H. Nishino, Kawahira, F. Machida, S. Hara, and H. I. Fujishiro: *Proc. 22nd Int. Conf. on IPRM* (2010) p. 156.

Table 1 Several band parameters of InSb.

	0% [1]	0% (Pseudopotential) [2]	-1.32% (Pseudopotential) [2]	0% (VASP) [This work]	-1.32% (VASP) [This work]
E_g (eV)	0.18	—	—	0.34	0.48
m_{Γ}^*	0.014	0.016	0.022	0.015	0.022
m_L^*	0.22	0.18	0.18	0.052	0.051
m_X^*	0.13	0.38	0.38	0.065	0.066
$E_{\Gamma-L}$ (eV)	0.76	1.04	1.00	1.04	1.06
$E_{\Gamma-X}$ (eV)	0.46	1.57	1.48	2.64	2.69

Calculations of Phonon Properties in Oxides, and of Dielectric Functions in Halides

Takayuki MAKINO

*Department of Electric and Electronics Engineering,
University of Fukui, Bunkyo Fukui, Fukui 910-8557*

I tried the phonon calculations for oxides by using “phonopy” to obtain its dispersion and density of states. Supercells with displacements are needed to be created for the calculations of phonon dispersion and/or their density of states. Number of the created configurations is dependent on the symmetry of the relevant crystal (see, for example, Table 1). In other words, a number of *ab-initio* supercell calculations have to be executed to obtain force on atoms, though they are binary materials ($N_{\text{atom}}=2$). Due to the abovementioned situations, I have not completed the tasks. Despite this fact, I have already successfully created a force constants file for one of these oxides. The related postprocess will be performed sequentially, because this package can be executed even under Linux-based personal computers.

material	symmetry	configuration	N_{typ}	N_{atom}
A	Pnma	40	40	2
B	Pnma	40	40	2
C	Pnma	60	40	2

I also tried dielectric function calculations for halide-based mixed crystals. Because the dielectric function cannot be directly converted from the spectral distribution of the density of states, so I tried to calculate them by using “RESPACK”. I was able to finally master how to convert the self-consistent field calculation results from “Quantum ESPRESSO” to “RESPACK” formats by communicating with the staffs. The validity and comparison with our experimental data of the partially obtained results are being checked currently.

Acknowledgments

I am indebted to kind suggestions and customization of the program from the RESPACK staffs (Professor K. Nakamura *et al.*).

References

- [1] K. Nakamura *et al.*: Phys. Rev. B **74** (2006) 235113.
- [2] L. Chaput, A. Togo, I. Tanaka, and G. Hug, Phys. Rev. B, **84** (2011) 094302.

Magnetic properties of rare earth mixed crystal magnet materials

H. Akai

*Institute for Solid State Physics, University of Tokyo
Kashiwa-no-ha, Kashiwa, Chiba 277-8581*

The purpose of the present study is to develop a system that can generate permanent magnet materials databases in the multi-dimensional composition spaces by using first-principles electronic structure calculation. Given a structure and a set of components, e.g., $\text{Sm}(\text{Fe}_{1-x}\text{Co}_x)_{12}(\text{N}_{1-y}\text{S}_y)$, we typically need calculations for 100~1000 different systems. Since these systems are compositionally disordered, usual band structure calculation is not suitable for realistic simulations. An efficient way to handle this problem is to use the KKR-CPA method, which can take a configurational average of such disordered systems rather accurately. Unfortunately, the full-potential scheme is not implemented in the present version of KKR-CPA used now[1] (full-potential KKR-CPA codes exist but they do not suit the present purpose because of their heavy computational demands). On the other hand, the pseudo-potential codes can calculate the ordered system quite efficiently although their accuracy has to be checked from time to time through comparisons with the results obtained by other more reliable method such as full-potential KKR and WIEN2k. Considering the above, one of the practical ways to take is to combine KKR-CPA and pseudo-potential codes: use pseudo-potential codes for the end points (i.e., ordered alloys) of composition space and use KKR-CPA to interpolate all the remaining region of the space. A computational system “HOFMAN” constructed under such a strategy is now running.

An example of the usage of HOFMAN system is seen in Fig. 1, where a new alloy system $\text{Sm}(\text{Fe}_{1-x}\text{Co}_x)_{12}(\text{N}_{1-y}\text{S}_y)$ is examined.

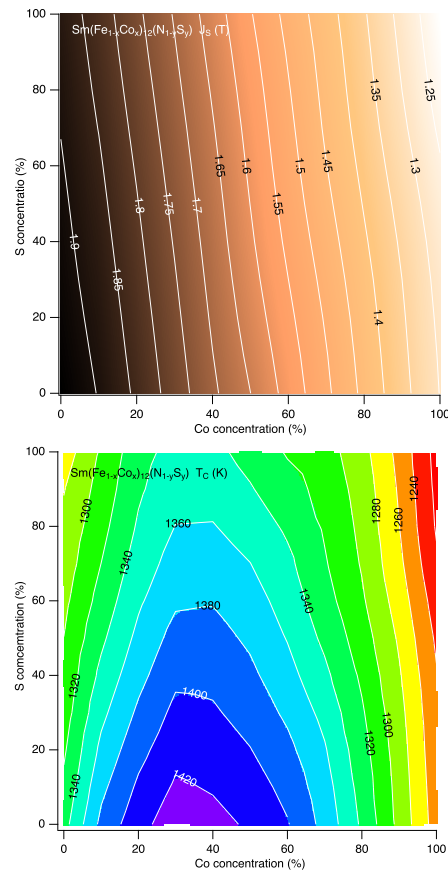


Figure 1: Magnetization (T) (top) and T_C (K) (bottom) of $\text{Sm}(\text{Fe}_{1-x}\text{Co}_x)_{12}(\text{N}_{1-y}\text{S}_y)$.

References

- [1] H. Akai, AkaiKKR, <http://kkp.issp.u-tokyo.ac.jp/> (2002).

Ab initio inspection on doping effects on rare-earth permanent magnets

Munehisa Matsumoto (Akai Group)
Institute for Solid State Physics, University of Tokyo
Kashiwa-no-ha, Kashiwa, Chiba 277-8581

April 26, 2019

We have been exploring possibilities to improve rare-earth permanent magnets (REPM's) on the basis of fundamental understanding for the intrinsic electronic structure. The champion magnet, Nd-Fe-B ternary alloy, is made of the main-phase compound $\text{Nd}_2\text{Fe}_{14}\text{B}$. Its excellent magnetic properties at room temperature are traded off with a drawback with poor high-temperature performance. The possible directions for improving the intrinsic properties of REPM's include raising the Curie temperature and/or enhancing the temperature resistance of magnetic properties.

A standard way to raise the Curie temperature is to make an alloy with Co. Thus it is important to understand how Co-doping works in $\text{Nd}_2\text{Fe}_{14}\text{B}$. Even though some experimental observation on the site preference of doped elements in $\text{Nd}_2\text{Fe}_{14}\text{B}$, it is only in recent days that *ab initio* investigations on $\text{Nd}_2\text{Fe}_{14}\text{B}$ have been in major trends. This is partly because the large unit cell of $\text{Nd}_2\text{Fe}_{14}\text{B}$ with 4 formula units or 68 atoms is demanding in terms of computational resource. Also this practical problem comes on top of the fundamental problem in dealing with 4*f* electrons. At the core of our calculations are open-source package for *ab initio* electronic structure calculations, AkaiKKR [1] and OpenMX [2]. With these the intrinsic properties of doped $\text{Nd}_2\text{Fe}_{14}\text{B}$ can be addressed in a reasonable time on System B. Continuous exploration of

the compositional space is done on the basis of coherent potential approximation using AkaiKKR. Effect of discrete replacement of host atoms by dopant atoms is investigated by OpenMX. Part of our recent results on Co-doped $\text{Nd}_2\text{Fe}_{14}\text{B}$ where one Co atoms replaces one Fe atom out of the possible 56 atomic sites in the unit cell of $\text{Nd}_2\text{Fe}_{14}\text{B}$ is shown in Fig. 1 for the mixing energy which is defined as follows.

$$\begin{aligned} \Delta E_{\text{mix}} = & U[\text{Nd}_2(\text{Fe}_{1-x}\text{Co}_x)_{14}\text{B}] \\ & - (1-x)U[\text{Nd}_2\text{Fe}_{14}\text{B}] \\ & - xU[\text{Nd}_2\text{Co}_{14}\text{B}] \end{aligned}$$

Here $U[M]$ is the calculated energy for a given material M . It is clearly shown that doped

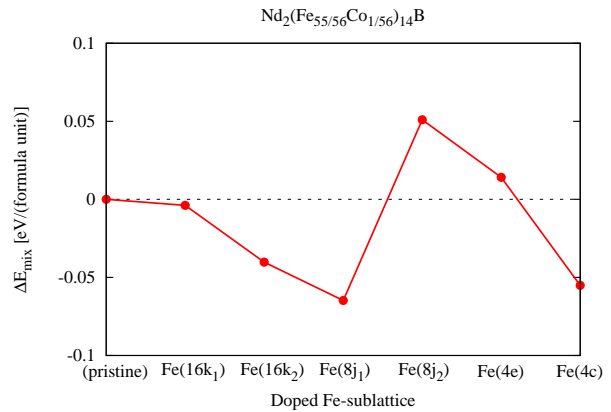


Figure 1: Calculated mixing energy of Co and $\text{Nd}_2\text{Fe}_{14}\text{B}$.

Co prefers Fe(8j₁) sublattice among the six

sublattices in the host $\text{Nd}_2\text{Fe}_{14}\text{B}$ [3]. Remarkably the numerically observed trend is consistent with past experimental claims in that Co prefers $\text{Fe}(8j_1)$ and avoids $\text{Fe}(8j_2)$. It also can be shown that this particular preference originates in the magnetic exchange couplings between the host Fe and dopant atoms. Such fundamental understanding should pave the way toward the improvement of intrinsic properties avoiding unnecessary tradeoff's between various desired properties to make a good REPM.

References

- [1] H. Akai: <http://kkr.issp.u-tokyo.ac.jp/jp/>. See also <https://ma.issp.u-tokyo.ac.jp/app/113>.
- [2] T. Ozaki *et al*: <http://www.openmx-square.org/>. See also <https://ma.issp.u-tokyo.ac.jp/app/594>.
- [3] M. Matsumoto, preprint (arXiv: 1812.10945)

Electronic structure and superconductivity based on a first-principles approach

Hiroaki IKEDA

*Department of Physics, Ritsumeikan University
Kusatsu, Shiga 525-8577*

Our aim is to develop the first-principles band structure calculations and understand the pairing mechanism of unconventional superconductivity in the strongly correlated electron systems. This year, we studied the following topics using Class B; material design of new high- T_c superconductors and the quasiparticle self-consistent GW (QSGW) band structure in the iron-based superconductors.

First of all, we tried material design of hydride superconductors using USPEX code after high- T_c H_3S . We performed it for some binary and ternary compounds of hydrogen. Obviously, it is difficult that the space group keeps high symmetry in ternary compounds under high pressure. This may be disadvantageous to realize high- T_c superconductors. On the other hands, in binary hydrides, 260K superconductivity in LaH_x was realized [1]. This motivated us to calculate superconductivity in YbH_x , since atomic configuration of Yb atom is fully-occupied f^{14} while that of La atom is fully-empty f^0 . Figure 1 shows enthalpy of formation in YbH_x . We can see that YbH_2 is the most stable, but there are some metastable structures, YbH_6 etc, under high pressure. Then we calculated the electron-phonon coupling constant λ in these structures. Finally, we found that YbH_6 indicates $T_c \sim 50\text{K}$ at 200GPa. Suppression of T_c , as compared with LaH_x , comes from the fact that Yb f orbitals are hybridized with ligand hydrogens, and phononic modes of ligand hydrogen are suppressed.

Next, we performed the QSGW calculations

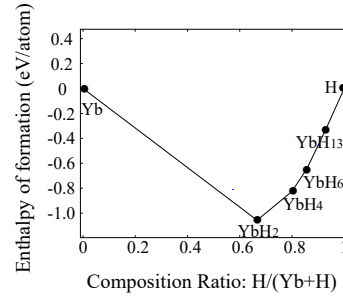


Figure 1: Enthalpy of formation at 200GPa in Yb-H system.

in a variety of iron-based superconductors. As well-known, the LDA/GGA calculations in the iron-based superconductors describe overall features of the electronic structure. However, size, curvature, and orbital characters of Fermi surfaces are significantly deviated from the experimental observations. This is a serious problem in understanding the superconducting pairing mechanism. As the iron-based superconductors are semi-metallic, this problem can have a similar aspect to the fact that the LDA/GGA cannot well describe the band gap of semiconductors. Here, we applied the QSGW method, which well explains the band gap in semiconductors. We found that the QSGW approach can improve the band structures. A part of this work was used in the dHvA analysis of FeS in [2].

References

- [1] M. Somayazulu *et al.*, Phys. Rev. Lett. **122**, 027001 (2019).
- [2] T. Terashima *et al.*, Phys. Rev. B **99**, 134501 (2019).

Development and control of spin texture by band engineering using quantum-well state

Shunsuke SAKURAGI

*Institute for Solid State Physics, University of Tokyo
Kashiwa-no-ha, Kashiwa, Chiba 277-8581*

We have studied a magnetism induced by quantum-well states using density functional theoretical calculation. This year, we focused on a mechanism by which the magnetism of Pd(100) ultrathin film, which shows ferromagnetism induced by quantum-well states, can be controlled by tailoring the Pd/stacking layer interface electronic states (i.e., scattering phase shift of the quantum-well states) [1].

For the experimental observation of the control of magnetism in metals using an external field, thin films with a few monolayers are generally used because of the screening effect. Although previous research showed the effect of the change in the Fermi energy and polarization of the orbital character of the electrons by applying the electronic field, the standpoint of tuning the quantum size effect which was occurred by nano-scaling of the materials was not well discussed. Our present study was focused on quantum-well induced ferromagnetism, which appeared after forming the ultrathin film. Using DFT calculation with PHASE/0 code [2], we clearly show the possibility of paramagnetic to ferromagnetic switching by modifying the interface electronic states of the quantum-wells. Our present discovery opens up a new way to control magnetism by tuning the size effect.

Generally, the quantum-well states, which is the origin of the ferromagnetism in Pd(100) ultrathin films, are described in a one-dimensional quantum-well model containing the phase shift, which is the effect of the elec-

tron scattering at the interfaces of wells. First, we expand the function of the phase shift from the real space to momentum space dependency. This theory means that controlling the shape of quantum-well band dispersion will be artificially achieved by modifying the interface electronic states. For the appearance of ferromagnetism, making a flat band at the Fermi energy is important, and we clearly show that stacking of the fcc *d*-electron transition metal layer on Pd quantum-wells makes a flat band, from the DFT calculation based on this theory. We expect that the control of magnetism predicted in our present theory will be experimentally observable in a system of a stacking layer/Pd ultrathin film on a piezo substrate. This can modify the layer spacing (i.e., tune the hybridizing of the wave functions at the interfaces of the wells), and the nonmagnetic to ferromagnetic switching using the multilayer nano film system should be easily achieved.

References

- [1] Shunsuke Sakuragi, Hiroyuki Kageshima, and Tetsuya Sato : submitted to Phys. Rev. B.
- [2] <https://azuma.nims.go.jp/software/phase>

Study of interaction between radiation damage and interstitial atom

Kazuhito Ohsawa

Institute for Applied Mechanics,

Kyushu University, Kasuga-koen, Kasuga, Fukuoka 816-8580

Introduction

The study of hydrogen (H) isotope retention in tungsten (W) are important issue in the field of fusion reactor because W is one of the plausible plasma facing materials (PFMs). Usually, H seldom dissolve in W. However, H atoms are trapped in the vacancy-type lattice defects created under the irradiation circumstance. Actually, a large amount of retention of deuterium (D) was observed in the irradiation damage zone of W specimen. In particular, tritium (T) retention in the PFM is one of the serious problem associated with fusion reactor because T is radioisotope whose half-life is 12 years. H atom trapping in monovacancy in W have been reported in some previous works. Therefore, we investigated the H atom trapping in divacancy in W in the present work.

Simulation method

The binding energies of H atoms to the divacancy and stable configurations of the H atoms in it were calculated in terms of first-principle calculations based on density functional theory. We used the Vienna ab-initio simulation package (VASP). Then, a large

simulation cell, containing 6x6x6 bcc lattice (432 atoms), were used in order to reduce the effects of periodic boundary condition imposed on the simulation cell.

Results

First, we examined the stable configuration of the divacancy in W. The divacancy in the first nearest neighbor configuration is the most stable structure. Second, we investigated stable structures of H atoms in the divacancy, as shown in Fig. 1. The H atoms are located in the vicinity of the octahedral interstitial sites (O-sites). There are 12 O-sites next to the divacancy. Then, six are located in the center of the divacancy where two monovacancies are in contact with each other. The other six O-sites are located outside of the center. H atoms preferentially occupy O-sites in the center of the divacancy. All H atoms occupy O-sites in the center of the divacancy in the case of $k=2$, and 4, where k is the total number of H atoms trapped in the divacancy. However, repulsive interactions usually act among H atoms in metals. So, H atoms gradually occupy the outside O-sites, as

the number of H atoms in the divacancy increases. Actually, two H atoms occupy outside O-sites in the case of $k=6$, even though all O-sites in the center are not occupied by H atoms.

Binging energies of H atoms trapped in the vacancy-type lattice defects, i.e., monovacancy and divacancy, in W are presented in Fig.2 as a function of the number of H atoms. A maximum of 12 H atoms can be accommodated in the monovacancy. While, 18 H atoms can be accommodated in the divacancy at least.

Discussion

We consider how to determine the stable structures of H atoms in the divacancy. There are two kinds of O-sites next to the divacancy. Therefore, the attractive interactions to an H are different by the types. Besides, the mutual repulsion acts among H atoms. As a result, the stable structures of H atoms are determined by the balance of the attractive and repulsive interactions.

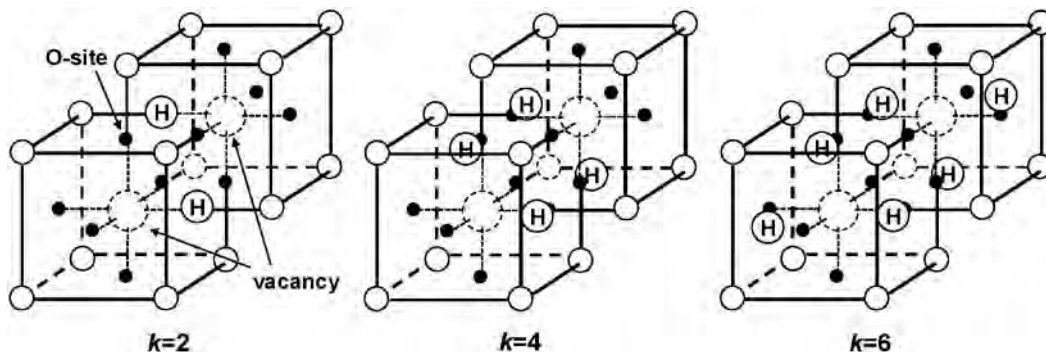


Fig. 1: Schematic view of stable configurations of H atoms trapped in divacancy in W. Number of H atoms is k . They are located close to O-sites.

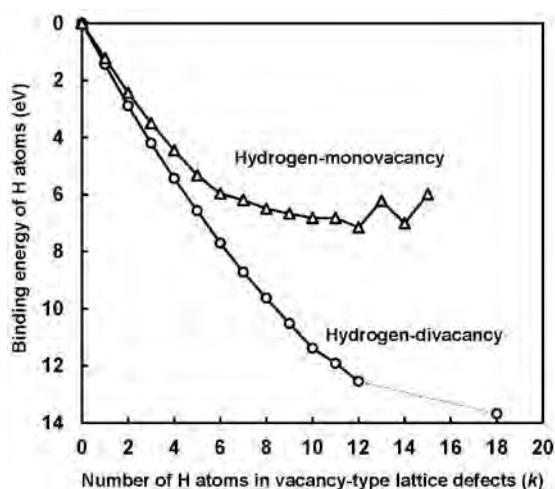


Fig. 2: Binding energy of H atoms to mono or divacancy in W.

Theoretical Study on the Aggregation-Induced Emission

Norifumi YAMAMOTO

Department of Applied Chemistry,

Chiba Institute of Technology, 2-17-1 Tsudanuma, Narashino, Chiba 275-0016

In this project, the mechanism of aggregation-induced emission (AIE) of tetraphenylethylene (TPE) was studied theoretically.

The TPE has been known to exhibit the AIE, which is non-emissive in dilute solutions but becomes highly emissive in solid or aggregates [1]. In this study, the AIE of TPE was investigated by using *ab initio* electronic structure calculations, together with molecular dynamics (MD) simulations.

In order to elucidate the characteristics of the potential energy profiles for the photochemical processes of TPE, the minimum energy paths for the photo isomerization reaction of TPE in an isolated phase were investigated using *ab initio* electronic structure calculations. The spin-flip approach within the time-dependent density functional theory (SF-TDDFT) method was used to compute the potential energies and analytical gradients for the electronic ground (S_0) and first excited (S_1) states of the molecule. All electronic structure calculations of CN-MBE presented herein were performed using the GAMESS program.

The results of SF-TDDFT calculations showed that the potential energies of TPE for electronic ground (S_0) and first excited (S_1)

states are degenerated at a conformation with the twist angle of 90° around its ethylenic C=C bond, which can lead the fluorescence quenching of TPE molecule in dilute solutions.

The free-energy profile of the photo isomerization of TPE in condensed phase was computed using MD simulations based on an empirical force field representation. All MD simulations of TPE presented herein were carried out using the GROMACS 2016.3 program.

The results of MD simulations revealed that TPE tends to assemble in close contact, where the ethylenic C=C bond rotation is markedly restricted in aggregates, preventing the fluorescence quenching via the S_0/S_1 conical intersection; TPE in THF solution, however, proceeds a barrierless non-radiative transition. These results gave a clear picture of the AIE mechanism of TPE, which is agree with that of a cyanostilbene derivative [2].

References

- [1] Hong, Y.; Lam, J. W. Y.; Tang, B. Z., *Chem. Soc. Rev.*, Vol. 40, pp. 5361–5388 (2011).
- [2] Yamamoto, N., *J. Phys. Chem. C*, Vol. 122, pp. 12434–12440 (2018).

Development of the determination technique of model parameters based on the accurate ab-initio quantum simulation

Hirofumi SAKAKIBARA

Department of Applied Mathematics and Physics,

Tottori University, Koyama-cho Minami, Tottori city, Tottori 680-8552

It is not so easy to treat strongly-correlated electrons only by first-principles calculation. Thus we often derive a low-energy from first-principles calculations. If the model describes strong correlations in some model calculations, it can be said that such strong correlation effect may be described in a (quasi-)first-principles method.

Especially for magnetism, metal-insulator transition, and superconductivity, single-band or multi-band Hubbard models are often adopted. In such Hubbard models, on-site electron interaction U is an essential parameter. Therefore, we have constructed a new method to determine U , named model-mapped RPA (mRPA) [1].

In the previous annual report, we have developed our mRPA code so as to be applicable to multi-orbital cases [2]. Then we obtained the model parameter of two single-layered cuprates La_2CuO_4 ($T_c \sim 40\text{K}$) and $\text{HgBa}_2\text{CuO}_4$ ($T_c \sim 100\text{K}$). Then we assume two-orbital Hubbard model consisting of the $d_{x^2-y^2}$ orbital and the d_{z^2} orbital [2,3]. The two-orbital model fully derived from first-principles

calculation explains the experimental difference of T_c in fluctuation-exchange approximation [4].

We also compare the results of mRPA and constrained RPA (cRPA) [5]. We found that the U of the $d_{x^2-y^2}$ orbital is larger in La_2CuO_4 than $\text{HgBa}_2\text{CuO}_4$ in cRPA, while smaller in La_2CuO_4 than $\text{HgBa}_2\text{CuO}_4$ in mRPA [4]. This result does not mean that our mRPA code does not work well.

To confirm this point, we applied mRPA to SrVO_3 . SrVO_3 is a famous benchmark material, in which the energy-bands are almost separated between the model space and the outside of the model space. Here the model space is spanned by the maximally localized Wannier functions. Separated band structure is desirable condition because the model space is well defined. Then we obtained $U=3.12$ eV in cRPA and $U=2.85$ eV in mRPA. It seems that these two methods agree with each other. This result means that mRPA code may work well.

Contrary to SrVO_3 , the band structure of the model space is not separated from the outside of the model space in the two cuprates. Namely, the model space is more ill-defined in cuprates

than SrVO₃. From the comparison between SrVO₃ and two cuprates, we can imagine that the well-definedness of the model spaces may affect methodological dependence of the Hubbard U . The detailed explanation of the dependence is shown in our recent paper [4]. In this annual report, we only give the conclusion that the projection method [7] adopted in cRPA may give rise to the dependence, where the projection method is used to define the model space.

In mRPA, such a projection method is not needed. In mRPA, we match the effective interaction obtained from first-principles and model calculations. Namely, we perform both of first-principles calculation and model calculation to determine U so that the both effective interactions become identical. Then the determination process is unique in mRPA. This is one of the advantages of mRPA.

For SrVO₃, we also obtained an extended Hubbard models consisting of not only the on-site interaction but also the nearest-neighbor site interaction V . We found U becomes larger ($U=3.29$ eV) when we consider an extended Hubbard model [4]. This is because that V weakens the local part of the effective

interaction and thus U should become larger to maintain the value of local term of the effective interaction, which is determined independently of the model we consider. Since this conclusion may be general for metallic system, we will investigate further materials on this point of view.

References

- [1] H. Sakakibara *et al.*: J. Phys. Soc. Jpn. **86**, 044714 (2017).
- [2] H. Sakakibara *et al.*, Phys. Rev. Lett. **105**, 057003 (2010).
- [3] H. Sakakibara *et al.*, Phys. Rev. B **89**, 224505 (2014).
- [4] H. Sakakibara and T. Kotani, arXiv:1812.03731 (2018).
- [5] F. Aryasetiawan, M. Imada, A. Georges, G. Kotliar, S. Biermann, and A. I. Lichtenstein, Phys. Rev. B **70**, 195105 (2004).
- [6] E. Sasioglu, in Lecture Notes of the 45th IFF Spring School “Computing Solids-Models ab initio methods and supercomputing” (Forschungszentrum Julich, 2014).

First-principles study on positron states in d0 ferromagnetics and at solid surfaces

Satoshi HAGIWARA

*National Institutes for Quantum and Radiological Science and Technology,
1233, Watanuki-machi, Takasaki, Gunma, 370-1292, Japan*

In this work, we studied the following two topics: 1) the positron state in the Ga vacancy in GaGdN, 2) developing the theory of positronium formation using realistic material surface. These works are collaboration with experimental group.

1) the positron state in the Ga vacancy in GaGdN: A spin-dependent positron annihilation spectroscopy is a powerful tool for investigating defect induced ferromagnetism, because positron is easily trapped by vacancy type defect and annihilates with electrons around the positron. In this respect, positron annihilation parameters provide information on electronic and magnetic states around vacancy type defects [1]. A previous study has reported that the Gd-doped GaN generates huge magnetization at room temperature ($\sim 4000\mu_B$). Afterwards, GGA+U study suggested that this huge magnetization is caused by Ga vacancy [2]. However, there are no reports on direct observation of defect induced magnetism of GaGdN. For this reason, we carried out the TCDFD calculation for spin-polarized positron annihilation parameters. The TCDFD calculation is performed using ABINIT code

[3]. We found that differential magnetic doppler spectrum depends on the spin-density around the Ga vacancy.

2) developing the theory of positronium formation using realistic material surface: A positronium (Ps) is a bound state between an electron and a positron like a hydrogen atom. Ps formation is caused in

positron re-emission process and is allowed outside of the metal surfaces, because Ps formation is prohibited inside of metal due to strong electron screening effect to a positron [4]. We found that the theoretical spectra including interaction between Ps and surface remaining hole [5] show in good agreement with experiment.

References

- [1] F. Tuomisto and I. Makkonen, *Rev. Mod. Phys.* **85**, 1583 (2013).
- [2] Y. Gohda and A. Oshiyama, *Phys. Rev. B* **78**, 161201(R) (2008).
- [3] X. Gonze et al., *Comput. Phys. Commun.* **205**, 106 (2016).
- [4] C. Hugenschmidt, *Surf. Sci. Rep.* **71**, 547 (2016).
- [5] A. Ishii, *Surf. Sci.* **209**, 1 (1989).

First-Principles Molecular Dynamics Study on Structural Properties of Fayalite Fe_2SiO_4 under High-Pressure

Masaaki MISAWA

Faculty of Science and Engineering, Kyushu Sangyo University, Fukuoka 813-8503

Fayalite (Fe_2SiO_4), the iron-rich end member of olivine ($\text{Mg}_x\text{Fe}_{2-x}\text{SiO}_4$), undergoes crystal-to-amorphous structural transformation under high-pressure (~ 40 GPa) at room temperature. Based on an in-situ infrared spectroscopy [1], it is explained that the pressure-induced amorphization is triggered by the deformation of tetrahedral SiO_4 structural units in the crystalline phase into octahedral SiO_6 , distorted octahedral SiO_6 or pyramidal SiO_5 units. However, it is not clear that the distribution of those structural units and what kind of atom is the network former/modifier in the amorphous phase.

To investigate the detailed structural properties of pressure-amorphous fayalite, we have carried out first-principles molecular dynamics simulations for the amorphization process of fayalite. The electronic states were calculated using projector augmented-wave method within the framework of density functional theory, in which the generalized gradient approximation was used for the exchange-correlation energy. In order to represent the electronic states of localized d-orbitals in Fe atoms, spin-polarization was taken into account and DFT+U method was

employed. First the pressure was increased from ambient pressure to 300 GPa to create the pressure-amorphous fayalite, and then return to ambient pressure to compare with experimental results. All of simulations are performed at room temperature.

As a result of the simulations, we confirm that massive structural change occurs and disordered structure was obtained at high pressure. In the obtained structure, both of pyramidal SiO_5 and octahedral SiO_6 units exist and those SiO_x units form corner-shared network structure at 40 GPa. On the other hand, at ambient pressure, most of Si atoms revert to tetrahedral SiO_4 units and Si-O network structure was disconnected. These disconnected SiO_x units form only monomer or dimer, which show good agreement with experimental prediction of the forsterite glass structure [2].

References

- [1] Q. Williams, E. Knittle, R. Reichlin, S. Martin and R. Jeanloz: *J. Geophys. Res.* **95** (1990) 21549.
- [2] S. Kohara, K. Suzuya, K. Takeuchi, C.-K. Loong, M. Grimsditch, J. K. R. Weber, J.A. Tangeman, and T. S. Key: *Science* **303** (2004) 1649.

Theoretical Design of Novel Magneto-Electric Oxides

Masayuki TOYODA

*Department of Physics, Tokyo Institute of Technology
Ookayama, Meguro-ku, Tokyo 152-8551*

Magneto-electric materials have promising potential for technological innovations, owing to their cross correlation between magnetism and electricity. A novel family of oxides represented by $\text{Ba}(\text{TiO})\text{Cu}_4(\text{PO}_4)_4$ [1] exhibit quadrupole-type alignment of localized $S = 1/2$ spin moments, which gives rise to the magneto-electric responses[2].

In this study, we performed systematic survey of the electronic structures and magnetic properties of $A(\text{TiO})\text{Cu}_4(\text{PO}_4)_4$ ($A = \text{Ba}, \text{Sr},$ and Pb) based on the density-functional theory. The computations have been done by using the ISSP supercomputer system B.

For all the oxides, the ground state is found to be antiferromagnetic (AFM) with the quadrupole-type alignment of the spin moments, which is the characteristic feature of this family. However, from the evaluation of the magnetic exchange interaction J , we found that the inter-layer interaction varies upon the replacement of the A ion. For the case of $A = \text{Ba}$ and Sr , the inter-layer interaction is AFM and, therefore, the materials show antiferroelectricity (AFE), which gives no macroscopic polarization. On the other hand, for the case of $A = \text{Pb}$, the interaction is ferromagnetic (FM) and the materials exhibits ferroelectric (FE) polarization.

From the analysis of the charge density distribution (Fig. 1), it is found that FM inter-layer interaction in $\text{Pb}(\text{TiO})\text{Cu}_4(\text{PO}_4)_4$ is mediated by the Pb- s states that has broader distribution than the other counterparts. Based on this insight, we also found that $A = \text{Sn}$ can be yet another magneto-electric oxide that

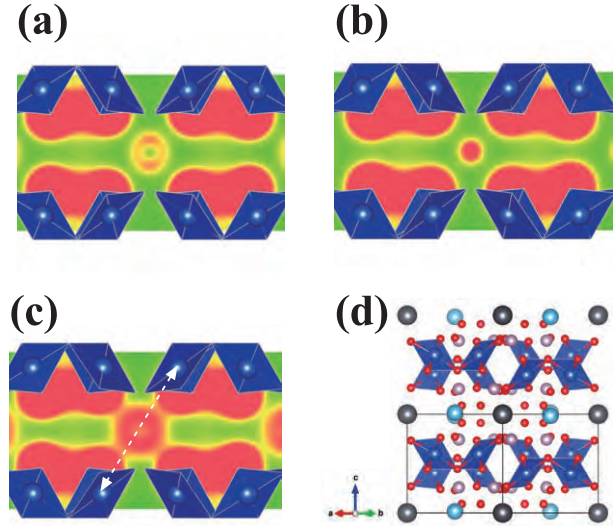


Figure 1: Partial electronic charge density distribution of the valence band states in (a) $\text{Ba}(\text{TiO})\text{Cu}_4(\text{PO}_4)_4$, (b) $\text{Sr}(\text{TiO})\text{Cu}_4(\text{PO}_4)_4$, and (c) $\text{Pb}(\text{TiO})\text{Cu}_4(\text{PO}_4)_4$ projected on (110) plane. The crystal structure viewed from [110] direction is also shown in panel (d).

shows AFM and FE ordering.

References

- [1] K. Kimura, M. Toyoda et al., Nat. Commun. **7**, 13039 (2016).
- [2] K.T. Delaney, Mj. Mostovoy, and N.A. Spaldin, Phys. Rev. Lett. **102**, 157203 (2009).
- [3] K. Kimura, M. Toyoda, P. Babkevich, K. Yamauchi, M. Sera, V. Nassif, H. M. Rønnow, and T. Kimura, Phys. Rev. B **97**, 134418 (2018).

Electronics structures of newly crystallized large aromatic organic semiconductors

Toshihiro Shimada, Ichiro Yamane, Nobuhiko Sakai, Takahiro Tamura, Wei Liu,
Meiqi Zhang, Takashi Yanase, Taro Nagahama
*Division of Applied Chemistry, Faculty of Engineering,
Hokkaido University, Kita 13 Nishi 8, Kita-ku, Sapporo, 060-8628 Japan*

We are studying synthesis reactions and properties of solid state materials, including new carbon materials[1], organic semiconductors[2], and nanostructures. We use computer to calculate electronic band structure and stability of various materials.

This year, we focused on electronic band structure of new organic semiconductor crystals which we have recently developed the method to make single crystals. The structure of the molecule (Benzo[*i*]benzo[6',7']quinoxalino [2',3':9,10]phenanthro[4,5-*abc*]phenazine; BBQPP in the following) is shown in Fig. 1. We grew single crystals of this and other molecules and determined the crystal structures by using x-ray diffraction.

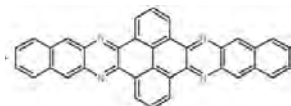


Fig. 1: BBQPP

Using ISSP supercomputer, we calculated the band structure of BBQPP based on the atomic positions determined from x-ray diffraction. The calculation was carried out using the Vienna Ab initio simulation package[3] which is based on DFT, plane waves and

pseudopotentials. Our calculation was performed with the projector augmented wave method and the exchange-correlation energy treated using the PBE functional[4] based on the generalized gradient approximation. The cutoff energy was 400 eV. The result is shown in Fig. 2. Strong one dimensional character of the electronic structure was noticed.

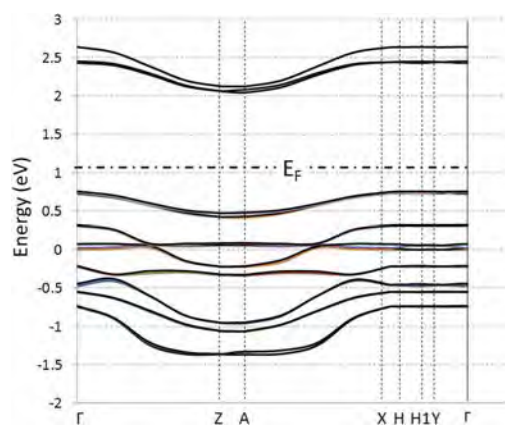


Fig.2: Band structure of BBQPP

References

- [1] I. Yamane et al., Jpn.J. Appl.Phys. 58, SBBG13 (2019).
- [2] N. Sakai et al., *ibid*, SBBG08 (2019).
- [3] G. Kresse J. Furthmüller, Phys. Rev. B54,11169 (1996).
- [4] J. P. Perdew, K. Burke, M. Ernzerhof, Phys. Rev. Lett. 77, 3865 (1996).

Elucidation of electronic states of caged compounds in aqueous solution

Miyabi HIYAMA

*Graduate School of Science and Technology, Gunma University,
Tenjin-cho, Kiryu, Gunma 376-8515*

Caged-luciferins are known as the compounds which can generate luciferin by UV photolytic reaction as shown in Figure 1. They are expected to be powerful tool in spectroscopic studies for catalytic reaction such as firefly bioluminescence.

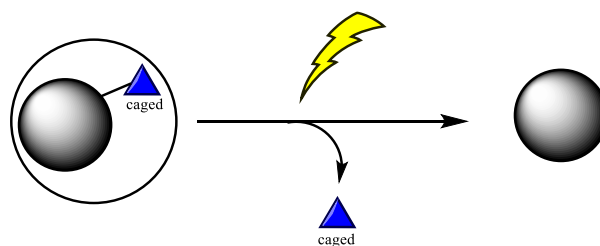


Figure 1: Conceptual diagram for Caged-luciferin

A new caged-luciferin designed in Akiyama group of ISSP was synthesized and its molecular structure was identified with NMR[1]. When we use this caged-luciferin for spectroscopic studies, we need the detail of electronic states of this molecule in aqueous solutions. In this year, we investigated the electronic structures of this caged-luciferin in aqueous solution by DFT calculations.

The polarized continuum model was used for the description of water solute molecules. All calculations were performed using the GAUSSIAN09 [2] program on system B of Super Computer Center in ISSP.

It was found that there are forty equilibrium structures for the caged-luciferin in aqueous solution and these structures are classified in terms of characteristics in their configurations[3, 4].

References

- [1] Kurata et al., *J. Photochem. Photobiol. B*, **189** (2018) 81.

- [2] Gaussian 09, Revision D.01, M. J. Frisch et al.

- [3] Usukura et al. The 12th Annual meeting of Japan Society for Molecular Science.

- [4] Hiyama, Symposium for reaction Path Search 2018.

Calculation of oxide surface properties for catalyst informatics

Yoyo HINUMA

Center for Frontier Science

Chiba University, 1-33 Yayoicho, Inage, Chiba, Chiba 263-8522

Surface point defects of metal oxides, for instance O vacancies, have a dominant effect on heterogeneous catalysis. The Mars-Van Krevelen mechanism is one of the most frequently encountered catalytic process. In one example, O vacancies on a metal oxide catalyst surface act as reaction sites. The energy required to remove O from a surface, which is denoted as the surface O vacancy formation energy (E_{Ovac}), can be used to rationalize and predict catalytic performance in such a catalytic process. Calculation of E_{Ovac} requires a slab-and-vacuum model with sufficient spacing between O vacancies, hence some estimation of E_{Ovac} from less costly calculations, such as slab-and-vacuum model calculations with minimum cell size and even bulk calculations, will be effective in screening materials for a given purpose.

A total of 33 binary oxide surfaces of insulating and semiconducting oxides was evaluated using the automated nonstoichiometric and nonpolar slab-and-model generation algorithm by Hinuma et al. [1,2]. A good correlation was found between E_{Ovac} and band gap, bulk formation energy, and electron

affinity was found. Moreover, the relation between subsequent small molecule (O_2 , NO, CO, CO_2 , and H_2) for 16 surfaces were assessed. The adsorption mode was strongly governed by E_{Ovac} , where a large E_{Ovac} benefits side-on adsorption for NO and CO as well as dissociative adsorption for energy showed CO_2 and H_2 . Furthermore, the side-on and dissociative adsorption energy is linearly dependent on E_{Ovac} . [3]

These findings serve as the basis for more efficient catalyst design because E_{Ovac} was found to influence the stability of O vacancies and the adsorption mode, which in turn can be estimated to some extent using cheaply obtained physical quantities, namely band gap, bulk formation energy, and electron affinity.

References

- [1] Y. Hinuma et al.: *Comp. Mater. Sci.* 113 (2016) 221.
- [2] Y. Hinuma et al.: *Phys. Rev. Mater.* 2 (2018) 124603.
- [3] Y. Hinuma et al.: *J. Phys. Chem. C.* 122 (2018) 29435.

Search and realization of novel electronic properties of solid surfaces and interfaces and of small particles

Takeshi INAOKA

*Department of Physics and Earth Sciences, Faculty of Science,
University of the Ryukyus, 1 Senbaru, Nishihara, Okinawa 903-0213*

We describe two of those subjects which we addressed this year.

Graphene is a very popular single-layer structure of carbon (C) atoms arranged in a hexagonal lattice. However, we consider that there might be different monolayer structures of C atoms. Last year, we presented another stable structure which is composed of tetragonal and octagonal patterns. It was found that the electron system is a semi-metal which is characterized by the electron pocket around the \bar{M} point and the hole pocket around the $\bar{\Gamma}$ point. This year, we proposed a similar stable structure which is constituted of tetragonal, hexagonal, and octagonal patterns.

In scanning tunneling microscopy (STM) light emission spectra of Ni(110)-(2x1)-O surface appear stepwise structures due to oxygen (O) atom vibration parallel to the surface [1]. These structures are considered to originate from the change in the local density of states (LDOS) below the STM tip owing to the vibration [1]. From this standpoint, we started first-principles calculations of this system at higher levels than in previous works.

We employed the program package 'Vienna Ab initio Simulation Package' (VASP) [2,3] on systems B and C.

(1) Proposal of a novel single-layer structure of carbon atoms [4]

By means of first-principles calculations with the generalized gradient approximation (GGA), we investigated a C monolayer structure shown in Fig. 1. We optimized the in-plane structure including the primitive unit cell size. Then, we checked the stability of this structure to the plane-normal atom displacement. It was found that the cohesive energy per C atom evaluated by separating the crystal

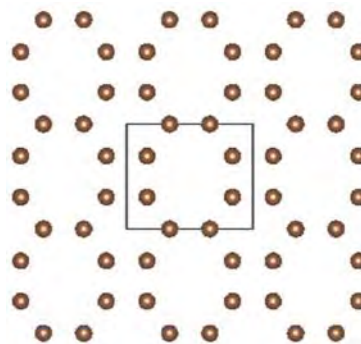


Fig. 1 Proposed monolayer structure of C atoms

into isolated atoms is comparable to that of graphene, and that the in-plane structure is stable.

The energy contour map of the twelfth band showed that there exists a hole pocket around the \bar{X} point which extends toward the $\bar{\Gamma}$ point. On the other hand, the energy contour map of the thirteenth band indicated that there lies an electron pocket around the \bar{M} point that spreads toward the \bar{Y} point. These pockets compensating each other asserts that this crystal is semi-metal with large electron or hole density estimated to be $1.4 \times 10^{14} \text{ cm}^{-2}$. From the electron density distribution, we realized that the twelfth and thirteenth bands are formed by hybridization of plane-normal p orbitals of C atoms. Each band has its own hybridizing character.

(2) Electronic structure of Ni(110)-(2x1) O surface [5]

To examine how the O atom displacement in phonon vibration changes the LDOS, we started first-principles calculation of this system.

Previously, first-principles calculations were performed for O-adsorbed Ni surfaces. However, slabs of several atomic

layers were treated because of limitations of computer performance at that time. In the present work, we intend to identify sufficient slab thickness to represent semi-infinite substrate by using slabs of several tens of atomic layers.

Figure 2 exhibits the optimized slab structure of 11 Ni atom layers with an adsorbed O atom at each surface. We assume the missing-row reconstructed O $p(2\times 1)/\text{Ni}(110)$ surface. Figure 3 displays the orbital-projected density of states (pDOS) for p_x orbital of the O atom (full curves) and for d_{xy} orbital of the topmost Ni atom (dotted curves). The black and red lines are for majority and minority spins, respectively. The p_x pDOS of the O atom for each spin shows a peak near the Fermi level E_F , which accords with a peak of the d_{xy} pDOS of the Ni atom. This peak-energy agreement is considered to indicate the bonding of the p_x state of the O atom and the d_{xy} state of the Ni atom. At the next stage, we will investigate the peak shift of the p_x pDOS of the O atom in surface phonon vibration.

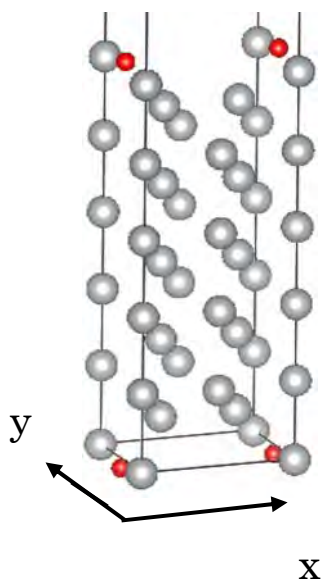


Fig. 2 Optimized slab structure of O $p(2\times 1)$ Ni(110) surface. The slab is composed of 11 Ni atom layers and an adsorbed O atom at each surface.

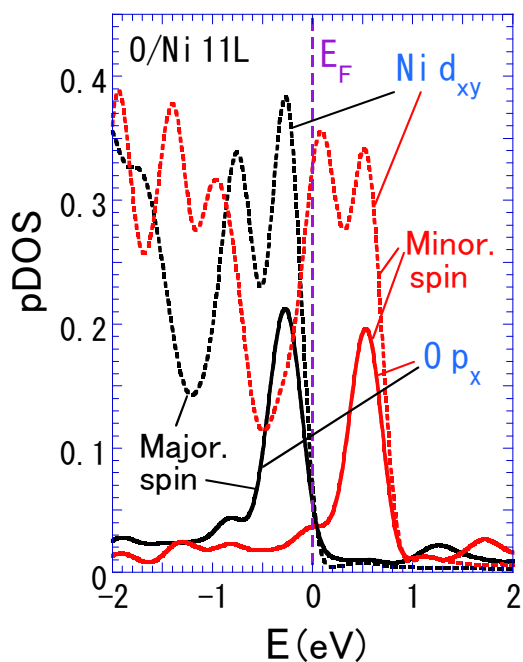


Fig. 3 Orbital-projected density of states of the adsorbed O atom and the surface Ni atom. For details, see the text.

References

- [1] Y. Uehara, T. Inaoka, T. Nishio, and S. Katano, *J. Appl. Phys.* **123** (2018) 224302 (8 pages).
- [2] G. Kresse and J. Hafner: *Phys. Rev. B* **47** (1993) 558–561.
- [3] G. Kresse and J. Furthmüller: *Comput. Mat. Sci.* **6** (1996) 15–50.
- [4] T. Inaoka and Y. Nakaema, to be prepared.
- [5] T. Inaoka and Y. Uehara, to be prepared.

Chemical doping of nano-structured PbS

Ken-ichi SHUDO

*Fac. of Sci/Eng., Yokohama National University
Tokiwadai 79-5, Hodogaya-ku Yokohama 240-8501*

Galium oxide family are wide-gap semiconductors, and their optical features, tunable by impurity dope, are expected to be useful for many applications. In order to analyze our experimental data of photo-absorption/luminescence affected by the impurities in Ga_2O_3 [1], electronic states of ϵ - and κ - Ga_2O_3 with Co dope were calculated using the VASP code [2] based on first principles theory.

Calculations were done for a single unit cell through supercells sized to $8 \times 4 \times 4$, with/without Co dope as an impurity atom. The calculation was typically done in one or four computer-nodes, in *hybrid* parallelism (8 MPI + 3 openMP par node, typically). We began with the optimization without the impurity. The lattice constants were fixed at the obtained optimized dimension, and a Ga atom was then replaced by Ge. As expected from the small lattice constant of **b** and **c** direction, $1 \times 1 \times 2$ or $1 \times 2 \times 1$ supercell of Ga_2O_3 gave unstable results, suggesting necessity of careful conformation of the impurity to avoid the Co-Co interaction at high density of the impurity.

The results in density functional theory (DFT) gave Co-induced states in the band gap (see the main panel of Figure 1). They are not satisfactory in that the calculated band gap did not agree with the experimental data, as often seen in DFT. Thus we concluded some modification should be introduced, such as empirical methods namely DFT+U or non-local external potential (NLEP) [3]. However, the tendency of bandgap increase/decrease in the calculated results (inset of Fig.1) was in good agreement

with our experimental results.

At the same time, we performed preliminary calculation of impurity states in PbS crystal, and detailed analysis of spin-polarization of monolayer film of metal organic framework (MOF) started as an ISSP project (H29-Cb-0009) from 2018.

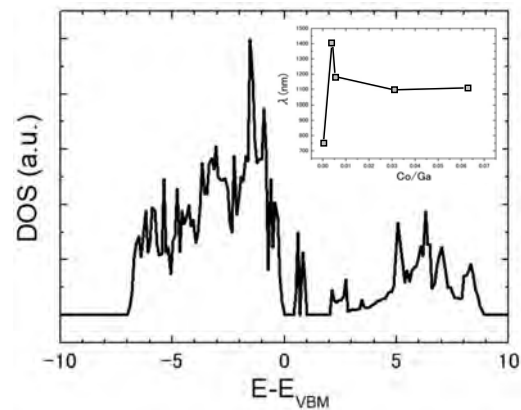


Figure 1: Calculated density of electronic states with a Co atom in a $8 \times 4 \times 4$ ϵ - Ga_2O_3 supercell. Inset: band-gap to varied density of the Co impurity.

References

- [1] K. Mukai, A. Tsuno, K. Shudo, and H. Otani: *Jap. j. Appl. Phys.* **58**, SBBK05 (2019).
- [2] G. Kresse: *Phys. Rev. B* **59**, 1758–1775 (1999); see also <https://www.vasp.at>
- [3] S. Lany, H. Raebiger, and A. Zunger: *Phys. Rev. B* **77**, 241201 (2008).

First-principles Study of Defects of Magnesium Alloys

Daisuke Matsunaka

*Department of Mechanical Systems Engineering,
Shinshu University, 4-17-1 Wakasato, Nagano 380-8553*

Magnesium (Mg) has been of increasingly interest from the engineering viewpoint, because of its low density and relatively high specific strength. Despite intensive research efforts, there remain various problems to be overcome; low ductility and low toughness at room temperature. As polycrystalline magnesium materials are applied for the engineering use, it is important to elucidate grain boundary properties. We have performed molecular dynamics analyses of symmetric tilt grain boundaries for [0001], [10-10], and [1-210] rotation axes using three types of interatomic potentials. The grain boundary energy vary for misorientation and there are energy cusp misorientations corresponding to twin boundaries for [10-10], and [1-210] rotation axes. On the other hand, for [0001], the misorientation dependence of grain boundary energy is relatively simple. These results imply that the anisotropy of hcp structure is reflected in the symmetric tilt grain boundaries.

In Mg alloys with rare earth elements, the addition in solid solution causes a significant increase in ductility. It is an important issue to

elucidate effects of an alloying element on each deformation mode such as deformation twinnings and non-basal slips. First-principles calculations give us valuable information of alloying elements. Development of interatomic potentials for alloys which can describe the first-principles results is necessary for atomistic simulations of deformation in Mg alloys. In this study, we tried to develop an interatomic potential for Mg alloy in terms of artificial neural network framework, based on first-principles results. As learning data, we calculated crystal structures such as fcc and bcc as well hcp and their deformed models and defective models, in which the number of atoms are relatively small. We have successfully implemented the developed potential into large-scale molecular dynamics simulations.

References

- [1] D. Matsunaka and K. Kawahara: Proc. 4th Multi-scale Mater. Mech. Symp. (2019) P20.
- [2] K. Oboso, Y. Fujioka, S. Yoshioka, and D. Matsunaka: Conf. Proc. Jpn. Soc. Comp. Eng. Sci. **24** (2019) A-03-04.

Calculation of Catalyst Electronic Structures for Catalyst Informatics

Takashi TOYAO

Institute for Catalysis,

Hokkaido University, N-21, W-10, Sapporo 001-0021,

Machine learning (ML) methods have gained much attention among the molecular and materials science communities for use in the prediction of various kinds of physical and chemical properties. ML methods could serve as a fast and high-precision alternative to the first-principles modelling. Several successful examples are already available for predictions and discoveries of organic chemistry reactions including ones that use homogeneous catalysts. However, targets of ML predictions for heterogeneous catalysis have been limited. Our group has been trying to contribute to establishing “Catalysis Informatics” by utilizing ML [1-2].

Here, we have calculated adsorption energies of CH₄ related species, namely CH₃, CH₂, CH, C, and H on the Cu-based alloys by using density functional theory (DFT), as shown in Figure 1 and 2. These DFT-calculated adsorption energies of CH₃, CH₂, CH, C, and H on Cu-based alloys will be used for ML predictions, and furthermore, for utilization of CH₄.

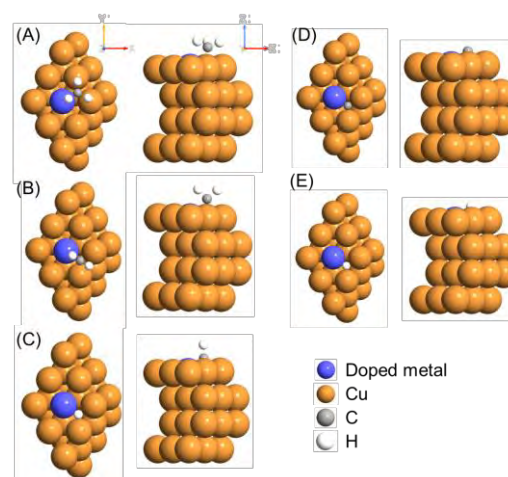


Figure 1. Adsorption models for (A) CH₃, (B) CH₂, (C) CH, (D) C, and (E) H on Cu-based alloys. Color code: gray: C; white: H; brown: Cu; blue: doped metal atoms.

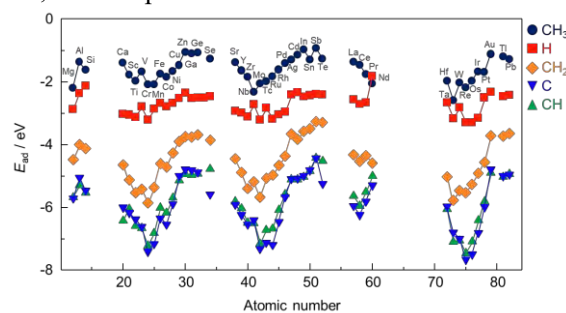


Figure 2. DFT-calculated adsorption energies of CH₃, CH₂, CH, C, and H on the Cu-based alloys.

References

- [1] I. Takigawa, K. Shimizu, K. Tsuda, S. Takakusagi, *RSC Advances*, **2016**, *6*, 52587-52595.
- [2] T. Toyao, K. Suzuki, S. Kikuchi, S. Takakusagi, K. Shimizu, I. Takigawa, *The Journal of Physical Chemistry C*, **2018**, *122*, 8315–8326

Structural study on surface reconstruction and solvent effects of nanoparticles

Akira YOKO

WPI – Advanced Institute for Materials Research (WPI-AIMR), Tohoku University

2-1-1 Katahira, Aoba-ku, Sendai 980-8577, Japan

Nanoparticle structures have been investigated because the nanoparticle structure is different from that of the bulk crystal. Surface reconstruction takes an important role in nanoparticle structure.

We have investigated nanoparticle structure of perovskite oxides, which have different surface energies depending on the composition [1]. The difference in particle size observed in experiments using supercritical water could be explained by the difference in calculated surface energies. Surface energies of nanoclusters are different from that of bulk surface calculated with slab model, and the calculation of nanoclusters was essential.

This year, calculation of interface energies of nanoclusters considering the effects of the solvent. The implicit solvent model which consider the effects of dielectric constant was applied. Calculations were conducted via VASPsol code with clusters consisting of 40 atoms. The dielectric constant of supercritical water was used (e.g., 5.9 for 400 °C, 30 MPa). Dielectric medium stabilized metal oxide nanoclusters resulting in the decrease in interface energy compared to the surface energy

in the vacuum. Interestingly, the dielectric medium affects nanocluster structures.

The effects of dielectric constant on nanoparticle structure were also investigated using BaTiO₃ as a model. The tetragonality defined as the ratio of the lattice of c-axis and a-axis was evaluated changing dielectric constant. As a result, the tetragonality of BaTiO₃ decreased with an increase in dielectric constant as shown in Figure 1. The previous experimental study elucidated that cubic and tetragonal BaTiO₃ formed at high and low water density conditions, respectively. The calculated results in this study could explain the tendency. Larger scale calculation would be required to elucidate this phenomenon.

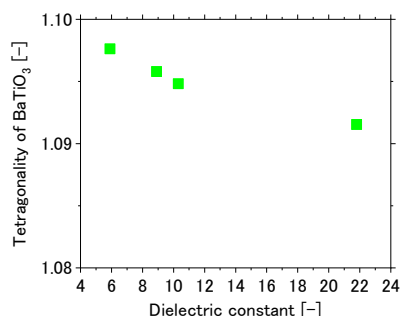


Fig. 1: Tetragonality of BaTiO₃ in dielectric medium.

References

[1] A. Yoko: *J. Phys. Chem. C*, **122(42)** (2018) 24350.

First-principles study on the structural stability of long-period stacking ordered structure in Fe based shape memory alloys

Takao Tsumuraya

Kumamoto University

2-39-1 Kurokami, Kumamoto 860-8555, Japan

Fe-Mn-Si based alloys is known to exhibit a shape-memory effect associated with deformation-induced martensitic transformation from face-centered cubic (fcc) γ -austenite to hexagonal closed packed (hcp) ϵ -Martensitic phase [1, 2]. Among them, Fe-15Mn-10Cr-8Ni-4Si (mass%) alloy appeared to have outstanding properties of low-cycle fatigue lives and is practically used in a seismic damping component of architectural constructions [3]. Recently, under cyclic push-pull loading of the Fe-Mn-Si-based alloys, a new phase different from ϵ phase was found by TEM. The new phase shows electron diffraction spots at the $1/3$ position of the 10-11 spots of the ϵ phase, which suggests the existence of a long-period stacking ordered (LPSO) structure.

In 1963, Lysak and Nikolin also discovered a new phase which is different from ϵ phase during heating and cooling cycles of Fe-Mn-C alloys using the x-ray diffraction measurements [4, 5]. This new phase is called ϵ' phase. Later, a similar phase was found by Oka *et al* using transmission electron microscopy (TEM). The ϵ phase is formed by stacking faults from fcc structure where $a/\sqrt{6}$ partial dislocation occurs every two layers on (111) plane of fcc structure which is parallel to (0001) plane of hcp structure. This type of dislocation is called Shockley's partial dislocation. However, such a long time, actual stacking sequence of the ϵ' (LPSO) phase and the relative stability with γ and ϵ phases still

remain unclear.

To understand the actual stacking pattern of the LPSO like structure and relative stability with γ and ϵ phases, we study phase stability and magnetic properties of pure Fe with 4H (dhcp), 6H₁, 6H₂, and 10H structures, together with 2H (hcp) and 3R (fcc) structures using first-principles density-functional theory (DFT) calculations within a generalized gradient approximation (GGA) (Fig. 1). The Kohn-Sham equation is solved by all-electron full-potential linearized augmented plane wave (FLAPW) method [6]. It is clearly shown that 6H₂ is the most stable structure. Therefore, we conclude that the LPSO phase adopts the 6H₂ structure. We also clarified the origin of structural stabilities from electronic structure point of view.

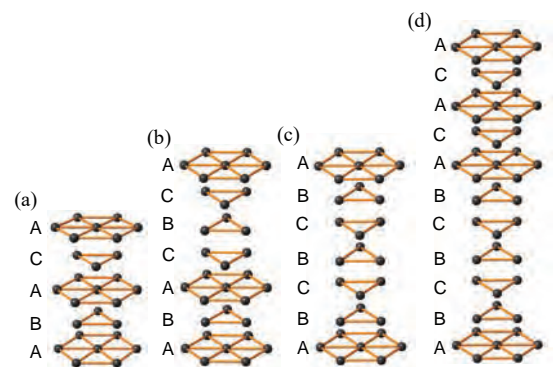


Figure 1: Candidates of long-period stacking ordered structure of Fe, (a) dhcp (4H), (b) 6H₁, (c) 6H₂, and (d) 10H.

References

- [1] A. Sato, Y. Yamaji, and T. Mori, *Acta Metall.* **34**, 287 (1986).
- [2] K. Ogawa and S. Kajiwara, *Mater. Trans.* **34**, 1169 (1993).
- [3] T. Sawaguchi, P. Sahu, T. Kikuchi, K. Ogawa, S. Kajiwara, A. Kushibe, M. Higashino, and T. Ogawa, *Scripta Mater* **54**, 1885 (2006).
- [4] L. I. Lysak and B. I. Nikolin, Martensitic phase with a multilayer structure, *Dokl. Akad. Nauk SSSR* **153**, 812 (1963).
- [5] Z. Nishiyama, *Martensitic transformation*, (London Academic Press, 1978).
- [6] E. Wimmer, H. Krakauer, M. Weinert, and A. J. Freeman, *Phys. Rev. B* **24**, 864 (1981).

Study on Electronic Properties in New Nanoscale Surfaces and Interfaces

Katsuyoshi KOBAYASHI

*Department of Physics, Ochanomizu University
2-1-1 Otsuka, Bunkyo-ku, Tokyo 112-8610*

In 2018 we have developed a method of calculation for spin and angle resolved photoelectron spectroscopy (SARPES). We have previously developed a new calculation method of SARPES [1]. In this method we used results of repeated-slab calculations with plane wave basis for the final states in photo-excitation. This was done because program packages for density functional calculations using plane wave basis are readily available, and the calculation of momentum matrix elements is easy. One point to consider is the boundary condition of final state wave functions in vacuum regions. We formed out-going plane-wave states in vacuum regions for final states by linear combination of repeated-slab states. This method was applied to the Bi(111) surface. Calculated results reproduced experimental ones [2]. A problem in the previous calculation is that the final states used for evaluating the matrix elements of photo-excitation are not the out-going states but time-reversed LEED states [3]. In 2018 we developed a method of forming the time-reversed LEED states using the results of repeated-slab calculations.

We performed density-functional calculations using the VASP program package to obtain self-consistent electron ground states. Bulk Bloch states of the excited states above vacuum levels were formed by linear combination of the wave functions given by the repeated-slab calculations. The time-reversed LEED states were made by eliminating the backward propagating Bloch states from the repeated-slab states. Matrix elements of photo-excitation were calculated using the time-reversed LEED states for final states.

This method was applied to the Bi(111) surface. Figure 1 shows calculated results of spin expectation values. The difference between the results of the out-going states [1] and the time-reversed LEED states is small. Calculated results reproduce experimental results [2].

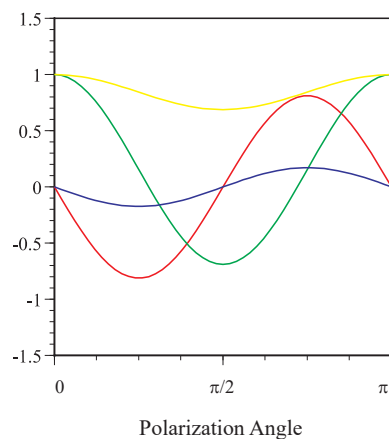


Figure 1: Spin expectation values calculated as a function of polarization angle of incident light. Red, green, and blue lines are x , y , and z components of spin expectation values. Yellow lines show intensity of photo-electrons.

References

- [1] K. Kobayashi *et al.*: Phys. Rev. B **95** (2017) 205436.
- [2] K. Yaji *et al.*: Nat. Commun. **8** (2017) 14588.
- [3] I. Adawi : Phys. Rev. **134** (1964) A788.

Coherent phonon spectroscopy of atomic layer materials

Ahmad Ridwan Tresna Nugraha

Department of Physics, Graduate School of Science

Tohoku University, 6-3 Aramaki-Aza-Aoba, Aoba-ku, Sendai, Miyagi 980-8578

Ultrashort (femtosecond) laser pulses applied to a solid-state material with duration less than a phonon period ($\sim 20\text{-}200$ fs) in the material may generate lattice oscillations coherently, known as coherent phonons. Excitations of coherent phonons are necessary to utilize the phonon modes as a basic component in phononic devices. In particular, we have to look for some materials that could host several coherent phonon modes.

Atomic layer materials, such as transition metal dichalcogenides (TMDs) and their hetero-structures, could be a good candidate for hosting the coherent phonons due to the presence of few-THz phonon modes that do not require sub-fs laser to excite them (50-fs laser is sufficient). A typical setup to excite and observe coherent phonons is shown in Fig. 1, in which the pump-probe technique is utilized.

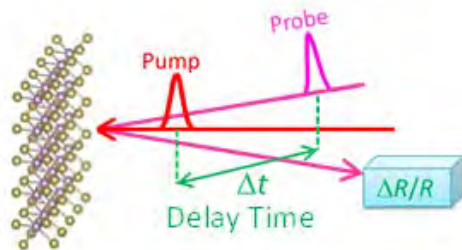


Fig. 1: Coherent phonon spectroscopy through ultrafast pump-probe technique.

In the pump-probe spectroscopy, an important physical quantity that can be measured is the change in either differential resistance ($\Delta R/R$) or different transmittance ($\Delta T/T$) as a function of delay time (Δt) between the pump and probe laser. The emergence of these quantities reflects the generation of coherent phonons because it is expected that there will be no macroscopic optical responses unless the lattices oscillate coherently. The changes in the optical quantities further indicate that the energy band of the materials might be modulated.

Therefore, to analyze the coherent phonon generation from the theoretical point of view, what we need to do firstly is to calculate the electronic band structure and phonon dispersion of the material under consideration. We can then modify the atom position in the material following the possible atomic displacement due to the coherent phonon oscillations. While such a calculation was possible without using supercomputer for some materials like carbon nanotubes that have a sophisticated tight-binding approximation [1,2], supercomputer is required to calculate band structure and phonon dispersion for most of TMDs.

In this 2018 fiscal year, we submitted several jobs in ISSP supercomputer system B to calculate the band structures and phonon dispersions of some atomic layer materials by considering displacement due to coherent phonon oscillations. An example given here is modulation of the band gap in monolayer MoS₂ by the oscillation of longitudinal acoustic (LA) phonon mode. The result is shown in Fig. 2.

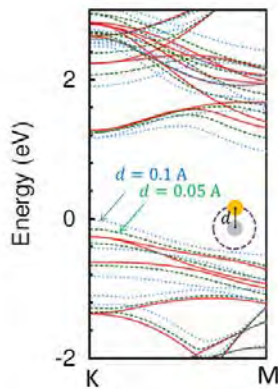


Fig. 2: Band gap modulation in monolayer MoS₂ by displacement d of the atoms due to the LA phonon.

In the particular calculation of MoS₂, we artificially exaggerate the amplitude of LA phonon oscillation as large as 0.1 angstrom to 0.05 angstrom so that we can see the effect of the phonon oscillation on the band structure of MoS₂ (Fig. 2). The ongoing work now is to calculate the absorption coefficient by this band gap modulation because the differential reflectance or differential transmittance is proportional to the change of absorption coefficient at different band structures [4].

References

- [1] A. R. T. Nugraha et al.: Phys. Rev. B **84**, (2011) 174302.
- [2] A. R. T. Nugraha et al.: Phys. Rev. B **91**, (2015) 045406.
- [3] A. R. T. Nugraha et al.: J. Phys. Condens. Matter **29** (2017) 055302 .
- [4] A. R. T. Nugraha et al.: *unpublished*.

First-principles meta-dynamics analysis of Catalyst Referred Etching method (reaction of water molecule on Ga₂O₃ surface)

Kouji INAGAKI

Graduate School of Engineering, Osaka University

Yamadaoka 2-1, Suita, Osaka 565-0871

Ga₂O₃ has been attracting attention as novel wide-bandgap material for power electronic and efficient optical devices, since recently an efficient crystal fabrication technic for the material has been developed. We studied interaction properties between water molecule and Ga₂O₃ surface, which plays crucial role in the most of fabrication processes for electronic devices such as polishing or chemical cleaning using water solvent in the polishing fluid or the chemicals. Water adsorption on Ga₂O₃ (100) surface which surface is the most stable has been already studied [1] with the purpose of analysis of catalytic properties of water splitting on the surface. In the device fabrication field, unstable (010) surface is important because it is the crystal growth surface with fast growth rate. Here, we report molecular and dissociative

adsorption of water molecule on Ga₂O₃ (010) surface as the first step of analyzing surface damage induced by etching or oxidation of the surface. We used STATE-senri code for first-principles calculations. The adsorption energies calculated as 0.79eV and 0.98 eV for molecular and dissociation, respectively. Only in the dissociative adsorption case, Ga atom at the adsorption site shows a substantial magnitude of displacement $\sim 0.5 \text{ \AA}$ as shown in Fig. 1. This indicates that once water molecule adsorbs on Ga₂O₃ surface, it become dissociated and impose a strain to the Ga atom. This indicates the initial stage of surface etching or oxidation.

References

[1] V.M.Bermudez, et.al.: Chem. Phys. 323 193 (2006).

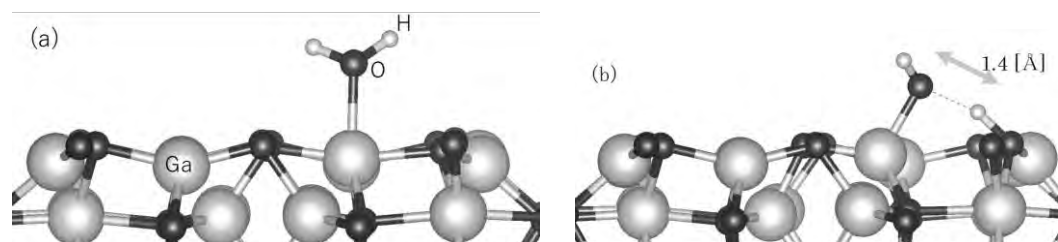


Fig. 1: Atomic configuration of H₂O molecule on Ga₂O₃ (010) surface. Molecular adsorption (a). Dissociative adsorption (b).